INVESTIGATIONS OF ADVANCED INJECTION AND COMBUSTION STRATEGIES ON DI DIESEL ENGINE PERFORMANCE AND EMISSIONS

by

RAOUF MOBASHERI

A thesis submitted to the School of Engineering and Informatics
for the degree of

Doctor of Philosophy

(Mechanical Engineering)

at the

University of Sussex

October 2012
Brighton, East Sussex

UNIVERSITY OF SUSSEX

INVESTIGATIONS OF ADVANCED INJECTION AND COMBUSTION STRATEGIES ON DI DIESEL ENGINE PERFORMANCE AND EMISSIONS

RAOUF MOBASHERI

Submitted for the degree of Doctor of Philosophy

October 2012

Abstract

The main driving force behind this research was the need for cleaner and more efficient engines to meet the ever-increasing demands on the modern automobile's emissions. In recent years different studies have been carried out to analyze the combined effects of high-pressure injection, boost pressure, multiple injections, included spray angle and combustion chamber geometry. Though considerable research has shown these technologies can meet the low emission regulations, the careful optimization of the engine operating conditions is still required in order to get the full benefit of the different strategies. With these issues as motivation, the first important objective of this study was to gain a detailed understanding of the mechanisms through which fuel injection interacts with other engine parameters and influences diesel combustion and emissions, and hence to attempt to generalize the adoption of multiple injection strategies with regards to improving diesel engine performance. For this purpose, a modified parameter called "Homogeneity Factor of in-cylinder charge" (HF) was introduced and proposed as a new measure in combustion theory to analyze the combustion characteristics and air-fuel mixing process of diesel engines in more detail. The second part of this research builds upon a detail investigation on the included spray cone angle concept and explores further their use in conjunction with multiple-injection strategies in diesel engines. In addition, an investigation was performed in third phase of this research to analyze the effects of piston geometry on combustion, performance and exhaust emission characteristics. The results showed that employing a post-injection combined with a pilot injection results in reduced soot formation from diffusion combustion and enhances the soot oxidation process during the expansion stroke, resulting in decreased soot emissions, while the NOx concentration is maintained in low levels. It was also found that spray targeting is very effective for controlling the in-cylinder mixture distributions especially when it accompanied with advanced injection strategies. Moreover, the results confirmed that a narrower width of piston bowl has a higher unburned fuel air mixture region and hence results in higher soot emissions but with slightly larger piston surface area the optimum operating point could be obtained.

ACKNOWLEDGEMENTS

First and foremost, I would like to take this opportunity to express my sincere gratitude to my supervisor, Dr. Zhijun Peng, for providing me with the opportunity to work under his supervision. His wisdom and guidance simultaneously challenged and supported my efforts and it has truly been an honor and privilege to work with him.

Thanks need to be given to my co-supervisors, Dr. Julian Dunne and Prof. Naser Sayma at the University of Sussex for their time and support.

I would also like to thank my thesis committee members Prof. Hua Zhao from the Brunel University and Dr. Evgeny Petrov from the University of Sussex for their constructive comments.

I want to express my gratitude to Dr. M. S. Shahrokhi-Dehkordi for his invaluable assistance. He has also been a good friend, who made living in Brighton more enjoyable.

Finally, words cannot adequately describe how much gratitude needs to be extended to my parents for their support and encouragement. Hopefully, I have made them proud.

PUBLICATIONS

i. **Mobasheri, R.**, Peng, Z. and Mirsalim, S.M., "CFD Evaluation of Effects of Split Injection on Combustion and Emissions in a DI Diesel Engine", SAE Technical Paper 2011-01-0822, 2011.

ii. **Mobasheri, R.**, Peng, Z. and Mirsalim, S.M., "Analysis the Effect of Advanced Injection Strategies on Engine Performance and Pollutant Emissions in a Heavy Duty DI-Diesel Engine by CFD Modeling", International Journal of Heat and Fluid Flow 33 (2012) 59–69.

iii. **Mobasheri, R.**, Peng, Z., "Investigation of Pilot and Multiple Injection Parameters on Mixture Formation and Combustion Characteristics in a Heavy Duty DI-Diesel Engine", SAE Technical Paper 2012-01-0142, 2012.

iv. **Mobasheri, R.**, Peng, Z., "Analysis of the Effect of Re-Entrant Combustion Chamber Geometry on Combustion Process and Emission Formation in a HSDI Diesel Engine", SAE Technical Paper 2012-01-0144, 2012.

v. **Mobasheri, R.**, Peng, Z., "3D-CFD Modelling of the Effects of Injection Timing on the Combustion Process and Emissions in a High Speed Direct Injection (HSDI) Diesel Engine", Proceedings of the ASME 2012 Internal Combustion Engine Division Spring Technical Conference ICES2012, Paper number ICES2012-81137, 2012.

vi. **Mobasheri, R.**, Peng, Z., "Using Large Eddy Simulation for Studying Mixture Formation and Combustion Process in a DI Diesel Engine", SAE Technical Paper 2012-01-1716, 2012.

vii. **Mobasheri, R.**, Peng, Z., "A Computational Investigation into the Effects of Included Spray Angle on Heavy-Duty Diesel Engine Operating Parameters", SAE Technical Paper 2012-01-1714, 2012.

TABLE OF CONTENTS

ABBREVIATIONS

AFR	Air to Fuel Ratio
ATDC	After Top Dead Center
BMEP	Brake Mean Effective Pressure
BSFC	Brake Specific Fuel Consumption
BTDC	Before Top Dead Center
CA	Crank Angle
CAD	Crank Angle Degrees
CFD	Computational Fluid Dynamics
CI	Compression Ignition
CO	Carbon Monoxide
CO_2	Carbon Dioxide
CR	Compression Ratio
DI	Direct Injection
ECFM	Extended Coherent Flame Model
EGR	Exhaust Gas Recirculation
EVC	Exhaust Valve Closing
EVO	Exhaust Valve Opening
FGT	Fixed Geometry Turbine
HC	Hydrocarbons
HCCI	Homogeneous Charge Compression Ignition
HRR	Heat Release Rate
HSDI	High Speed Direct Injection
IMAP	Intake Manifold Air Pressure
IMAT	Intake Manifold Air Temperature
IMEP	Indicated Mean Effective Pressure
ISFC	Indicated Specific Fuel Consumption
IVC	Inlet Valve Closing
IVO	Inlet Valve Opening
LES	Large Eddy Simulation
NOx	Nitrogen oxides
PCCI	Partially Premixed Compression Ignition

RPM	Revolutions per minute
SI	Spark Ignition
SOI	Start of Injection
TDC	Top Dead Center
TED	Two Equation Turbulence
TKE	Turbulent Kinetic Energy
UHC	Unburned Hydrocarbons
VCR	Variable Compression Ratio
VGT	Variable Geometry Turbine
VNT	Variable Nozzle Turbine
VVT	Variable Valve Timing

SUBSCRIPTS

α	index for chemical species
b	backward
e	equilibrium
eff	effective
f	Forward
fu	Fuel
st	stoichiometric
I	Number of oxygen atoms
m	Number carbon atoms
n	Nucleation; number of hydrogen atoms
o	Oxidation
pr	Products; prompt

LIST OF FIGURES

LISTS OF TABLES

Chapter 1

Introduction

1.1. Background

Efficient use of fossil fuels and reducing CO_2 emissions are very high on the priority list for the automotive industry. Although efficiencies of gasoline-type powertrains have been dramatically improved with gasoline direct injection and hybrid electric vehicle technologies, diesel engines still have superiorities on fuel economy over them, especially on motorways. Without the increasing contribution of diesel engines and newer diesel technologies, it would not be possible to achieve the fuel consumption and CO_2 emission reduction targets [1].

As diesel engines play more and more important roles in global car markets, it is necessary to continuously optimise their performances. New technologies of diesel engines not only require improving their integrations with drivetrain such as diesel hybrid technologies, but also need innovations on in-cylinder combustion.

In diesel engines, fuel is injected as liquid and it must evaporate before it can burn. Thus, there is an ignition delay between the start of injection and start of

combustion. During the ignition delay, some fuel is evaporated and mixes with air to levels that are within the flammability limits. Since it is mixed before combustion starts, the combustion rate of this premixed fuel-air mixture is controlled by fast chemical rates. When rapid combustion of this premixed mixture occurs, the gas temperature rises rapidly, causing higher NOx formation rates. The formation of NOx can't be prevented in the high temperature combustion of lean fuel-air mixture because nitrogen is the main component of ambient air. Following premixed combustion stage, the combustion rate is controlled by the mixing and diffusion rate, which are usually slower than the premixed combustion rate. Soot forms in the fuel-rich regions, although partially oxidized in the expansion stroke, also remains in considerable amounts at Exhaust Valve Opening (EVO) [2]. Basically soot is formed when oxygen is insufficient to oxidize the hydrocarbon compounds in diesel fuel during combustion. Since the combustion of sprays in a diesel engine is heterogeneous, soot formation is controlled by local ratio of hydrocarbon and oxygen during combustion process. Therefore, in DI diesel engines, the highest soot concentration is found in the core region of each fuel spray where local average equivalence ratios are very rich. Much soot is oxidized later in the cycle as more air is entrained into the fuel spray. Consequently, the net soot is the results of a competition between the soot formation and oxidation process in the cylinder.

When NOx and soot emissions may provide barrier for the application of diesel engines, the difficulty for dealing with the problem comes also from the trade-off feature between NOx and soot emissions. It is always very difficult to reduce both kinds of emissions simultaneously since factors that tend to decrease one usually increase the another. For example, retarding the fuel injection timing is an efficient method to decrease NOx emission. However, this method usually results in an increase of soot

production and causes lower thermal efficiency and higher Brake Specific Fuel Consumption (BSFC) [1]. Increasing EGR rate can decrease the NOx emission level as well, however less oxygen due to high ERG rate reduces the possibility to oxidize soot.

Increasing environmental concerns and more and more stringent emission legislations have let to the necessity of considering both conventional and unconventional means for reducing soot and NOx emissions in diesel engines.

Numerical simulation, compared to expensive engine experiments, is an efficient way to investigate various novel ideas to improve current engine performance, and hence it has become essential part of engine research and development. Although it is still challenging to achieve adequate accuracy with numerical simulation for modelling engine emissions, in particular for NOx and soot emissions, numerical simulations can play very important role for investigating those complicated the transient properties of physical process, e.g. diesel spray combustion and emission formation, whose characteristics are difficult or impossible to obtain with the current measurement technologies.

It has long been recognized that diesel engine combustion quality highly depends on the mixing of fuel and air. High injection pressures and multiple injections are commonly adopted in diesel engines to achieve better mixing of the fuel and air and to enhance the breakup of the fuel droplets. The common rail injection system has brought a great deal to flexibility to diesel engine development, since it decouples the three parameters of engine speed, injection pressure, and injector operating closing times. This feature provided the possibility of performing multiple injections per engine cycle. With the increased freedom of injection control, the multiple injection strategy has been

studied and practised in recent years with regard to its capability to improve engine performance, which mainly includes:

- Reducing pollutant emission, due mainly to very precise control of injection timing and rail pressure over the entire operating ranges.
- Reducing combustion noise, due mainly to the addition of a small pre-injection (pilot injection) which enables a reduction of the main injection ignition delay.

1.2. Research Objectives and Motivations

The main driving force behind this research was the need for cleaner and more efficient engines to meet the ever-increasing demands on the modern automobile's emissions. As discussed in the next chapter, different studies have been carried out in recent years to analyze the combined effects of high-pressure injection, boost pressure, multiple injections, EGR and combustion chamber geometry. Though considerable research has shown these technologies can meet the low emission regulations, the careful optimization of the engine operating conditions is still required in order to get the full benefit of the different strategies. Split injection, with two injection pulses in an engine cycle, along with EGR and boost pressure has been widely studied in recent years for evaluating its effects on engine performance and amount of pollutants emissions. However, influence of multiple injection strategies with three or more pulses in an engine cycle, in particular its combination with ERG and various included spray angles have not been understood clearly.

With these issues as motivation, the most important objective of this study was analyzing the combustion process and emission formation in DI diesel engines to examine the possibility of emission reduction by using different combustion and

injection strategies. For this purpose, the effects of wide range of split and multiple injection strategies in conjunction with the effects of various included spray angles and combustion geometries have been studied.

1.3. Organization of Thesis

This thesis is organized into eight chapters to help the reader in understanding the nature of this work, as follows.

Chapter 1 provides an introduction to the study.

Chapter 2 reviews some of the previous works related to this research in order to provide background for the subsequent chapters. A literature review of experimental and modeling studies is presented in this chapter.

Chapter 3 presents the theory behind diesel combustion process. Additionally, a modified parameter called “Homogeneity Factor of in-cylinder charge” (HF) has been introduced and proposed as a new measure in combustion theory to analyze the combustion characteristics and air-fuel mixing process of diesel engines. It has been shown in next chapters that this parameter can be used as an efficient tool for further exploring the effects of different injection strategies on combustion process in more detail.

Chapter 4 describes the theoretical background of the Computational Fluid Dynamic (CFD) Code and the mathematical equations adapted in this research for validation.

Chapter 5 elaborates on the emission reduction capability of combined effects of multiple injections and EGR. The main purpose of this part was to gain a detailed understanding of the mechanisms through which fuel injection interacts with other

engine parameters and influences diesel combustion and emissions, and hence to attempt to generalize the adoption of multiple injection strategies with regards to improving diesel engine performance.

Chapter 6 builds upon a detail investigation on the included spray cone angle concept and explores further their use in conjunction with multiple-injection strategies in diesel engines. Different optimum multiple injection strategies obtained in previous part is adopted for this assessment. CFD analysis of different included spray angles in comparison with the traditional spray injection angle reveals that narrow spray cone angle nozzles provide an opportunity to achieve further reductions in NOx and soot, with minor penalties in fuel economy.

Chapter 7 presents a CFD investigation that has been carried out to study the effect of Re-Entrant combustion chamber geometry on mixture formation, combustion process and engine performance. For this purpose, a wide range of combustion chamber configurations have been considered based on four categories including piston bowl depth, piston bowl width, piston bottom surface and lip area.

Chapter 8 summarizes the major conclusions derived from this thesis. Possible areas for future investigation are discussed as well.

Chapter 2

Literature Review

2.1. Background

Internal combustion engine has had many variations during the past century. Compression Ignition (CI) engines are one of the oldest and are also one of the leading possibilities for the automotive industry. As it is well known, NOx and soot emissions are problematic in diesel engine combustion. After-treatment systems to control these emissions have been developed in recent years but they are usually expensive, complicated and will reduce fuel economy and thus reduce the primary advantages of diesel engines. Hence, there is still a great interest to optimize in-cylinder combustion technologies for the emission minimization which offer low NOx and low soot emissions.

In this chapter, the operation of different types of compression ignition engines (CI, HCCI/PCCI) is firstly discussed to establish a context for this research work. Then, combustion technology advancement over the past two decades is reviewed with special focus on advanced in-cylinder combustion strategies.

2.2. Engine Combustion

2.2.1. CI Engine Combustion Process

The diesel combustion process is characterized by heterogeneous mixture formation and combustion. In diesel engines, fuel is directly injected under high pressure, usually shortly before the top dead center, into the combustion chamber [3]. The fluid fuel entering the combustion chamber is atomized into small droplets, vaporized and is mixed with air, resulting in a heterogeneous mixture of fuel and air. Combustion is initiated by the high temperatures and pressures by an auto-ignition process, hence the alternative name compression ignition (CI) engine [3]. The load of the engine is controlled by the amount of injected fuel and combustion start is controlled by the start of injection. Diesel engines are usually operated with a globally lean air-fuel ratio, but direct injection leads to different mixture areas ranging from very lean through stoichiometric to very rich mixture ratios. Such mixture stratification leads inevitably to the formation of pollutant emissions, especially soot particles and nitrogen oxides [3]. Chapter 3 reviews the diesel combustion process in more details.

In the conventional diesel combustion process, usually there is only a very short amount of time available for mixture formation. A fast injection and as good as possible atomization of the fuel are, therefore, the prerequisites for a fast and intensive mixing of fuel and air [3]. It has been shown that the particulate emissions can be reduced with increasing fuel injection pressure because of increased mixing via enhanced spray penetration [4]. Therefore, higher pressure injection systems have been incorporated into modern diesel engines. This allows the use of smaller injection holes for the same fuel delivery rate, resulting in smaller fuel droplets.

Badami et al. [5] accomplished up to 27% reduction in particulate emissions with 2.7% reduction in BSFC when the injection pressure was increased from 1300 to 1500 bar in a HSDI diesel engine at 4000 rev/min. Shimazaki et al. [6] observed the combustion process in a single cylinder two-stroke DI diesel engine with a gas sampling methods and found that in the case of high injection pressure, the O_2 concentration decreased faster, and air dilution was more active and occurred earlier. They concluded that this might explain the decrease of soot emissions due to accelerated soot oxidation.

However, increasing the injection pressure generally results in higher NOx emissions. Shundoh et al. [7] accomplished significant smoke reduction by increasing the injection pressure at a 1000 rev./min full-load condition on a DI diesel engine, while NOx emission increased. They asserted that to achieve NOx reduction, the injection pressure must be controlled according to the load condition because NOx emission increases dramatically from a full load to a partial load operating condition. Pierpont and Reitz [8] found that increasing the injection pressure on a heavy duty engine at 75% load, 1600 rev./min resulted in a reduction of particulate emissions but an increase in BSFC, if NOx levels were held the same by retarding the timing.

2.2.2. HCCI / PCCI Combustion

The application of Homogeneous Charge Compression Ignition (HCCI) engine has been studied since 1979 when it was applied to two stroke engines by Onishi et al. [9] and Noguchi et al. [10] through use of hot residual gas retained in the cylinder. Since then a large number of studies of HCCI engines have been carried out. The HCCI engine contains attributes of both the SI and CI engine. HCCI engines use an intake charge that is a homogeneous mixture of fuel and air as in a SI engine, but the mixture is compression ignited, as in a CI engine. In contrast to both SI and CI engines, an

HCCI engine does not contain a direct trigger to start the combustion process like the other two engines, but depends on the thermochemical path of the mixture being compressed. Thus, ignition depends on the temperature and pressure history of the gas mixture.

The HCCI auto-ignition process is very much like knocking in SI engines, except that HCCI occurs homogeneously throughout the cylinder, not ahead of a flame front. The high compression ratios needed to auto-ignite the mixture can yield efficiencies similar to that of CI engines, provided that the indirectly controlled ignition starts at the right time. Moreover, these engines have neither throttling nor a high-pressure fuel injection system, and are usually operated at part load with their very lean premixed homogeneous mixtures burning at relatively fast velocity and low temperature. They have the advantage of low particulates and NOx emissions while maintaining higher efficiency at light load conditions than spark ignition and diesel engines. However, the difficulty in controlling the start of combustion, high heat release rates, very high unburned HC and CO emissions, and limited power output are remaining obstacles to the wide application of such engines [11, 12]. Some of the main disadvantages due to the inherent nature of HCCI combustion can be summarized as follows:

- Combustion control: The absence of a direct mechanism to trigger ignition has resulted in a major challenge to control combustion during HCCI operation. HCCI combustion occurs when the charge composition and temperature are favorable for auto-ignition. This means that combustion control would have to be achieved by regulating the charge composition and the time history of the temperature. Several promising methods such as variable valve timing (VVT),

variable compression ratio (VCR), EGR and etc are being used to indirectly control combustion.

- High CO and UHC emissions: one of the significant drawbacks of HCCI operation is high CO and UHC emissions.
- Operating range extension: At very low loads/cold start, the compressed gas temperature is not sufficiently high to initiate auto-ignition. This results in misfire and consequently high carbon monoxide (CO) and unburned hydrocarbon (UHC) emissions. HCCI operation at very high loads is limited due to higher rate of pressure rise and significant NOx emissions.

Recent HCCI engine researches mainly focus on the following issues:

- Extension of the operational limits in both the lower and higher load ranges, including the improvement of the power output, and the application of HCCI combustion in multi- cylinder engines
- Improvement of the performance of HCCI engines under the conditions of cold start/warm up and very low load operation

Furthermore, the investigation of the combustion characteristics of HCCI engines is a fundamental approach that needs to be followed to find effective solutions to their limitations.

A promising development in the HCCI strategy utilized two injection events: an early injection of a portion of the total fuel, in order to prepare an ignitable mixture, followed by a second injection of the remaining fuel close to top dead center in order to trigger the combustion. These injection strategies in DI diesel HCCI engines lead to the creation of a partially premixed mixture of fuel, air and residual gases that undergoes low temperature combustion. This regime, referred to as Partially Premixed

Compression Ignition (PCCI) combustion. For both HCCI and PCCI combustion, the role of chemical kinetics is very important. Particularly in HCCI engines, the onset of combustion as well as the rate of heat release depends strongly on chemistry. While the timing of ignition can be controlled by the presence of spray in PCCI, accurate description of the chemistry is still a primary issue even in PCCI combustion.

2.3. Diesel Combustion Technology Advancement

2.3.1. Common Rail Injection System

The improvement of DI diesel engines for passenger cars to comply with the stringent exhaust emission standards is closely linked to continued development of the injection system. A growing trend in the diesel engines industry is towards wider use of electronically controlled high pressure injection system which can inject fuel at any point in the cycle without the injection rate changing owing to injection timing or engine speed.

The major difference between common rail system and a standard diesel injection system is the free choice of the injection pressure and timing [4]. In addition, modern electronically controlled common rail injection systems are capable of multiple high pressure injections at various engine speeds.

Figure 2.1 shows the common rail system schematically. Common rail injection systems employ a high pressure pump to supply an accumulator that is common to all the injectors in the system. The pressure is controlled with a pressure regulating valve. Fast acting solenoid valves that control the start of injection, combined with an injection pressure which is independent of injection timing (and relatively independent of engine speed) has made the common rail an attractive option for automotive engines.

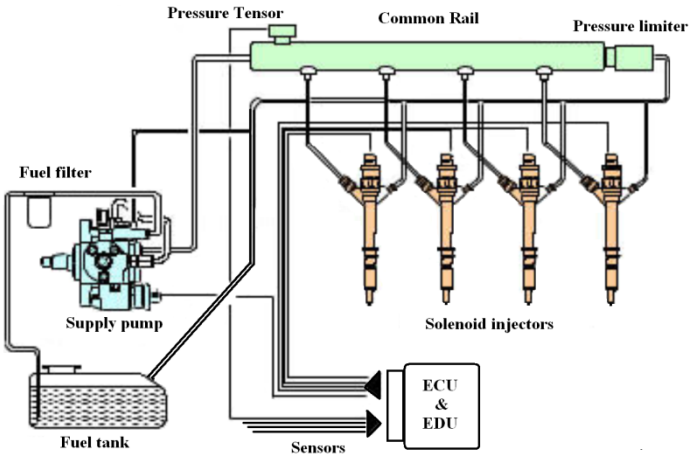

Figure 2.1 – Common rail fuel injection system [4]

2.3.2. In-Cylinder Air Motions

In-cylinder flow patterns including swirl, squish and tumble motion are well known to strongly influence both engine performances and pollutant emissions, by playing a fundamental role on mixture formation, early ignition development stages, mixing-controlled combustion and late-combustion fuel consumption. Swirl is usually defined as organized rotation of the charge around the vertical axis of the cylinder, which can be obtained by the geometry of the intake ports and also by the geometry of the valve seats [3]. The squish flow is generated when the piston approaches top dead center, displacing the air in the squish area. Both the squish and the swirl flow can improve the mixing between the induced air charge and the injected fuel. Tumble flow is defined as a swirling motion of cylinder air around the transverse axis of the cylinder in the direction of the crankshaft axis [3].

An appropriate level of swirl improves fuel efficiency, due to the shortening of combustion duration and the more effective phasing of the heat release curve. The higher mixing rate provided by swirl also reduces smoke emissions, due to decreased soot formation and enhanced late cycle oxidation [13-15]. While many other flow

structures generated during the intake process decay very quickly, swirl can survive throughout the compression process, and even into combustion and expansion processes. This feature is very useful in enhancing the mixing between the fuel spray and air, and therefore has a marked effect on the combustion process [16].

Diesel engines with cylinder diameters greater than 300 mm can normally operate efficiently without additional air movement in the combustion chamber and the mixture is essentially prepared by atomising the fuel as it emerges from the injection nozzle. The injection nozzles used are multi-hole nozzles containing up to 12 holes. Combustion processes with high swirl ratios usually use fewer nozzle holes in order to avoid an interaction of adjacent fuel jets [3]. Modern large four-stroke engines as used in trucks, heavy-duty, power generation and marine applications usually use a combustion process with low swirl and a more shallow piston bowl compared to passenger car engines. The advantage of a low-swirl combustion process is the improved volumetric efficiency, since the generation of directed flow structures always increases gas exchange losses. The mixing energy is supplied mainly by the injection system [3]. With smaller engines and therefore higher engine speeds, the charge movement that normally occurs as a result of the intake process, injection of fuel and piston motion is no longer sufficient to prepare the mixture effectively. Special measures are required to increase the relative speed of fuel and air in the combustion chamber. The inlet ports are designed as swirl and/or tangential ports, an intensive rotational movement of air occurs around the cylinder axis (swirl) when air enters the combustion chamber. This is superimposed on the turbulence that already exists in the combustion chamber and has the effect of distributing and mixing the fuel vapour that immediately forms in the area around the injection jet when fuel is injected with the air already in the combustion chamber (macro mixture preparation).

The in-cylinder flow after spray injection is dominated by the spray-induced flow because the injected droplets have much higher speeds. The surrounding gas flow is dragged by droplets and interacts with the piston bowl movement. This can form a tumble flow, which has a significant impact on the consequent processes of mixing, combustion, and pollutant formation [17]. Tumble is similar to the swirl except it is in a vertical plane in the flow field. A tumble flow is usually formed in the late stage of the intake stroke and survives through the compression stroke until the piston approaches top dead centre (TDC) [18].

In recent years, various studies have been applied in CFD upfront optimization of the in-cylinder flow and tumble motion. Iyer and Yi [19] assessed the effects of intake port design and spray injection timings on the tumble intensity using the MESIM 3D CFD code. By quantification and visualization of engine tumble flows they concluded that the effect of intake valve masking was beneficial for improving the air–fuel mixing, especially at part load. Delaying the start of injection timing allowed for the generation of higher tumble flow that, in turn, generated higher turbulence intensity at TDC [18].

The advantage of squish turbulence over swirl is that its intensity increases as it approaches the piston at TDC (fuel injection phase) whereas swirl generated during the intake process begins to subside at this point. A combination of both methods is applied as the high running speed capability of engines increases. In order to achieve best values for fuel consumption and exhaust emissions, the design of the combustion chamber geometry and fuel injection system must be optimised and matched to each other.

It has long been recognized that engine out emission levels depends greatly on swirl due to its mixing characteristics. However, this effect cannot be controlled by a

single parameter as simple as the swirl number, since induction swirl and piston configuration interact each other in diesel engines. Arcoumanis et al. [20] measured the three components of velocity and their fluctuations by Laser-Doppler anemometry mainly near TDC of compression at 200 rev./min. They observed that interaction of swirl, carried from intake and persisting through compression, with squish generated near TDC profoundly altered the axial flow structure. In the case of a cylindrical bowl, the sense of the vortex was reversed by swirl and, in a re-entrant bowl, swirl increased the number of vortices to two.

Because of these flow complexities it is not possible to specify an ideal amount of swirl that should be used for all cases. However, optimal levels of swirl for minimum levels of emissions are often observed at certain operating conditions. Espey et al. [21] used an optically accessible DI diesel engine to investigate the effect of swirl on fuel-air mixing and flame evolution. They found in a mixing study (performed with nitrogen to prevent combustion) that the spray plume penetration length was reduced by 17%, while the mixed area was increased by 25% with induced swirl. They also observed that, initially, the visible flame grew more rapidly with swirl, but it penetrated more slowly into the squish region. They asserted that this slower penetration was related to the reversal in the rotational direction of the vortex in the combustion chamber when swirl is added to the flow, which tends to carry fuel from the wall towards the center of the combustion chamber.

Ogawa et al. [22] used a modified version of the KIVA code to analyze the combustion and emission characteristics of a DI diesel engine and found that increasing the swirl ratio reduced soot emissions, but increased NOx. Further increases in the swirl ratio produced an increase in soot emissions. They asserted that the reason for greater soot emissions with a higher swirl ratio was related to increased fuel vapor

concentration at the center of the combustion chamber. Fuchs and Rutland [23] modelled intake, compression, and combustion of a Caterpillar diesel engine using a modified version of the KIVA-II and KIVA-3 CFD codes. Their results revealed that high swirl ratios distributed the fuel such that it remained in the bowl, thus depleting almost all of the bowl oxygen during combustion, which resulted in a poor late diffusion burn.

2.3.3. Pressure Charging Including VGT/VNT

Boosting, which refers to increasing the air (or mixture) density by increasing its pressure prior to entering the engine cylinder, has been considered as a method of increasing the specific performance of diesel engines. Recently, many studies investigating the effects of boosting have shown favorable results in terms of exhaust emission and fuel economy. Therefore, variable boost pressure systems have become an important tool for adapting diesel engines to meet future emissions and performance requirements, since a variable boost system allows flexible control of boost pressure for different load and speed conditions [24].

Matching a turbocharger to a given heavy-duty diesel engine in vehicles is considerably more difficult due to the wide speed and load variations encountered. If a big turbocharger with a fixed geometry turbine (FGT) is used to match a diesel engine well at high speed, the engine can obtain proper performance at high speeds, with low fuel consumption, and low smoke emissions, but the engine performance will deteriorate at low speeds. If a small turbocharger is used to match the diesel engine well at low speed, the engine can get good performance and low smoke at low speeds, but the expansion ratio across the turbine will be very high at the maximum engine speed when air flow is greatest. Thus the piston must pump the exhaust gases out against a

high backpressure, resulting in poor net power output and fuel consumption. In addition, the engine will exceed the allowable limits of maximum cylinder pressure and turbocharger speed. Clearly the turbocharger should not match heavy-duty diesel engines at one high or low speed and a compromise must be reached in the engine speed range.

A simple method of avoiding the above problem is to use a waste-gate valve through bypassing some of the exhaust gas around the turbine at high speeds. Thus when a small turbine is fitted to achieve good low-speed boost, the massive increase in specific available energy at the turbine at high speed is alleviated by increasing the effective flow area out of the exhaust manifold. This has two effects. Firstly, only part of the exhaust gas flow goes through the turbine. Secondly, the increase in flow area reduces the exhaust pressure that would otherwise build up. Both measures reduce turbine work and hence boost pressure. In addition, the second factor reduces pumping work during the exhaust stroke and would moderate the loss in brake mean effective pressure (BMEP) and deterioration in fuel consumption at high speeds [25, 26].

Ideally the best method to solve the above problem is to use a variable geometry turbine (VGT). So far, VGT technology has found wide use in current heavy-duty diesel engines to achieve the desired diesel engine performance [25]. The turbochargers have variable nozzle turbines, which are controlled electronically. The VGT feature enables the turbocharger boost to be controlled across the engine speed and load range. In VGT turbochargers the turbine housing contains movable vanes that control the effective size of the housing, and direct the flow of the exhaust gas to the turbine wheel. When the vanes are closed, the exhaust gas is accelerated between the vanes and across the turbine wheel, producing higher turbine speeds and higher boost at low engine speeds. In effect, this shows that the engine uses a smaller turbocharger at these conditions, which means

that the turbocharger works at high-efficiency status. At higher speeds and loads, the vanes are opened to control the amount of boost desired, and prevent over-speeding of the turbocharger. This shows that the engine uses a large turbocharger. Thus, the turbocharger still works under high-efficiency conditions. Overall, the VGT turbocharger provides a much wider range of high-efficiency operation and a higher boost level compared with a standard FGT turbocharger [25, 26].

One of the main drawbacks of employing a variable nozzle turbine (VNT) is the increased pumping loss associated with vane closure, leading to poorer fuel economy. The dynamic behaviour introduced in the exhaust flow, as a result of movement in the EGR (valve) and the VNT (vanes), defines the state and composition of the air charge entering the engine. Hence, much attention is paid to the development of the control of EGR and VNT to improve exhaust emissions, fuel economy and engine performance [25, 27].

Since its first introduction by Garrett Turbochargers in 1991 for the Fiat Croma, the VNT turbocharger has been progressively developed for smaller frame sizes, higher efficiency and volume production. Today the VNT turbocharger is standard equipment for high-power-density diesel engines and all manufacturers of diesel passenger cars offer high-power output engines using VNT turbochargers. The most notable are the new premium V8 engines from Audi, BMW, Mercedes and Ford. These engines are fitted with twin VNT Garrett turbochargers that have electric actuators to enable the electronic engine management system to directly control the turbine vane position. Garrett Turbochargers has led the field in this technology and the demand for VNT turbochargers has risen dramatically over the last 10 years [25].

Uchida et al. [28] studied the effect of supercharging on DI diesel combustion. They reported that supercharging could favorably reduce ignition delay and enhance diffusion combustion, resulting in improved fuel economy and reduced emissions, except for NOx, at retarded injection timing. Tanin et al. [29] studied boost pressure effects using a single-cylinder version of a heavy-duty diesel engine. They found that particulate emissions decreased significantly with increased intake boost pressure due to the increased available air for soot oxidation at elevated intake pressure, while holding brake specific NOx constant. Zhang et al. [30] conducted an experimental study to investigate the effects of supercharging on an optically accessible DI diesel engine. They observed that in the diffusion combustion stage, the flame movement was less active and the impingement effect of the fuel jet was smaller in the case of high boost pressure during the injection period, indicating that the turbulent effect caused by the fuel injection was weakened. As a result, they argued that, although higher boost pressure brought more air into cylinder, the entrance of air to the flame covered sprays would not be imported much. Consequently, at higher boost pressures, the relatively small flame area and relatively little flame movement might reduce the advantage of increased air available. However, they observed that the soot formed was soon oxidized around the surface of flames because of the large amount of air at their engine operating conditions.

2.3.4. Exhaust Gas Recirculation

It is well known that exhaust gas recirculation (EGR) is effective for the reduction of NOx emissions [31]. The application of EGR in diesel engines helps to replace part of oxygen in the inlet air with carbon dioxide and water vapor from the exhaust that have higher specific heat capacities. The inclusion of CO_2 and H_2O

together with the reduction in oxygen concentration in the combustion process reduces the gas temperature within the engine cylinder during combustion. The NO formation and decomposition can be described by the Zeldovich mechanism which is very temperature sensitive [32].

However, the reduction in oxygen availability in the burning regions of the combustion chamber impairs the soot oxidation process and the reduction in the local combustion temperature reduces the soot oxidation rate. Consequently, the use of EGR is often associated with an increase in exhaust smoke and particulate levels.

Ladommatos et al. [33] conducted a detailed study of the effects of EGR in a 2.5L, four-cylinder DI diesel engine. Their results showed that the reduction in NOx emissions and the increase in particulate emissions due to EGR could mainly be attributed to the dilution function of residual gas to inlet charge oxygen.

Hentschel and Richter [34] investigated the formation of soot in a 1.9L DI diesel engine and found that with increasing EGR rates, the amount of soot formed was increased only slightly, but the amount of soot oxidized during combustion decreased significantly. Ladommatos et al. [35] also observed that use of EGR caused an increase in the ignition delay and shift in the location of the whole combustion process further towards the expansion stroke. This resulted in the combustion gases spending shorter periods at high temperature, leading to lower thermal NOx formation as well as a reduced rate of soot oxidation.

EGR is usually considerably hotter than the inlet air, which results in an increase in the charge temperature. Dürnholz et al. [36] found that EGR not only helps to reduce NOx, but it also contributes to achieve lower HC emissions when hot EGR was used. Ladommatos et al. [37] found that at a given engine speed and load, cooling the EGR

increased the density of the inlet charge and the volumetric efficiency of the engine in comparison to cases with hot EGR. They showed that a substantial improvement in the trade-off between exhaust NOx and soot emission could be achieved by cooling the EGR.

Ladommatos et al. [37] found that introducing EGR as an additional component of the inlet air in such a way as to keep the oxygen concentration constant could alleviate the detrimental effects of EGR on particulate emissions. Arcoumanis et al. [38] reported that cold EGR resulted in lower NOx emissions at EGR rates below 30%, but at higher EGR rates cold EGR seemed to offer marginally higher NOx emissions in comparison to hot EGR. Mattarelli et al. [39] studies the effect of EGR in a 2.5 L, four valve, turbocharged DI diesel engine with and without cooling. They found that cooler EGR was demonstrated to be effective for improving NOx emissions, particularly at high load. As its influence is so complicated, normally the application of EGR must be considered to combine with other optimizations, such as fuel injection strategy.

2.3.5. Injection Strategies

Multiple injections strategy is another method which has been proposed as an efficient tool to decrease the amount of pollutant emissions. Multiple injections divide the total quantity of fuel into two or more injections per combustion event. Splitting the injection sequence into two events is called pilot or split injection. A pilot injection is also usually defined as an injection where 15% or less of the total mass of fuel is injected in the first injection. Many researchers are now investigating pilot and split injection as an effective means to simultaneously reduce NOx and soot emissions.

Yamaki et al. [40] investigated the effects of pilot injection on exhaust emissions in a turbocharged heavy duty DI diesel engine and found that with partial load, when

the pilot fuel quantity was increased, fuel consumption and soot increased, but NOx was found to decrease and then increase. Minami et al [41] studied the effects of pilot injections in a turbocharged DI diesel engine and found that the pilot injection was effective to reduce NOx and HC at low load conditions, though it deteriorated soot to some degree. Zhang [42] used a single cylinder HSDI diesel engine to investigate the effect of pilot injection with EGR on soot, NOx and combustion noise, and found that pilot injection increased soot emissions. The author observed a linear relationship between smoke and luminous flame area fraction within the piston cavity when the main injection starts. The author also showed that reducing the amount of fuel in the pilot injection and increasing the interval between pilot and main injections could reduce the pilot flame area when the main injection starts, resulting in lower soot emissions. Nehmer and Reitz [43] studied the effect of split injection in a heavy-duty diesel engine by varying the amount of fuel in the first injection from 10 to 75 % of the total amount of fuel. They found that split injection better utilized the air charge and allowed combustion to continue later into the power stroke than for a single injection case, without increased levels of soot production.

Mendez et al. [44] studied the effects of different multiple injection strategies on combustion process. In this work, investigations were conducted on low compression ratio Diesel engine at high EGR rate operating conditions to evaluate the potential of multiple injections. These experiments have highlighted that in the thermodynamic conditions specific to low CR engines and high EGR rate interesting effects on the combustion process could be obtained via multiple injections. It was observed when the CR is reduced ignition delay increases and the peak heat release associated with the combustion of the pilot injection is greatly reduced. For CR 14:1 the distinct initial heat release associated with the fuel injected during pilot injection is very often close to be

null unless the fuel amount injected during the pilot injection is greatly increased. No distinct combustion of the pilot injection can be identified from the heat release analysis.

Figure 2.2 shows an illustration of pilot injection that does not burn before main injection. This is due to a low CR engine (14:1) and a high EGR rate (46%) that lead to a so long ignition delay that the fuel of the pilot injection is over dispersed and that the resulting very lean mixture never reaches auto-ignition condition before the main combustion phase. As a consequence, for identical EGR rates, single and double injection strategies exhibit similar heat release profile. This is due to the fact that the fuel from the first and second injection burns at the same time.

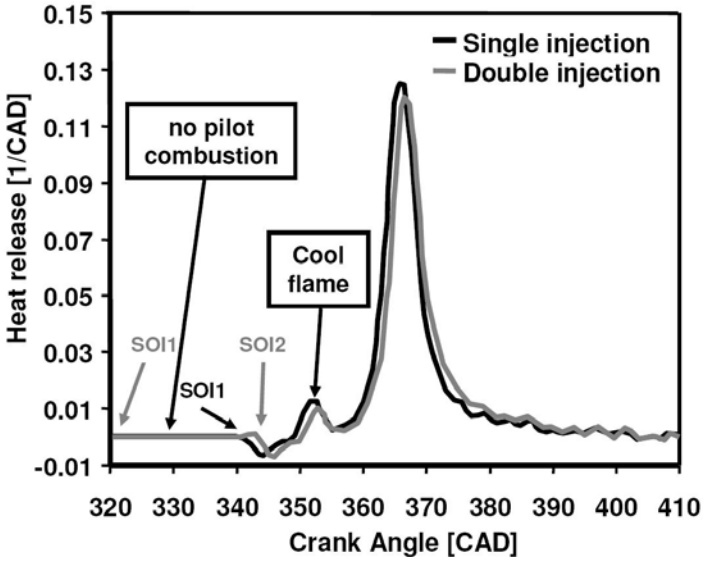

Figure 2.2 – Effect of low CR and high EGR rate on ignition of pilot injection [44]

It is usually admitted that combustion noise measured and maximum heat release are in most case well correlated [44]. So to decrease combustion noise it is advisable to limit the level of maximum heat release. A promising approach is to split the fuel combustion process into two parts in order to get two separate heat release peaks triggered by two or more injections. The maximum amplitude of the split heat

release is lower than the peak heat release obtained with a single injection and this leads to a lower combustion noise.

As shown in Figure 2.3, splitting heat release by using two injections allowed to reduce heat release maximum value to a lower one than with the single injection. Consequently, combustion noise is decreased by 7 dB.

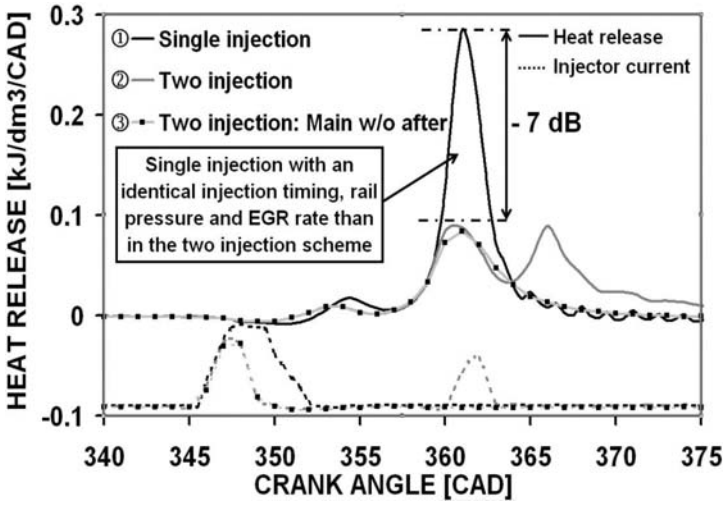

Figure 2.3 – Single and double injections heat release [44]

Tow et al. [45] pointed out that the dwell between injections was very important to control soot productions and there would exist an optimal dwell at a particular engine operating condition. Their optimal dwell of a double injection was found to be about 10˚ CA at 75% load and 1600 rev/min for their engine conditions.

Han et al. [46] carried out a three-dimensional computation to understand the mechanism of soot and NOx emission reduction in a heavy duty diesel engine with multiple injections. The mechanisms of the soot reduction using split injections are illustrated schematically in Figure 2.4. As can be seen in Figure 2.4, in single injection combustion, the high momentum injected fuel penetrates to the fuel rich, relatively low temperature region at the jet tip and continuously replenishes the rich region, production soot. However, in a split injection, the second injection enters into a relatively fuel-lean

and high temperature region that is left over from the combustion of the first injection. Therefore, soot formation is significantly reduced because the injected fuel is rapidly consumed by combustion before a rich soot producing region can accumulate. They also pointed out that the dwell between two injections should be optimized long enough that the soot formation region of the first injection is not replenished with fresh fuel, but short enough that the in-cylinder gas temperature environment seen by the second pulse remains high enough to prompt fast combustion, reducing soot formation.

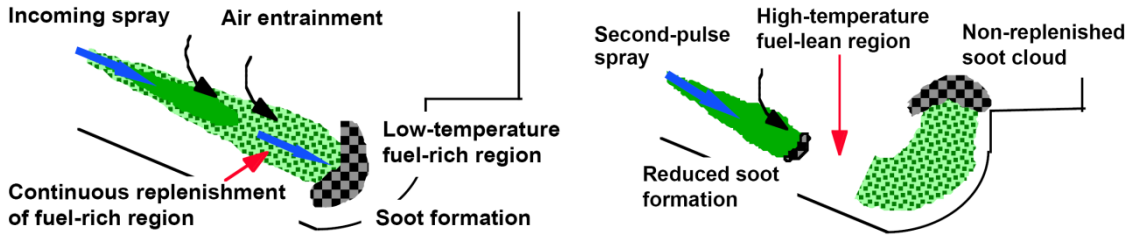

Figure 2.4 – Schematics diagram showing soot-reduction mechanisms of split injections. Left: Single injection. Right: Split injection [46]

The benefits of multiple injections have been found to be highly dependent on the specification of the quantity of fuel in each injection and the dwell between injections. Dürnholz et al. [47] investigated the influence of pilot injection for a turbocharged and intercooled DI diesel engine for passenger cars. Their optimized pilot injection contained about 1.5 mm^3 of the fuel in the pilot injection independent of engine load and their optimal dwell was 15˚ CA.

Ricaud et al. [48] experimentally optimized HSDI diesel engine performance by adopting a multiple injection strategy. With more flexibility and more precise control of the injection characteristics provided by a common rail injection system, a series of multiple injection strategies including “1 pre-injection + main injection”, “2 pre-injections + main injection”, and “2 pre-injection + main injection + post injection” were experimented at several operating points. The study showed that there is

practically no advantage in long pre-injection dwell times, unless completely homogeneous combustion is desired. The fuel quantity in each pulse, the dwells between pulses, the injection pressure, and the start of injection timing, as well as EGR ratio, must be carefully determined to achieve optimized performance. The injection pressure should be increased with more injection pulses, since multiple injection leads to combustion almost entirely occurring in the mixing-controlled regime. Combustion noise can be limited because multiple injection strategies also offer the freedom to adjust the in-cylinder pressure rate. However, combustion noise and soot emissions were revealed to be very sensitive to the injected fuel quantity in the pre-injections, which could be a difficulty in the practical use of multiple injection, since a high degree of control is required. They also concluded that with the increased number of parameters associated with multiple injection strategies, it is necessary to use efficient optimization methodologies.

Dronniou et al. [49] investigated the effects of combination of high EGR rates and multiple injection strategies to reduce pollutant emissions. Results showed the soot level can be dramatically reduced if an early pilot injection is combined with a main injection. Results presented in Figures 2.5 and 2.6 show that the addition of a post-injection improves emissions results. The post-injection enhances soot burnout by reintroducing some turbulent energy within the cylinder (e.g. improved mixing with air). However, using advanced injection timings has major mechanical drawbacks, because fuel spray impinges the wall and causes unacceptable levels of oil dilution [49]. Nevertheless, these tests did prove the high potential of a combustion strategy that would combine massive EGR and partially premixed combustion.

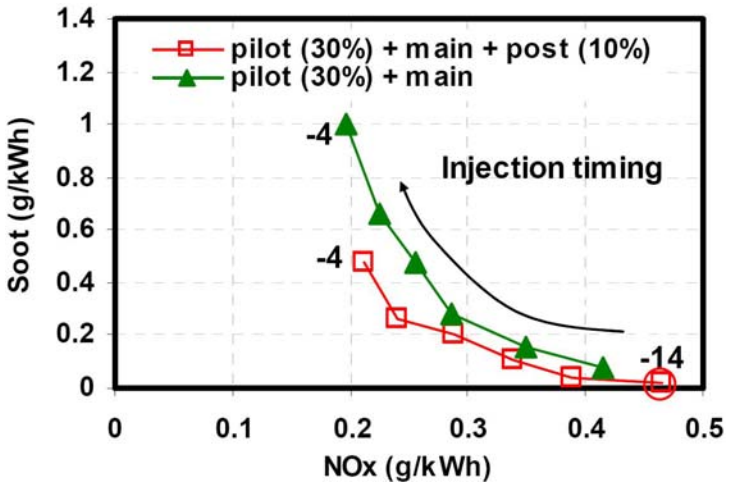

Figure 2.5 – Influence of post-injection on NOx -Soot trade-off [49]

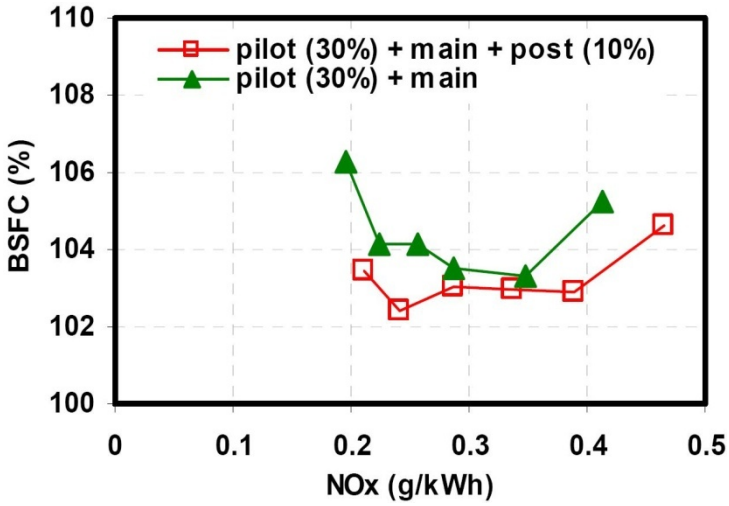

Figure 2.6 – Influence of post-injection on NOx vs. BSFC [49]

EGR is known to be effective to reduce NOx emissions, but usually increases particulate emissions. On the other hand, multiple injections are considered as an effective means to improve particulate emissions. Thus, it is of interest to explore the possibility of simultaneous reduction in particulate and NOx emissions with the combined use of EGR and multiple injections. Mikulic et al. [50] investigated the effects of pilot injection with EGR on engine emissions and fuel consumption and found that the lowest NOx emissions could only be reached using a combination of EGR and

pilot injection. They also found that pilot injection in combination with EGR provided no deterioration of fuel consumption and HC emissions. Uchida et al. [51] found that the combined use of pilot injection with EGR results in little advantages for the NOx-BSFC trade-off since smoke increased, especially under low load conditions. They argued that the smoke deterioration might be caused by the interference of the main injection sprays in a hot and higher equivalence ratio zone near the injector nozzle.

Ladommatos et al. [37] found that introducing EGR as an additional component of the inlet air in such a way as to keep the oxygen concentration constant could alleviate the detrimental effects of EGR on particulate emissions. Therefore, it is also of interest to explore the combined effects of EGR and supercharging. Uchida et al. [28] conducted an experimental study to examine the effects of EGR combined with supercharging on diesel combustion characteristics. They observed that by combining supercharging with EGR, the ignition delay was shortened with increased intake boost pressure. Furthermore, it was found that supercharging enhanced the air-fuel mixing and diffusion combustion so that smoke emissions were not greatly deteriorated, except at excessively retarded injection timings. They also observed that, as the intake boost pressure was increased, the limit of the EGR ratio due to misfiring could be extended widely.

The interaction of fuel injection and swirl/supercharging is another important aspect of study. Shundoh et al. [7] investigated the effects of swirl at 1000 rev/min and full load with 150 MPa injection pressure. They found that by increasing the swirl ratio, both NOx and soot emissions increased while the fuel economy worsened. Those results were fairly different from their previous results obtained with 50-90 MPa injection pressures except for the NOx emission trend. They concluded that the effect of swirl might be closely affected by injection pressure.

Traditional injector design is often suitable for injection timing close to TDC and can not satisfactory meet the requirement for early or late injection timings [52]. Various attempts have been made to mitigate problems encountered with these injection strategies. One attempt utilizes three injectors [53], to avoid spray-wall interaction. Another alternative uses narrow spray cone angle fuel injector nozzles (less than 100-degrees) to avoid spray-wall interaction at early injection timings [54].

A number of the direct injection strategies have employed early injection timings to extend the ignition delay to a long enough period for complete fuel vaporization to occur prior to combustion. For instance, one proposed strategy uses two injections; an early injection that introduces 50% of the total fuel prepares an ignitable mixture lit off by the second injection of the remaining fuel closer to top dead center (TDC) [55]. Similarly, others have demonstrated a split injection strategy where an early first pulse injected fuel 54° to 4° before TDC, with a late second pulse occurring 13° after TDC [56].

2.3.6. Combustion Chamber Geometry

Most DI diesel designs can be categorized as either an open chamber or a re-entrant chamber design. Most small-bore diesel engines use a small diameter, relatively deep, re-entrant type bowl. The fuel spray is typically aimed at the bowl lip. This design has been used for its high swirl and strong squish flows, which tend to promote sufficient mixing, especially at high engine speeds. Some researchers have found that when modern high-pressure injection systems are used along with sufficiently small bowl throat diameter chambers, liquid impingement occurs on the piston at certain operating conditions. They contend that the traditional small diameter bowl may be inappropriate when used with modern high-pressure injection systems.

The effect of combustion chamber shape on the engine performance is very complex due to its influence on the flow field and the air-spray interaction. The results in literature confirm that it is difficult to define an optimized combustion chamber, because of the influence of engine specification and injection system [57]. From results in literature, Heywood [31] deduced that for a fixed compression ratio, the swirl levels at TDC increases if the bowl diameter is reduced, leading to less smoke, higher NOx levels and HC emissions. The squish-swirl interaction, instead, is influenced by the offset of the bowl with respect to the cylinder axis [57]. Middlemiss [58] performed an extensive experimental study on the effect of chamber geometry in a small-bore high-speed diesel engine. Many different designs were tried. The designs included a baseline, open-type chamber with a small center crown and a host of re-entrant designs, where the throat diameter and angle of the re-entrant portion of the bowl were varied. One of the re-entrant designs included a center crown. Four bowl lip designs were tried along with a variety of compression ratios in a parametric study. In general, it was found that re-entrant chambers resulted in higher mixing rates thereby allowing retarded injection timings and higher speed operation. This resulted in low soot and NOx emissions with no degradation in fuel economy. Saito et al. [59] performed an experimental study of bowl geometry in a small-bore diesel engine. Two open-type chambers were tried, one shallow and one deep. A re-entrant chamber was also tried, with equal maximum bowl diameter to the open chambers. The throat diameter of the re-entrant bowls was varied. It was found that a 40 mm throat diameter was optimal. They found that the re-entrant chamber produced shorter ignition delays, lower fuel consumption, and lower soot and NOx emissions when used with retarded injection timings. Sakata et al. [60] performed a combined experimental and computational study of piston bowl design in a small-bore diesel engine. They found that a specially designed bump (so-called “reflex” edge) on

the re-entrant portion of the bowl increased fuel spray air entrainment and mixing. This resulted in increased performance and reduced hydrocarbon (HC) emissions.

An experimental study of the effects of the spray orientation, injector hole size and number, compression ratio, and combustion chamber geometry was carried out by Corcione et al. [61]. They used a small-bore aircooled DI diesel. Two bowl shapes were tried, a parallel sided open chamber (so-called toroidal) and a re-entrant chamber. In general, it was found that the toroidal chamber performed better at low engine speeds and the re-entrant bowl was better at high speeds. Zhang et al. [62] performed an experimental study on the effect of chamber geometries on combustion behavior. Three geometries were investigated, a right-circular-cylinder dish type open bowl, a flat bottom re-entrant bowl, and the re-entrant bowl with a pronounced center crown. They concluded that the re-entrant bowl with the center crown resulted in the fastest combustion. They also found it was important to achieve a good fuel/flame distribution inside and outside the bowl to reduce soot emissions.

Zolver et al. [63] performed a computational study on piston bowl shapes in a small-bore diesel engine. The bowl design and volume balance (between the bowl and squish regions) were found to play an important role in defining the flow near TDC. Raising the swirl level and turbulence or destroying swirl to create turbulence was found to be productive approaches. NOx emissions were reduced through chamber-geometry-generated turbulence. De Risi et al. [57] performed a combined experimental and computational study on the effects of chamber geometry and engine speed on emissions in a small-bore diesel. The basic chamber shape investigated was a Mexican hat-type bowl. Five different variations of this shape were tried, one of which was an open-type bowl. They also tried a bowl with a reflex edge, similar to that of Sakata et al. [60]. They found the effect of bowl geometry more prevalent at low engine speeds. At

higher engine speeds a smoother bowl lip resulted in lower soot and higher NOx. The highly re-entrant bowl was found to have performance more independent of engine speed, however the spray angle and injection timing became more critical. The best results were found when aiming the fuel spray at the bottom of the bowl. Bianchi et al. [64] performed a computational study on the use of a larger diameter, less re-entrant bowl configuration along with high pressure common rail fuel injection and low swirl in a small-bore diesel engine. The concept was to use a bowl design better suited to the modern injection system, thereby eliminating spray-wall impingement and the need for high swirl. This would increase the volumetric efficiency and possibly allow for simultaneous reductions in exhaust emissions and fuel consumption. The spray angle and number of injector holes was also changed. It was found that the high-pressure common rail injection system provided sufficient mixing without a highly re-entrant bowl and high swirl. They were able to reduce soot and NOx emissions, while paying only a small indicated mean effective pressure (IMEP) penalty.

2.4. CFD Modeling of Flow and Combustion in IC Engines

The combustion processes of IC engines are characterized by complex heat transfer, gas dynamics, multi-phase flows, and turbulence-chemistry interactions. IC engine combustion spans multiple regimes that include premixed flame propagation, mixing-controlled burning, and chemical-kinetics-controlled processes, which may occur simultaneously. The task of modeling IC engines is to completely or partly describe these physical and chemical processes using mathematical models with stable and accurate numerical schemes so that the output of the modeling can reveal desirable information about engine cycles [65].

The infancy of Computational Fluid Dynamics (CFD) in-cylinder engine modeling started from the 1970s. However, until the 1980s, engine CFD modeling was not generally applied in engine development due to two facts: first, the computer capacity was still a limiting factor; second, general engine CFD code or software was not available. Instead, engine modeling with phenomenological models was the main stream in this period [18].

In 1985, a group at the Los Alamos National Laboratory developed an open source code called KIVA [66] that integrated different components of engine CFD modeling, including moving meshes, compressible flows, spray and droplet evaporation, and fuel combustion chemistry. KIVA provides an open source CFD modeling tool for engine reactive flow simulations, which has significantly stimulated the development of engine physical and chemical models. Reitz and Rutland [67] reviewed various advanced diesel engine submodels within the framework of KIVA 3 and concluded that the CFD modeling tool was able to match experimental engine pressure traces and heat release well over investigated conditions and good quantitative agreements in NOx and soot emissions were also attainable. With the rapid increase of computational power of personal computers and demands for better simulating advanced engine combustion techniques, detailed fuel chemistry solvers have also become a standard part of many engine CFD tools since 2001 [65, 68].

In recent years CFD has been successfully established for the calculation of fluid flow, mixture formation and combustion in internal combustion engines as a complementary tool to in-cylinder pressure analysis and optical mixture formation and combustion diagnostics. The accuracy of the calculation results and hence the potential contribution of the CFD simulation to major design decisions within the engine development process strongly depends on the achievable project turnaround times and

the reliability of the models adopted for the treatment of the individual in-cylinder physical and chemical processes, such as cavitating injector flow, liquid fuel spray propagation, evaporation and mixing with the in-cylinder charge, auto-ignition, turbulent combustion and pollutants formation. As the result of intense world-wide research and development efforts over the last decades, a variety of models exhibiting different levels of complexity and sophistication is available today [65, 69].

OpenFOAM is an open source CFD software package produced by a commercial company, OpenCFD Ltd [70]. It consists of a flexible set of C ++ modules for different engineering applications including IC engine simulation. A 3D unstructured mesh of polyhedrals is used in Open FOAM. Commercial software that is capable of IC engine simulation include Star-CD [71], FLUENT [72], FIRE [73], VECTIS [74], CONVERGETM [75, 76], and FORTÉTM [77-79]. Star-CD and VECTIS are multi-purpose CFD software codes with advanced automatic meshing techniques. FLUENT are FIRE are also a multi-purpose CFD software with dynamic unstructured mesh technique. CONVERGETM uses an orthogonal structured mesh with adaptive mesh refinement and mesh embedding, which simplifies mesh generation. FORTÉTM is mainly based on the KIVA3v Release 2 code and has implemented the most advanced chemistry solvers and pioneers detailed chemistry applications in IC engine simulation.

The workflow description including the CFD solver and modeling details as well as all calculation results used in this study are based on the CFD AVL FIRE code. An overview of the theoretical background of the different models and modeling approaches used in this study is presented in Chapter 4.

The CFD simulation of internal combustion engine processes can be divided into three major steps, i.e. the generation of the computational meshes required to cover the fluid domain over the crank-angle interval of interest, the specification of the initial and boundary conditions, of the flow solver settings and of the physical and chemical models adopted to simulate the governing in-cylinder processes and, finally, the post-processing and interpretation of the simulation results [65].

In order to meet the demands concerning accuracy and hence reliability of the numerical results, the quality of the computational grids has to fulfill certain requirements. Besides a reasonable overall spatial resolution for representation of the in-cylinder flow domain, including proper resolution of the near wall layer, an accurate modeling of valve and piston movement is required for modeling the engine configuration in the CFD simulation. Due to the often symmetric arrangement of IC-engine injector/piston bowl configurations, as it is typically the case for modern diesel engines, the analysis and optimization of the spray injection and combustion processes is usually done by simulating an engine segment model only. The flow domain under investigation is then limited to the combustion chamber part around one single fuel spray applying cyclically symmetric boundary conditions for the crank-angle interval from inlet valve closure to exhaust valve opening. In this case the computational grid generation can be based on parameterized 2D curves, describing the combustion chamber and optionally the injector geometry. Based on this input the generation of the grids required to cover the simulation period between intake valve closing and exhaust valve opening is performed automatically within AVL FIRE Engine Simulation Environment Diesel (ESE Diesel). The AVL FIRE ESE Diesel user interface moreover offers the full functionality to set up and run the entire diesel engine spray injection and

combustion calculation and to perform all relevant application specific post-processing activities [65, 69].

Computational optimization of IC engines has become more accepted in assisting practical engine designs in recent years. The task of computational optimization of IC engines is to identify optimal combinations of design variables that can achieve minimum or maximum objective functions of interest [65].

In practice, engine optimization over all operating conditions is of more interest, but it is also more challenging due to two facts. First, the optimal sets of design variables achieved from an optimization study of a specific operating condition are usually not applicable to other conditions. Second, many engine design variables are not adjustable under different operating conditions, such as the piston geometry. To tackle this difficulty, Ge et al. [80] proposed a methodology for engine development using multi-dimensional CFD and computer optimization. A multi-objective genetic algorithm NSGA II and the KIVA3v2 code were used to optimize a light-duty diesel engine. Design parameters of the diesel engine were divided into two categories: hardware design (piston geometry, number of nozzle orifices, injection angle) and controllable design (SOI, swirl ratio, boost pressure, and injection pressure). Hardware design parameters were optimized first under the full (high)-load condition, as suggested by Shi and Reitz [65, 81]. Then, the optimal hardware design was fixed for subsequent optimizations of the controllable parameters under different operating conditions. They illustrated that with fixed optimal hardware design and optimal sets of controllable parameters for each case, optimal designs which simultaneously reduce fuel consumption and pollutant emissions were obtained in all cases except for a very low load case. In addition, strong correlations among the controllable design parameters

were not observed, which implies that these controllable parameters can be optimized separately.

Many studies have proven that engine CFD modeling tools with simplified ignition and combustion models, such as the Shell/CTC (Characteristic Time Combustion) model [82], can be reliable simulators for diesel engine optimization within conventional operating regimes where fuel/air mixing and diffusion flames dominate the combustion and pollutant formation processes [83, 84]. The individual simulation using such approaches only requires a few hours on the latest personal computers, so the whole optimization process can be completed within a week or two with multiobjective evolutionary methods, which is highly attractive for industrial optimization designs. But the advanced combustion techniques in modern diesel engines, such as HCCI, PCCI, and Modulated Kinetics (MK), are primarily controlled by fuel chemistry. In this case, accurate engine CFD simulations require a detailed description of the chemical kinetics of the fuels. It is not uncommon to find one to two orders of magnitude increase in the required computer time when solving detailed reaction mechanisms in engine CFD simulations compared to using simplified combustion models. Therefore, engine optimization using CFD simulation with detailed chemistry is generally not practically feasible, given the excessively long optimization cycle.

Significant efforts have been made recently to accelerate engine CFD simulations with detailed chemistry, which can be categorized into four major approaches. First, the development of mesh-independent spray models [85-87] enables engine CFD simulations using coarser meshes without losing accuracy compared to those of fine meshes [88]. Second, multi-zone or multi-grid methods [77, 89, 90] divide computational domains into subdomains by grouping thermodynamically-similar cells,

which largely reduces the calling frequency to the chemistry solver in engine CFD simulations. Third, efficient parallelization schemes [77] take advantage of the multi-core architecture of latest central processing units. Finally, reaction mechanism reduction techniques [91-93] and the on-the-fly model reduction schemes [94, 95] greatly decrease the reaction mechanismsize needed to describe the chemical kinetics of fuel oxidation and combustion.

Chapter 3

Relevant Combustion Theory and Definition of Homogeneity Factor

3.1. Background

In diesel engines the liquid fuel is injected at high pressure directly into the combustion chamber when the piston is near compression TDC. The fuel injector nozzles atomize the fuel, which evaporates and mixes with the compressed air in the high-temperature and high-pressure environment. Once the vapour and air mixture forms and the local temperature reaches or exceeds the auto-ignition temperature, this region will ignite undergoing premixed combustion. This initial energy release is followed by a period of mixing controlled combustion which will consume all fuel. Although the diesel engine improves fuel economy compared to SI engines, the reduction of its NOx and Particulate Matter (PM) emissions is still a challenging work [96].

In the first part of this chapter the relevant theory behind the combustion process in diesel engines is discussed and then a new parameter named “Homogeneity Factor (HF)”is introduced and proposed as a new measure to investigate the air-fuel mixing and combustion process.

3.2. Diesel Engine Combustion

3.2.1. Mixture Formation

The injection nozzle represents the link between the injection system and the combustion chamber. The fuel leaves the nozzle at high speed through small holes with diameters in the order around 0.12 mm for passenger car engines up to about 1.5 mm in the case of very large two-stroke diesel engines. Figure 3.1 shows a qualitative sketch of the fuel spray exiting the injection nozzle [3].

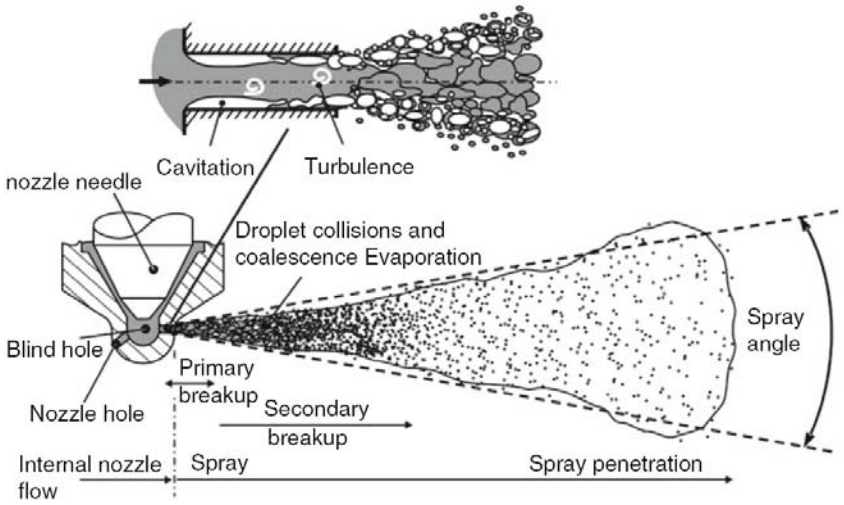

Figure 3.1 – Schematic representation of nozzle flow and spray propagation [97]

The spray generated during injection can be roughly subdivided into two regions, one with a dense spray near the nozzle exit and a thin spray region further down the flow. The first decomposition of the cohesive fuel spray into ligaments and droplets is called primary spray break-up. In modern high-pressure injection systems,

cavitation and turbulence are the most important mechanisms of primary spray break-up [98]. In the injection nozzle, the liquid fuel is accelerated into the nozzle holes in the transition from the nozzle blind-hole. The change of flow direction on the edge of the nozzle hole leads to the formation of a "vena contracta", which further lowers the static pressure in the fluid [99]. This reduction is strongly dependent on the geometry of the nozzle and especially on the radius of curvature of the inlet edge of the nozzle hole. If the pressure at the vena contracta falls below the vapour pressure of the fluid, hydrodynamic cavitation is initiated and vapour bubbles are created. Depending on the flow parameters, the cavitation can either be stabilized to reach the nozzle hole outlet or the flow can fully or partly reattach [100]. Cavitation reduces both the effective flow area of the nozzle as well as friction. In case of small needle lifts, cavitation structures can also arise in needle seat areas which either break up in the blind hole and thus increase turbulence or enter the nozzle holes, thus promoting further cavitation. When they leave the nozzle holes, the cavitation bubbles collapse very quickly due to the high pressures in the combustion chamber, which leads to an increase of turbulence and faster primary spray break-up [3].

Break-up of already existing droplets into smaller droplets due to aerodynamic forces caused by the relative speed between droplet and the environment is called secondary spray breakup. In addition, droplets can collide with each other and coalesce. The spray momentum leads to air entrainment of the surrounding combustion chamber air into the spray. In the combustion chamber, the droplets are heated up as a result of convective heat transfer and temperature radiation of the hot chamber walls, and the fuel finally begins to evaporate. Besides the physical properties and the combustion chamber conditions (pressure, temperature), the rate of fuel evaporation is determined by the size

of the droplet surface formed and thus on primary and secondary break-up as well as on the amount of air entrained into the spray [3].

In diesel engines, mixture formation cannot be considered independently of combustion. It is indeed the distinctive feature of diesel engine combustion that spray propagation, mixture formation, and combustion progress are in partial simultaneity. Only a small amount of the injected fuel mixes nearly homogeneously with the air in the combustion chamber during ignition delay. After ignition, this amount combusts almost instantly. Afterwards, mixture formation and combustion proceed simultaneously, and combustion is mainly controlled by the mixture formation processes [3].

3.2.2. Auto-Ignition and Combustion Sequence

The period of time between injection start and combustion start is called the ignition delay. The physical and chemical processes occurring during this time are very complex. The essential physical processes are the atomization of the fuel, vaporization, and mixing of fuel vapour with air, forming an ignitable mixture. The chemical processes that lead to auto-ignition of the hydrocarbons contained in the fuel under typical diesel conditions are characterized by a highly complex, degenerated chain branching mechanism [3, 69, 101].

The ignition delay can be controlled by means of temperature and pressure at the start of injection, which in turn depend on the inlet temperature and pressure, the compression ratio, injection start and the wall temperatures. In addition, the ignitability of the fuel (cetane number) and further parameters such as injection pressure, the geometry of the nozzle holes and the in-cylinder flow have a major effect on the ignition delay duration and the ignition location [3].

Figure 3.2 provides a schematic representation of the injection and combustion sequence of a diesel engine with direct injection. As it can be see, the sequence of diesel engine combustion can be subdivided into three phases including pre-mixed combustion, main combustion (mixing-controlled) and post-combustion (reaction-kinetically controlled).

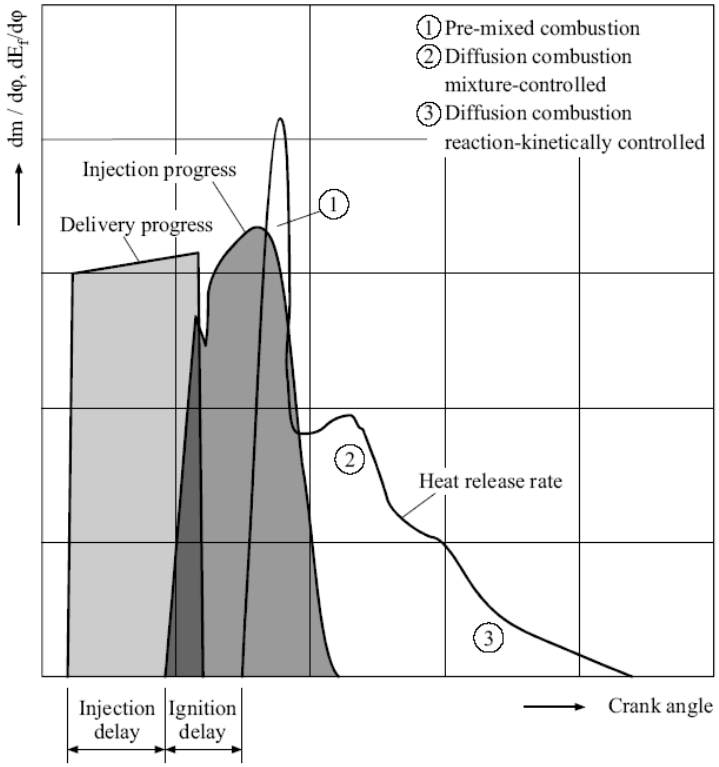

Figure 3.2 – Injection and combustion sequence in a diesel engine [3]

3.2.2.1. Initial Premixed Combustion

The first phase follows immediately after ignition. The fuel injected during ignition delay mixes with the air in the combustion chamber and forms a nearly homogeneous and reactive mixture. After the ignition delay, which is physically and chemically controlled, this mixture burns very quickly. Since areas with premixed combustion arise in the main combustion phase as well, this phase is called initial premixed combustion. The rate of heat release is controlled in this combustion phase by

the speed of the chemical reactions and by the amount of fuel/air mixture formed during ignition delay. The combustion noise of typical diesel engines is caused by the high speed of pressure rise at the start of combustion. This speed of pressure rise can be influenced by changing the timing of injection. The combustion noise can be considerably reduced by a pre-injection. In this case, at first only a small fuel amount of about 1~2% is injected which leads after the ignition delay to only a small amount of heat release and to a small pressure increase. The increased temperatures lead however to a significant reduction of the ignition delay of the main injection, which leads to a reduction of the amount of premixed combustion with a positive effect on noise [3].

3.2.2.2. Main Combustion

In the second phase, heat release is controlled by the turbulent mixing processes between the fuel and air and is therefore also called mixture-controlled combustion. In this phase, injection, spray break-up, droplet evaporation, mixing with air, combustion, and pollutant formation all take place simultaneously. Figure 3.3 shows a cross-section through a reacting diesel injection spray following the conceptual model of Dec [102] and Flynn et al. [103].

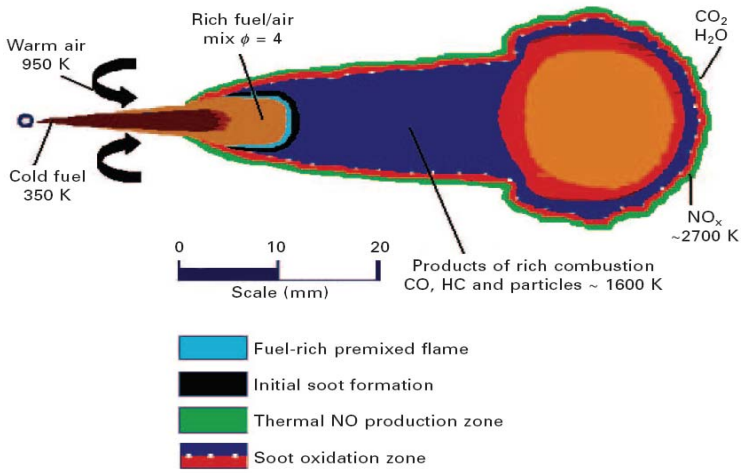

Figure 3.3 – Conceptional model of diesel combustion, Dec [102] and Flynn et al. [103]

The model describes the quasi-steady phase during main combustion and is, strictly speaking, only valid in quiescent conditions. The fluid fuel spray penetrates into the combustion chamber, mixes with air and evaporates. The air ratio in the spray increases both with increasing distance to the injection nozzle as well as with the distance to the spray axis. Downstream of the liquid penetration length, a rich mixture zone is formed which leads to partial oxidation of the fuel and temperatures up to 1,600 K. According to the work of Flynn et al. [103], the air ratio in this zone is in the range between 0.25-0.5, and about 15% of the total heat is released in this zone [3].

A diffusion flame is formed around the injection spray on an iso-surface with a stoichiometric air fuel ratio. The partially oxidized products of the rich premixed combustion and the particles formed move further downstream and are transported into the diffusion flame, where they are completely oxidized into carbon dioxide and water. Due to the high temperatures, nitrogen oxides are formed on the lean side of the diffusion flame. Near the injection nozzle, vaporization processes and chemical reactions in the spray determine the distance from the injection nozzle at which the diffusion flame establishes itself. The axial distance between the injection nozzle and the diffusion flame is called the lift-off length and is an important property of a diesel flame with regard to soot formation [3, 69, 104].

3.2.2.3. Post Combustion

After the injection process, no additional momentum is added to the spray by the injection and the flame jet structure evolves into a pocket of rich premixed products surrounded by a diffusion flame. The exact properties of this zone depend on the injection system. If the nozzle needle closes very quickly, then the last fuel parcels still have high speed, so that they have a similar combustion sequence as in main

combustion. On the other hand, a slow closure of the needle leads to low speeds of the last fuel parcels with low entrainment of oxygen and consequently increased formation of soot. With the expansion of the piston in the direction of the bottom dead center, the temperatures in the combustion chamber are lowered. The reaction rates go down with the temperatures, so that combustion is chemically controlled again. This phase is of extreme importance for the oxidation of the previously formed soot, of which over 90% is decomposed again. The temperatures during this combustion phase should be high, since soot oxidation is very slow below 1,300 K [3, 69, 105].

3.2.3. Pollutant Formation

In the complete combustion of a so-called C_xH_y fuel, consisting only of C and H atoms, the exhaust gas contains the components oxygen (O_2), nitrogen (N_2), carbon dioxide (CO_2), and steam (H_2O) [106].

In real combustion, however carbon monoxide (CO), unburned hydrocarbons (HC), hydrogen (H_2), nitrogen oxide (NOx), and particulates also appear in addition to the above components. As opposed to these substances, which are detrimental to human health, CO_2, which is partially responsible for the greenhouse effect, is not viewed as a pollutant, since it does not pose a direct health hazard and appears as the final product of every complete oxidation of a hydrocarbon. A reduction of CO_2 in the exhaust gas is thus only to be achieved through a reduction in fuel consumption or through an altered fuel having a smaller amount of carbon with reference to its heating value [106].

In Figure 3.4, the typical composition of the exhaust gasses (without a catalytic converter) of diesel engines is shown [106].

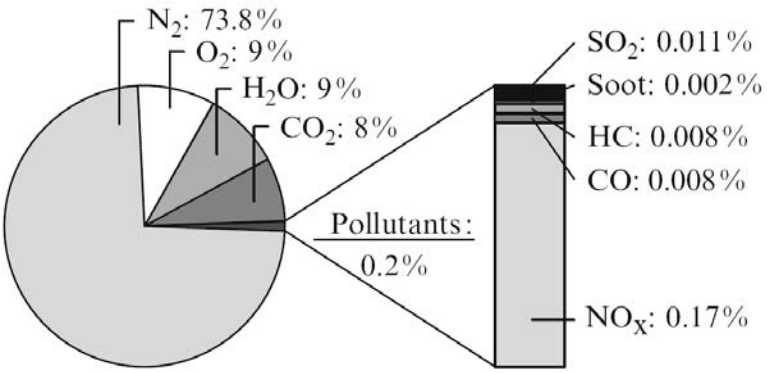

Figure 3.4 – Typical engine-out exhaust gas composition of diesel engines (without catalyst) in percent by volume [106]

A distinction is made between the concepts of complete and incomplete combustion as well as between perfect and imperfect combustion. For relative air-fuel ratios $\lambda \geq 1$, the ratio between the mass of air and the mass of fuel in the air-fuel mixture, there is theoretically enough oxygen for the fuel to burn completely. In actuality however, combustion progresses under such air ratios at most until chemical equilibrium, i.e. always incompletely, even under ideal conditions. As a result, there is always a certain amount of CO and unburned hydrocarbons after combustion, even if the supply of oxygen is sufficient. In the case of air-fuel ratios $\lambda < 1.0$, the fuel cannot burn completely because of the lack of O_2. Under ideal conditions, combustion proceeds at best until chemical equilibrium. At all air ratios, combustion can also be incomplete due to imperfect air fuel mixing or because certain reactions proceed so slowly that chemical equilibrium is not reached [106].

3.3. Homogeneity Factor

In this section a modified parameter named “Homogeneity Factor of in-cylinder charge” (HF) has been introduced as a new measure for supporting the understanding of the air-fuel mixing and combustion process in diesel engines.

The mixing quality in diesel engines is very critical for controlling the ignition and pre-mixed combustion and mixing controlled combustion, consequently for energy conversion efficiency and emissions (HC, CO, NOx and Soot). So far, for diesel combustion development and research, there is no a measure for quantitatively describing fuel-air mixing quality. Although qualitative description/result of mixing quality can be used for assessing the mixing quality and for studying its influence on ignition, combustion and emission, a quantitative description is desired for having a more accurate control to the mixing and combustion, in particular for HCCI/PCCI combustion for which a measure of charge mixing quality will be very helpful as a control medium for used in the controller to real-time control the ignition and combustion.

Nandha and Abraham [107] was proposed a parameter named Degree of Heterogeneity (DOH), defined as following, to measure the degree of heterogeneity in the mixture:

$$\mathrm{DOH}\ (\theta) = \frac{\sqrt{\sum_{i=0}^{N_{cells}}[(\varphi_i-\varphi_O)^2\delta m_i]/M}}{\varphi_0} \tag{3.1}$$

$$\varphi_0 = \frac{\sum_{i=0}^{N_{cells}}\varphi_i\delta m_i}{M} \tag{3.2}$$

$$M = \sum_{i=0}^{N_{cells}}\delta m_i \tag{3.3}$$

Where, φ_i is the equivalence ratio and δm_i is the mass of the mixture in the computational cell i, N_{cells} is the total number of computational cells, φ_O is the overall average equivalence ratio of total mixture and M is the mass of total mixture. The equivalence ratio is defined as the ratio of the actual fuel/air ratio to the stoichiometric fuel/air ratio. Stoichiometric combustion occurs when all the oxygen is consumed in the reaction, and there is no molecular oxygen (O_2) in the products.

$$\varphi = \frac{m_{fuel}/m_{ox}}{(m_{fuel}/m_{ox})_{st}} \quad (3.4)$$

where, m is the mass. If the equivalence ratio is equal to one, the combustion is stoichiometric. If it is < 1, the combustion is lean with excess air, and if it is >1, the combustion is rich with incomplete combustion.

Nandha and Abraham's original definition for Degree of Heterogeneity (DOH) [107] actually represents the standard deviation of the equivalence ratio normalized by the overall equivalence ratio.

In another study performed by Peng et al. [108] this parameter was modified using a new definition, Homogeneity Factor (HF), for finding the effects of the mixture homogeneity, as following:

$$HF(\theta) = 1/DOH(\theta) \quad (3.5)$$

They showed this parameter can be used as a measure for analyzing the fuel-air mixing and controlling the ignition timing and adjusting combustion phasing at different operating points. As shown in Figure 3.5, it is the effects of different main injection timing on the Homogeneity Factor with different fuel proportion in the main injection pulse. When more fuel was injected in the first injection pulse, it leaves more time for the mixing of most fuel, then the Homogeneity Factor at TDC can be increased [108].

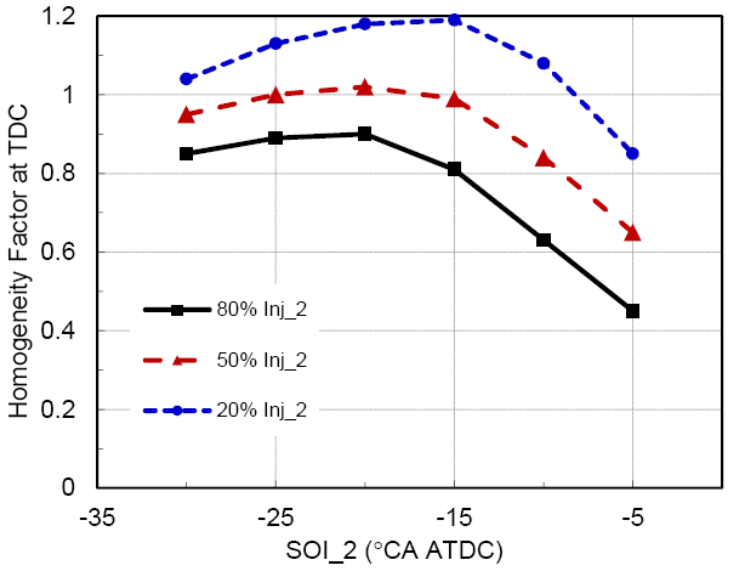

Figure 3.5 – Effects of the main injection timing on Homogeneity Factor at TDC, with different fuel proportions [108]

In the new definition, the HeterF is the standard deviation of fuel amount normalized by the overall fuel amount. This will be a more reasonable measure to the non-uniformity in the mixture.

In current study, a modified definition has been proposed for investigating the Homogeneity Factor (HF). As the increased fuel amount in a cell actually comes from the decrease of fuel amount in other cells, the half of the standard deviation is used in the new definition to reflect the non-uniformity more accurately. Then a homogeneity factor (HF) is derived basing on HeterF for having a more appropriate demonstration to the charge mixing quality. In this method, compared to the average equivalence ratio (φ_0), the fuel difference in Cell i is defined as following:

$$\frac{\varphi_i}{AFR_{st}+\varphi_i}\delta m_i - \frac{\varphi_O}{AFR_{st}+\varphi_O}\delta m_i = \frac{AFR_{st}(\varphi_i-\varphi_O)}{(AFR_{st}+\varphi_i)(AFR_{st}+\varphi_O)}\delta m_i \quad (3.6)$$

Where AFR_{st} is the stoichiometric air-fuel ratio. The total fuel amount will be:

$$\frac{\varphi_O}{AFR_{st}+\varphi_O}M \quad (3.7)$$

Therefore, Heterogeneity Factor (HeterF) is:

$$\mathrm{HeterF}(\theta) = \frac{\sum_{i=0}^{N_{cells}} \frac{\sqrt{(\varphi_i - \varphi_O)^2}}{AFR_{st} + \varphi_i} \delta m_i}{2\varphi_O M} \tag{3.8}$$

The Homogeneity Factor (HF) is defined as follows:

$$\mathrm{HF}(\theta) = \big(1 - \mathrm{HeterF}(\theta)\big)\% \tag{3.9}$$

3.3.1. An Evaluation of Homogeneity Factor by CFD Results

Based on the above definition of Homogeneity Factor (HF) definition, a CFD study are presented here to show the general trend of homogeneity factor at various operating points and to evaluate its effects on air-fuel mixing and combustion process. The CFD results are achieved at 1600 rev/min for a conventional injection case (single injection) and no EGR rate in a DI diesel engine. The same initial and boundary conditions are used for all the computations. To study the effect of injection timing, Start Of Injection (SOI) was swept from 30° to 10° CA BTDC. The main characteristics of the injection system are listed in Table 3.1. Note that in all figures 360˚ CA corresponds to TDC position.

Table 3.1 – Injector fuel system specifications

Injector type	Electronically controlled, common rail
Number of nozzle holes	6
Fuel mass	0.1622 g/cycle
Nozzle hole diameter	0.26 mm
Start of injection	30, 25, 20, 15, 10˚ ATDC
Injection duration	21.5˚ CA

Figures 3.6, 3.7 and 3.8 illustrate the amount of homogeneity factor as a function of crank angle compared to in-cylinder pressure and injection rate at three different injection timings (30, 25 and 20 CA BTDC), respectively.

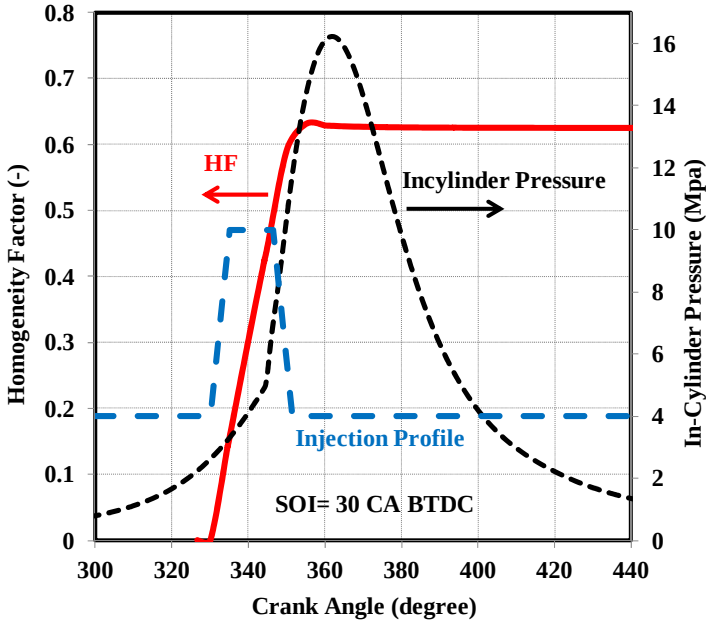

Figure 3.6 – Homogeneity factor, in-cylinder pressure and injection rate as a function of crank angle, SOI=30 CA BTDC

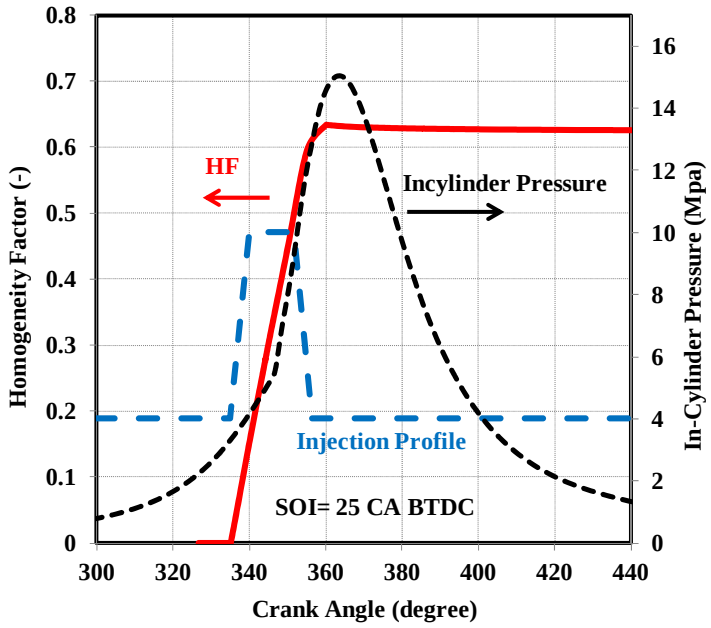

Figure 3.7 – Homogeneity factor, in-cylinder pressure and injection rate as a function of crank angle, SOI=25 CA BTDC

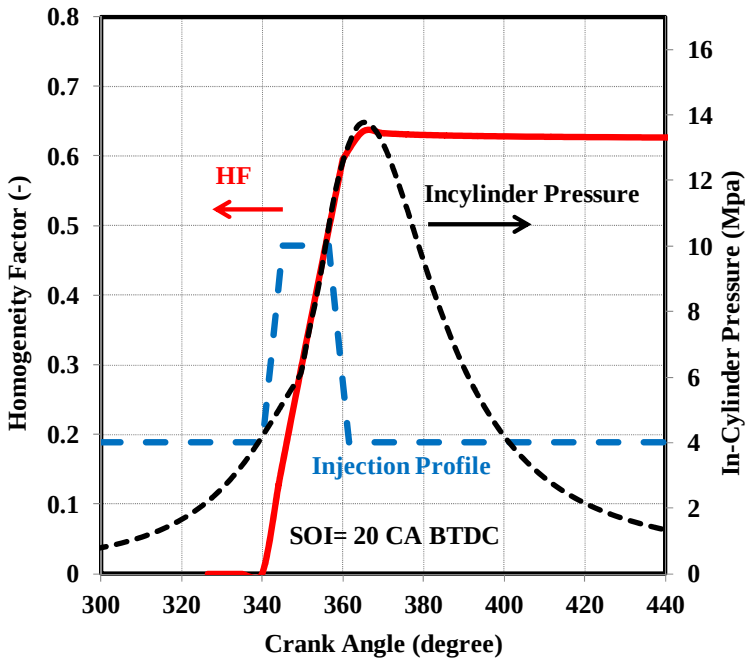

Figure 3.8 – Homogeneity factor, in-cylinder pressure and injection rate as a function of crank angle, SOI=20 CA BTDC

As can be seen in Figures 3.6-3.8, when SOI advances, the in-cylinder pressure increases and the maximum amount of Homogeneity Factor (HF) is achieved at an earlier time. As a result, for earlier SOI timing, more mixing time is available to achieve a large portion of premixed mixture which produces the higher amount of temperature and thus higher rate of in-cylinder pressure. The more advanced SOI timings produce a more homogeneous, locally fuel-lean in-cylinder mixture at the time of ignition since a sufficient mixing time is available to achieve a large portion of premixed mixture.

Figures 3.9 shows the amount of homogeneity factor as a function of crank angle at five different injection timings (30, 25, 20, 15 and 10 CA BTDC).

As shown in Figure 3.9, the maximum amount of homogeneity factor for two cases (SOI= 15 and 10 CA BTDC) are obtained after top dead center. It can be concluded that the best operating point of the combustion and the air-fuel mixing can be achieved by adjusting the homogeneity factor and start of injection timing. As SOI is

retarded to 10 CA BTDC, the ignition delay becomes shorter due to the higher ambient temperature, results in increased amount of diffusion burn and lower peak in-cylinder pressure which was caused to sweep the maximum amount of homogeny factor at a later point.

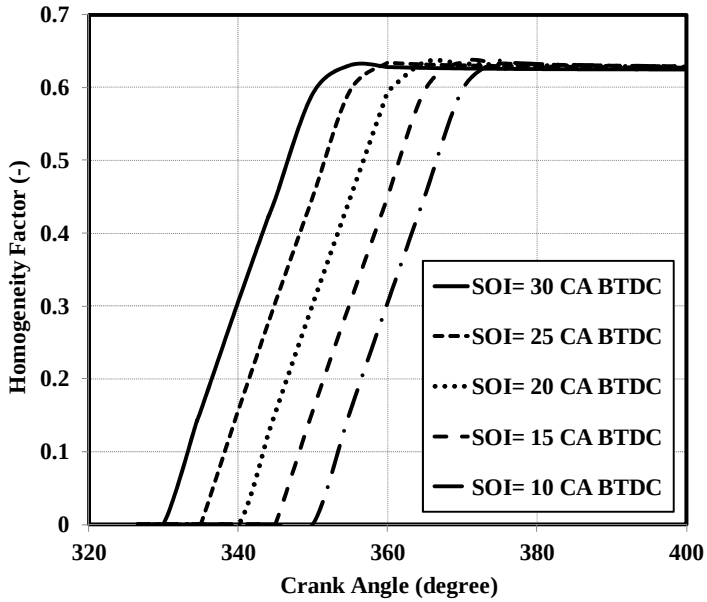

Figure 3.9 – Homogeneity factor as a function of crank angle at different injection timings

By the new definition of Homogeneity Factor, it is expected that this parameter can be used as a useful measure to analyze the air-fuel mixing and combustion process in diesel engines to adjust and control the injection timing and combustion phasing more precisely. For this purpose, the effects of different engine parameters on the Homogeneity Factor and the correlation of the Homogeneity Factor with combustion characteristics and emissions for further exploring the effects of different injection strategies and included spray angles is discussed in in chapter 5.

Chapter 4

Model Description

4.1. Introduction

This chapter provides an overview of the CFD workflow adopted for simulation of the in-cylinder physical and chemical processes governing engine performance and emission characteristics which have been used in this research. The workflow description including the CFD solver and modeling details in the present chapter are based on the commercial CFD code AVL FIRE [73, 109].

4.2. Turbulent Flow and Heat Transfer

Most IC-engine related fluid flow problems are turbulent flows. Hence, as a basis for precisely simulating the real flows, it is of utmost importance to be able to accurately model the phenomenon of turbulence. This is in particular necessary, since turbulence not only determines the details of the fluid flow itself, but also strongly influences the physical and chemical processes taking place during mixture formation and combustion. For example, in IC-engines the turbulent kinetic energy is a major

influencing factor on the propagation and evaporation of liquid fuel spray droplets and the subsequent combustion of the air/fuel mixture [109]. In addition to the well known, standard turbulence models, such as e.g. $k-\varepsilon$, Spalart-Allmaras, Reynolds Stress, etc., AVL FIRE1 offers the $k-\xi-f$ turbulence model, recently developed and validated for IC-engine related flow, heat transfer and combustion processes [110].

For IC-engine flows the $k-\xi-f$ model leads to more accurate results than the much simpler two-equation eddy viscosity models of the $k-\varepsilon$ type by simultaneously exhibiting a high degree of numerical robustness. In combination with a hybrid wall treatment, as proposed by Popovac and Hanjalic [111], combining the integration up to the wall with standard wall functions, the $k-\varepsilon$turbulence model is universally applicable to computational meshes and flow situations. In this study, the $k-\xi-f$ model is used as default model for turbulence and turbulent wall heat transfer modeling. One of the main advantage of this model is its robustness to be used for computations involving grids with moving boundaries and highly compressed flows as it is the case in IC-engines [109].

4.3. Fuel Spray and Wallfilm

The spray model most commonly adopted in AVL FIRE for IC-engine spray and mixture formation simulations is based on the Lagrangian Discrete Droplet Method (DDM). While the continuous gaseous phase is described by the standard Eulerian conservation equations, the transport of the dispersed phase is calculated by tracking the trajectories of representative droplet parcels [109]. A parcel consists of a number of droplets and it is assumed that all the droplets within one parcel have the same physical properties and behave equally when they move, break up, hit a wall or evaporate.

Droplet parcels are introduced in the flow domain with initial conditions of position, size, velocity and temperature [73, 109].

The standard WAVE model, described in [73, 112-114] was used for the atomization modeling. In this model the growth of an initial perturbation on a liquid surface is linked to its wave length and to other physical and dynamic parameters of the injected fuel and the domain fluid.

If the standard Wave model with blob injection (=> initial droplets have the diameter of the nozzle orifice) is used for the simulation, it often happens that there is hardly any fuel vapor close to the nozzle. This is due to the fact that the droplets are still very large at the beginning and therefore hardly evaporate. One way of producing some vapor close to the nozzle is to inject a bimodal spectrum with about 90 % of the mass as blobs and 10 % as very small droplets that should come from the stripping process. The Wave child option more or less does the same automatically. If a certain user defined amount of mass has been shed from the parent drop, a new child droplet with a stable diameter is created. The differences between these two options are illustrated in Figure 4.1.

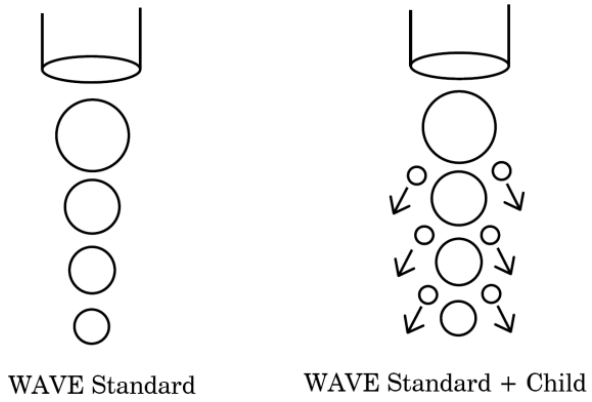

Figure 4.1 – Different Ways of WAVE Break-up [73]

Wall interaction of liquid droplets can play a major role for diesel and gasoline engines. Especially for small bore diesel engines the distance between the injector and

the bowl can be very small, so that large parts of the fuel are not yet evaporated or atomized when they hit the wall. This influences the combustion process and consequently the production of emissions, as an incomplete combustion in the vicinity of the wall will result in high HC emissions and soot particles.

The behaviour of a droplet at wall interaction depends on several parameters like droplet velocity, diameter, droplet properties, wall surface roughness and wall temperature. At very low inlet velocities the droplet sticks to the wall or to the wall film. When the inlet velocity increases a vapour or gas boundary layer is trapped underneath the droplet and causes the liquid to rebound. During the rebound parts of the kinetic energy are dissipated and the outgoing normal velocity is usually lower than the incoming normal velocity. A further increase of the velocity leads either to the spread or the splash regime. In the spread regime the complete liquid spreads along the wall with hardly any normal velocity. In the splash regime a part of the liquid remains near the surface and the rest of it is reflected and broken up into secondary droplets [73, 109].

4.4. Evaporation

The Dukowicz model [73, 115] was applied for treating the heat-up and evaporation of the droplets. This model assumes a uniform droplet temperature. In addition, the rate of droplet temperature change is determined by the heat balance, which states that the heat convection from the gas to the droplet either heats up the droplet or supplies heat for vaporization.

The heat and mass transfer processes are described by a model originally derived by Dukowicz [115]. Essentially it is based on the following assumptions:

- Spherical symmetry
- Quasi steady gas-film around the droplet
- Uniform droplet temperature along the drop diameter
- Uniform physical properties of the surrounding fluid
- Liquid – Vapor thermal equilibrium on the droplet surface

In the evaporation model of Dukowicz [115] it is considered that the droplet is evaporating in a non-condensable gas. Therefore, it uses a two-component system in the gas-phase, composed of the vapour and the non-condensable gas, even though each component may consist of a mixture of different species.

4.5. Combustion Modeling

The $\mathrm{ECFM-3Z}$ combustion model which is based on the Coherent Flame Model has been used for combustion modeling in this study. The $\mathrm{ECFM-3Z}$ (E stands for extended) model [73, 116-119] distinguishes between all three main regimes relevant in Diesel combustion, namely auto-ignition, premixed flame and non-premixed, i.e. diffusion combustion, as illustrated in Figure 4.2. The auto-ignition pre-reactions are calculated within the premixed charge of fuel and air, with the ignition delay governed by the local temperature, pressure, fuel/air equivalence ratio and the amount of residual gas. Local auto-ignition is followed by premixed combustion in the fuel/air/residual gas mixture formed during the time period between start of injection and auto-ignition onset within the $\mathrm{ECFM-3Z}$ modeled according to a flame propagation process. The third regime is the one of diffusion combustion where the reaction takes place in a thin zone which separates fuel and oxidizer. In the $\mathrm{ECFM-3Z}$, it is assumed that the chemical time in the reaction zone is much smaller than the time needed for the diffusion process. Therefore the rate of reaction during diffusion

combustion is determined entirely by the intermixing of fuel and oxidizer. This distinct separation of the different ignition/combustion regimes makes the ECFM – 3Z model specifically applicable to conventional as well as alternative diesel combustion modes. In the conventional case most part of the combustion can be assumed as diffusion type, in the case of recently introduced alternative concepts a large amount of fuel is consumed within premixed combustion [109].

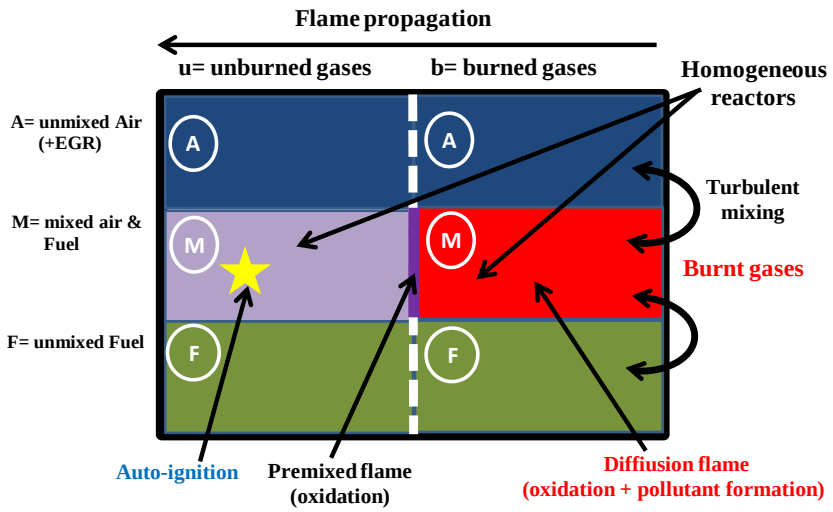

Figure 4.2 – Zones in ECFM-3Z Model

For prediction of the auto-ignition delay tabulated ignition data are used which are stored in look-up tables that are available in AVL FIRE for different fuels, generated based upon chemical kinetic calculations adopting complex reaction schemes. The tabulated values are stored as functions of the parameters pressure, temperature, fuel/air equivalence ratio and residual gas content. The range of these parameters has been chosen in a way to be able to cover the relevant in-cylinder pressure, temperature and charge-mixture composition conditions prior to combustion.

For the actual determination of the auto-ignition delay time in the CFD simulation, a transport equation for an auto-ignition indicator species is solved with the formation rate derived from the tabulated values. Once the local value of the indicator

species attains a certain threshold value, auto-ignition is initiated. Fuel consumption is then controlled by a characteristic chemical time-scale which ensures rapid combustion after auto-ignition [120].

The hydrocarbon oxidation process during high temperature combustion is separated into three major reaction steps. First the fuel is partly oxidized to CO and to CO_2, followed by CO oxidation, and finally a post-flame equilibrium chemistry approach is applied which results in the final species concentrations [109].

The above described combustion reactions cover the relevant range of mixture composition from lean to rich and the different levels of residual gas content. In addition to the amount of heat that is released within the flame the procedure provides all relevant information about CO and radical species which are important for the subsequent calculation of the pollutants [109].

4.6. Post Flame Chemistry

From the modeling point of view the main combustion process is separated into three steps. First the fuel is partly oxidized to CO and to CO_2, followed by CO oxidation and finally a post-flame equilibrium chemistry approach is applied which results in the final species concentrations including minor chemical species which are relevant e.g. for the pollutant formation. Assuming the mean fuel composition is C_nH_m and the local mean equivalence ratio $\overline{\emptyset}$, then the main fuel oxidation is defined in the $ECFM-3Z$ model with the following reactions in Eq.4.1.

$$\left\{\begin{array}{c} \alpha(1-r_{CO})\left[C_nH_m+\left(n+\frac{m}{4}\right)O_2 \rightarrow nCO_2+\frac{m}{2}H_2O\right] \\ \alpha r_{CO}\left[C_nH_m+\left(\frac{n}{2}+\frac{m}{4}\right)O_2 \rightarrow nCO_2+\frac{m}{2}H_2O\right] \\ (1-\alpha)\left[C_nH_m+\frac{n}{2}O_2 \rightarrow nCO_2+\frac{m}{2}H_2\right] \end{array}\right\} \quad (4.1)$$

Where r_{CO} is a constant value which presumes the amount of CO formed under lean conditions and α depends on the local equivalence ratio as follows, Eq.4.2.

$$\left\{\begin{array}{c} \overline{\emptyset} < \overline{\emptyset}_1 \rightarrow \alpha = 1 \\ \overline{\emptyset}_1 < \overline{\emptyset} < \overline{\emptyset}_2 \rightarrow \alpha = \frac{1}{2n+m}\left(\frac{4\times 0.98(n+m/4)}{\overline{\emptyset}} - 2n\right) \\ \overline{\emptyset}_2 < \overline{\emptyset} \rightarrow \alpha = 0 \end{array}\right\} \quad (4.2)$$

Where $\overline{\emptyset}_1 = 0.99$ and $\overline{\emptyset}_2 = 0.9\overline{\emptyset}_{crit}$, as the critical equivalence ratio above which there is not enough oxygen to complete the oxidation of fuel into CO,

$$\overline{\emptyset}_{crit} = \frac{2}{n}(n + \frac{m}{4}) \quad (4.3)$$

It can be seen from the equation above that for a lean mixture with $\alpha = 1$ the first two reactions are considered, which means that CO can also be formed under lean conditions. The third reaction describes the CO formation under rich conditions where there is not enough oxygen to burn all the fuel to CO_2. The oxidation of CO is described by the following reaction Eq.4.4.

$$CO + OH \rightarrow CO_2 + H \quad (4.4)$$

And the post-flame equilibrium chemistry is covered by the following set of reactions Eq.4.5.

$$\left\{\begin{array}{c} N_2 \leftrightarrow 2N \\ O_2 \leftrightarrow 2O \\ H_2 \leftrightarrow 2H \\ 2OH \leftrightarrow O_2 + H_2 \\ 2H_2O \leftrightarrow O_2 + 2H_2 \end{array}\right\} \quad (4.5)$$

The above described combustion reactions cover the relevant range of mixture composition from lean to rich and the different levels of residual gas content. In addition to the amount of heat that is released within the flame the procedure provides

information about CO and other species which are important for the subsequent calculation of the pollutants.

4.7. Emission Models

4.7.1. NO Formation Models

This section describes the extension of the FIRE code to simulate nitric oxide formation. In general, the nitric oxide formation stems from three principal sources [121-124]:

- Thermal NO which is formed due to the dissociation of the molecular air-nitrogen
- Prompt NO (Fenimore NO)
- NO formed from nitrogen containing components in the fuel

Fuel-NO formation can principally be neglected during the combustion process in internal combustion engines. Prompt NO formation can also principally be neglected since this process plays no dominant role in comparison to the thermal NO formation (< 5 [%] of NO is produced via this path). NO is formed in both the flame front and post-flame gases.

4.7.1.1. Principles of NO Formation

In engines, the cylinder pressure rises during the combustion process, so earlier burnt gases are compressed to a higher temperature level as they have immediately after their combustion. Hence, the thermal NO formation in the burnt gases always dominates in comparison to the NO formed in the flame front and represents the main source of the nitric oxide in engines whose reaction paths are effective at high temperatures (> 1800

[K]). The reaction mechanism can be expressed in terms of the so-called extended Zeldovich mechanism:

$$N_2 + O \overset{K_1}{\leftrightarrow} NO + O \tag{4.6}$$

$$N + O_2 \overset{K_2}{\leftrightarrow} NO + O \tag{4.7}$$

$$N + OH \overset{K_3}{\leftrightarrow} NO + H \tag{4.8}$$

The first reaction represents the rate limiting step in comparison to the other reactions. A very high activation energy (or temperature) is necessary to decompose the stable triple-bond of the molecular air-nitrogen. Accordingly, this reaction is significantly fast at high temperatures (hence thermal). In principal, it can be seen that the thermal nitric oxide formation is mainly determined by only five chemical species (O, H, OH, N and O_2) but not by the fuel being used. In order to obtain the required concentrations of the radicals, a complex reaction mechanism must be used in order to determine NO concentration. In the literature different possibilities are suggested to represent the rate law for NO [125].

Complex kinetic mechanisms are applicable only for simple flame computations (e.g. one-dimensional, laminar, etc.). For real turbulent flame calculations, their use is impractical due to the complexity of the interacting processes (turbulence, radiation, heat transfer, etc.) which must be considered to obtain realistic results. Therefore, simplified approaches must be used for complex applications, whereby essential information is not lost due to the reduction procedure [126, 127]. This reduction is based on the partial equilibrium assumption of the considered elementary reactions using the extended Zeldovich mechanism describing the thermal nitrous oxide formation.

4.7.1.2. Extended Zeldovich Model

The first two reactions were originally proposed by Zeldovich [124] and extended later by including the third reaction [73]. It was observed later that the nitrogen atoms released at reaction are oxidized to nitric oxide mainly by hydrogen radicals at near-stoichiometric conditions and in fuel-rich mixtures. The third reaction is usually negligible except in fuel rich flames.

The reaction mechanism is known as the extended Zeldovich mechanism that considers the effect of oxygen, nitrogen and hydrogen radicals on NO formation. It is very important to point out that all three chemical reactions that represent the Zeldovich mechanism exhibit strong temperature dependency.

The temporal change of NO concentration (or net rate of NO formation) via reactions is given by:

$$\frac{\partial c_{NO}}{dt} = k_{1f} c_O c_{N_2} + k_{2f} c_N c_{O_2} + k_{3f} c_N c_{OH} - k_{1b} c_{NO} c_N - k_{2b} c_{NO} c_O - k_{3b} c_{NO} c_H \qquad (4.9)$$

considering forward and backward directions where the concentrations c are given in mol/cm^3.

The thermal NO reactions are highly dependent on temperature, residence time and atomic oxygen concentration. The first reaction has very high activation energy and it is usually accepted as being the rate-limiting step of the thermal NO formation. Due to the high activation energy required to split the strong N_2 triple bond, the rate of formation of NO is significant only at high temperatures (greater than 1800 K).

All the required radicals for this NO formation model are calculated based on the equilibrium approach known and used in the ECFM combustion model (As it

described in section 4.5) where conditional approaches are used in order to determine burned species mass fractions based on mean and fresh gas species mass fractions and the reaction progress variable, respectively.

4.7.1.3. Prompt NO Mechanism

Under specific operating conditions, such as alternative diesel combustion, the rate of NO generated during combustion of hydrocarbon substances can be considerably higher than that predicted by the Zeldovich mechanism. This enhanced NO formation is attributed to the presence of hydrocarbon species, which result from fuel fragmentation during the combustion process. Prompt NO is formed by the reaction of atmospheric nitrogen with hydrocarbon fragments, which is subsequently oxidized to form NO. The prompt NO mechanism forms NO from nitrogen much earlier in the flame than the thermal NO mechanism, as its name suggests.

Fenimore [123] was the first who identified this NO formation mechanism. Prompt NO becomes important at low temperatures (below 1000 K), fuel-rich mixtures and short residence times. Prompt NO emerges during hydrocarbon combustion at the flame front by recombination of CH radical and molecular nitrogen into HCN. Atomic nitrogen further oxidizes to NO. From the reaction of HCN with free radical OH, the CN is formed which is further oxidized to NO. Those reactions are given as follows:

$$N_2 + CH \leftrightarrow HCN + N \tag{4.10}$$

$$N + O_2 \leftrightarrow NO + O \tag{4.11}$$

$$HCN + OH \leftrightarrow CN + H_2O \tag{4.12}$$

$$CN + O_2 \leftrightarrow NO + CO \tag{4.13}$$

Prompt NO formation occurs in fuel-rich regions where hydrocarbon radicals increase the formation of HCN where some species resulting from fuel fragmentation have been suggested as the source of prompt NO in hydrocarbon flames (e.g., C_2, CH, CH_2, C_2H), but the major contribution is from CH and CH_2, via:

$$CH_2 + N_2 \leftrightarrow HCN + NH \tag{4.14}$$

The products of these reactions could lead to formation of amines and cyano compounds that subsequently react to form NO by reactions similar to those occurring in oxidation of fuel nitrogen, for example:

$$HCN + N \leftrightarrow N_2 + \cdots \tag{4.15}$$

Prompt NO formation is proportional to the number of carbon atoms present per unit volume and is independent of the parent hydrocarbon identity (i.e. fuel). The quantity of HCN formed increases with the concentration of hydrocarbon radicals, which in turn increases with equivalence ratio. As the equivalence ratio increases, prompt NO production increases at first, then passes a peak and finally decreases due to a deficiency in oxygen.

In the early stages of the flame, where prompt NO is formed under fuel-rich conditions, the O concentration is high and the N radical almost exclusively forms NO rather than nitrogen. Therefore, the prompt NO formation rate will be approximately equal to the overall prompt NO formation rate:

$$\frac{\partial c_{NO}}{dt} = A f c_{O_2}^{a} c_{N_2} c_{fu} e^{\left(-\frac{Ea}{RT}\right)} \tag{4.16}$$

De Soete [128] defined rate data for $C_2H_4 - air$ flames for above expression:

$$A = A_1 \left(\frac{RT}{P}\right)^{a+1} \quad (4.17)$$

Where a is the oxygen reaction order, R is the universal gas constant and P is the pressure. The rate of prompt NO formation is found to be of the first order with respect to nitrogen and fuel concentration, but the oxygen reaction order, a, depends on experimental conditions. It should be noted that the model of De Soete differ significantly from data obtained experimentally under fuel-rich conditions and for higher hydrocarbon fuels. To reduce this error and predict the prompt NO adequately for all conditions, the De Soete model was modified using the available experimental data by a correction factor, f, which incorporates the effect of fuel type (i.e. number of carbon atoms) and air-to-fuel ratio for gaseous aliphatic hydrocarbons. The correction factor f is a polynomial which approximates a curve obtained on the basis of experimental data valid for aliphatic alkane hydrocarbon fuels and for equivalence ratios φ between 0.6 and 1.6:

$$f = a_0 + a_1 n + a_2 \varphi + a_3 \varphi^2 + a_4 \varphi^3 \quad (4.18)$$

Where n is the number of carbon atoms per molecule for the hydrocarbon fuel. a_0 to a_4 are constants. Oxygen reaction order, a, depends on flame conditions. According to De Soete, oxygen reaction order is uniquely related to oxygen mole fraction in the flame and has different values depend on the oxygen mole fraction.

4.7.1.4. Fuel NO Mechanism

It is well known that nitrogen-containing organic compounds present in fossil fuels can contribute to the total NO formed during the combustion process. This fuel nitrogen is a particularly important source of nitrogen oxide emissions for residual fuel oil and coal, which typically contain 0.3-2% nitrogen by weight.

The extent of conversion of fuel nitrogen to NO is dependent on the local combustion characteristics and the initial concentration of nitrogen-bound compounds. Fuel-bound nitrogen-containing compounds are released into the gas phase when the fuel droplets or particles are heated during the devolatilization stage.

From the thermal decomposition of these compounds in the reaction zone, radicals such as HCN, NH_3, N, CN and NH can be formed and converted to NO. In the proposed NO formation model all those radicals are taken as HCN or NH_3 only.

4.7.2. Soot Formation and Oxidation Models

Under high temperature and fuel rich conditions, as typically found in diesel combustion, hydrocarbon fuels exhibit a strong tendency to form carbonaceous particles-soot. Usually, under engine running conditions, most of the soot formed in the early stages of the combustion process is depleted due to oxidation. This takes place in oxygen rich areas of the combustion chamber later in the engine cycle. In diesel engines, it is the amount and completeness of the soot oxidation process that actually determines the engine particle emission characteristics.

The formation of particulates involves a large number of different chemical and physical processes, like the formation and growth of large aromatic hydrocarbons, their subsequent conversion to particles, the coagulation of primary particles, and the growth of solid soot particles due to the accumulation of gaseous components [129].

The soot particle formation process is characterized by a gaseous-solid conversion, whereby the solid phase does not exhibit a uniform chemical and physical topology.

It is evident that the formation of soot, i.e. the conversion of hydrocarbon rich, aliphatic compounds involving only a relatively small number of carbon atoms into an agglomerate comprising millions of them, is the result of a highly complex chemical process involving hundreds of reactions and as many intermediate and radical species. Particle oxidation mainly occurs due to the attack of atomic oxygen onto the carbonaceous particles under high temperature conditions.

In spite of the high complexity of the underlying processes, the individual reactions contributing to the soot formation and oxidation rates can be related to known flame parameters, such as fuel mass fraction, partial pressure of oxygen, flame temperature and/or turbulent mixing intensity.

A number of different sub-models have been proposed in the past in order to capture the individual aspects of relevant contribution of nucleation, particle growth and oxidation to the soot emission level in engines [130, 131]. These sub-models are based upon different simplifying assumptions concerning the relative contributions of the individual chemical and physical processes to the overall net formation rate. The soot formation model currently implemented in FIRE is based upon a combination of suitably extended and adapted joint chemical/physical rate expressions for the representation of the processes of particle nucleation, surface growth and oxidation. In this study, soot emission is modelled by the Kennedy, Hiroyasu and Magnussen mechanism [73].

4.7.2.1. Influence of Temperature

The temperature is one of the main parameters influencing the soot formation processes [132]. An increased soot formation rate was observed using an increased initial temperature of the air/fuel mixture [133]. Up to 1600 [K] the soot concentration

is increasing through a progressive surface growth rate, and above 1650 [K] the amount of soot becomes reduced by increased oxidation.

4.7.2.2. Influence of Pressure

Surface growth through the soot formation process is done by hydrocarbon and acetylene addition. With increasing pressure, the surface growth rate is increased, whereas the acetylene concentration decreases [134]. At high pressure (10 bar) the soot formation can become independent of the fuel composition.

4.7.2.3. Influence of Residence Time

The residence time affects the mechanism which limits the soot formation process [132]. The soot concentration is turbulence controlled in turbulent diffusion flames. The turbulent mixing rate is larger than the chemical reaction rate. In this case, the soot concentration increases with the residence time.

Soot formation is controlled by the chemistry in laminar diffusion flames. The soot concentration is a function of the local species concentration and temperature, and independent of the residence time.

Chapter 5

Multiple Injections

5.1. Background

As discussed in chapter 2, while EGR and split injection have been suggested as useful ways to improve NOx emission and also reduce soot emissions, it is of interest to explore the combined influence of these two technologies on possibility of simultaneous reduction in particulate and NOx emission. The main purpose of this chapter is to gain a detailed understanding of the mechanisms through which fuel injection interacts with other engine parameters and influences diesel combustion and emissions, and hence to attempt to generalize the adoption of various multiple and pilot injection strategies with regards to improving diesel engine performance.

5.2. Multiple Injection Strategies

In this section, an advanced CFD simulation has been applied to model the combination of split injection and EGR in a DI diesel engine. For this purpose, the effect of split injection parameters including the amount of injected mass and the delay dwell between injection pulses has been analyzed with different EGR rates. Based on

those simulations, the optimum operating points for obtaining the minimum amount of NOx and soot emissions have been demonstrated. The results presented in this chapter have been published in [135-137] .

5.2.1. Computational Grid

The computational mesh was created using AVL ESE Diesel Tool [73]. Because of the symmetrical location of the injector at the centre of the combustion chamber, the CFD calculations are performed on 60˚ sector meshes. Exhaust and intake ports are not included in the computational mesh by concentrating this simulation on in-cylinder flow and combustion processes. Calculations begin at Intake Valve Closure (IVC) and end at Exhaust Valve Opening (EVO). The same initial and boundary conditions are used for all the computations. The final mesh consists of a hexahedral dominated mesh. It should be noted that in any CFD simulation, it is vital to ensure that the results are not dependent on the utilized mesh. For this purpose, meshes of three different densities were pre-investigated. A coarse grid with about 14000 cells, medium resolution grid with about 28000 cells and a fine grid with about 37000 cells at TDC have been generated. In order to study the capability of these grids, the simulation was performed from IVC to EVO. Combustion has been switched off in these simulations to focus on the engine flow and fuel-air mixing. The medium dense mesh was selected due to its best suitability for the computations. For this case, the fluctuation of pressure and temperature curves was lowest compared to the measured data. The cell size along the piston bowl was set to 0.9 mm. Exact number of cells in the mesh was 28725 and 56311 at TDC and BDC, respectively, with the plot at TDC and 90˚ BTDC as shown in Figure 5.1.

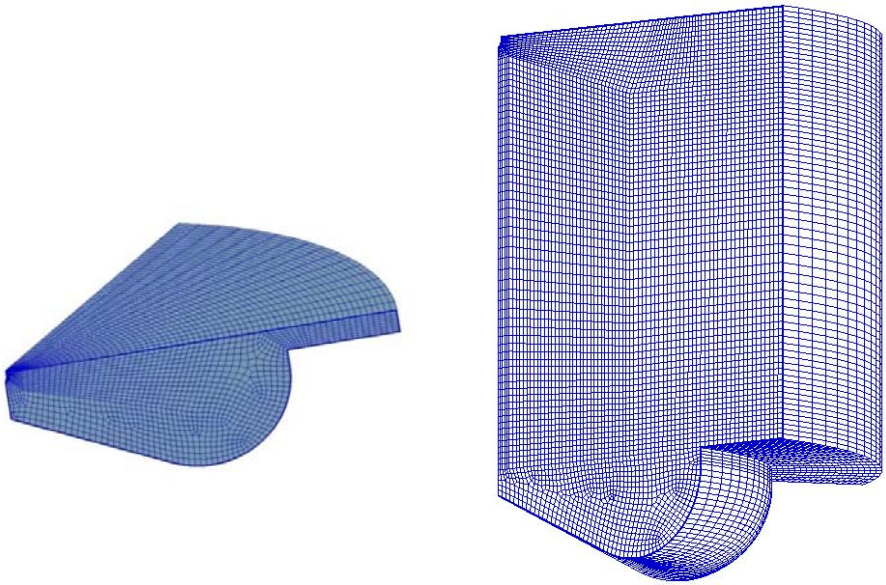

Figure 5.1 – Computational grids at TDC and 90˚ BTDC

5.2.2. Model Validation

The diesel engine used for the model validation is a single-cylinder version of a Caterpillar 3401 heavy-duty truck engine. The experimental results for this part of study have achieved from the University of Wisconsin-Madison [138]. The engine specifications are given in Table 5.1 [138] with a constant engine speed of 1600 rev/min for all mentioned cases.

Table 5.1 – Engine specifications

Engine type	Caterpillar 3401
Bore	13.719 cm
Stroke	16.51 cm
Compression Ratio	15.1:1
Displacement	2.44 l
Connecting rod length	26.162 cm
Squish clearance	4.14 mm
Inlet Valve Opening	-32˚ ATDC
Inlet Valve Closing	-147˚ ATDC
Exhaust Valve Opening	134˚ ATDC
Exhaust Valve Closing	29˚ ATDC
IMAP	184 KPa
IMAT	310 K
Piston Shape	Mexican Hat style

The fuel delivery system was an electronically controlled, common rail fuel injection system [138]. In all the injection cases studied, the same amount of fuel (0.1622 g/cycle) is injected in each engine cycle. The main characteristics of the injection system are listed in Table 5.2.

Table 5.2 – Injector fuel system specifications

Injector type	Electronically controlled, common rail
Injection pressure	Variable (up to 120 MPa)
Number of nozzle holes	6
Nozzle hole diameter	0.26 mm
Included Spray Angle	125˚
Start of injection	-9˚ ATDC
Injection duration	21.5˚ CA

Figure 5.2 shows comparisons between the predicted and measured in-cylinder pressure and heat release rate. The result is based on the assumption of uniform wall temperature 425 K for the cylinder wall, 525 K for the cylinder head and 525 K for the piston top.

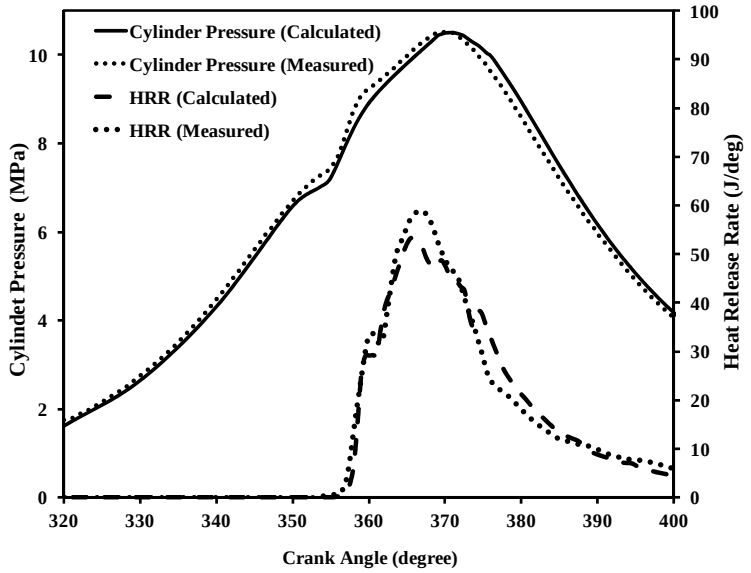

Figure 5.2 – Comparison of calculated and measured in-cylinder pressure

The trend predicted by the model is reasonably close to experimental results, although there are still some differences as can be seen in Figure 5.2. These discrepancies could be related to experimental uncertainties in input parameters to the computations such as the precise injection duration, start of injection timing and gas temperature at IVC.

Figures 5.3 and 5.4 present comparisons between the predicted and measured engine-out soot and NOx values for EGR levels of 0% and 10%. As illustrated in Figure 5.3, increasing EGR, which causes dilution of intake charge, and insufficient oxygen in intake charge, leads to lower combustion temperature and therefore decreases NOx emission. In contrast, as it can be seen in Figure 5.4, this variation has a reverse effect on soot formation.

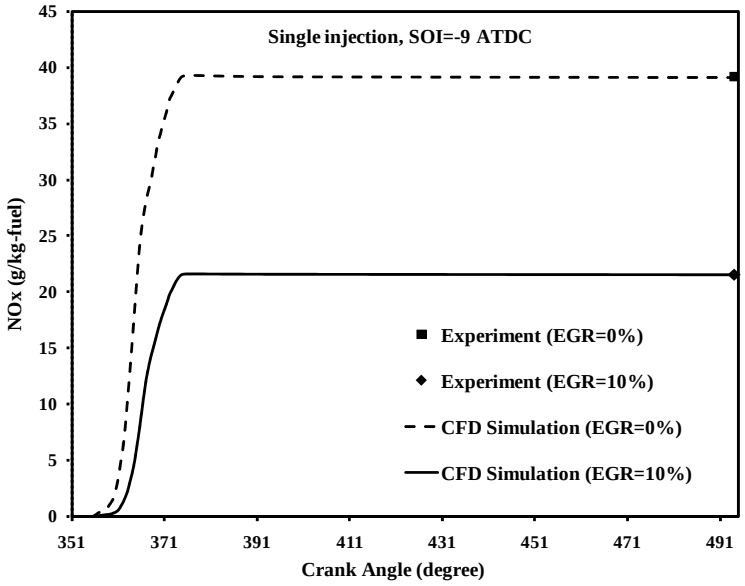

Figure 5.3 – Predicated NOx in comparison with measured data [138]

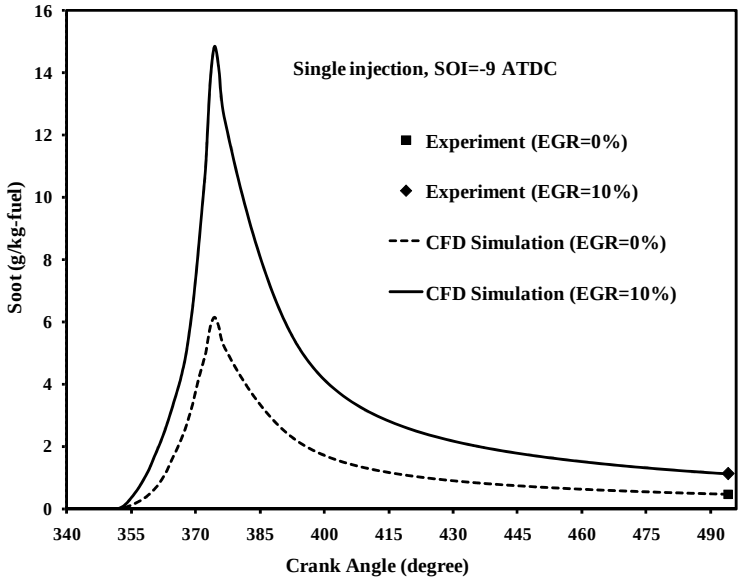

Figure 5.4 – Predicated soot in comparison with measured data [138]

It should be stated the particle oxidation process that accurately determines the soot emission level is modeled according to a hybrid chemical kinetics/turbulent mixing controlled rate expression. Oxygen partial pressure, local flame temperature as well as actual soot concentration and local turbulent mixing time scale, obtained from the solution of the two equations turbulence model, contribute to the soot oxidation source. Alternatively, NOx formation as well as soot formation is calculated by adopting the combustion and pollutant formation models.

While NOx and soot emissions processes can be predicted but there is only one measured value for these two components, necessary adjustments on emission model parameters were made for the validations demonstrated Figure 5.3 and 5.4. Then to achieve optimum validation results, the trade-off between NOx and soot was simulated with several different injection timing. Results shown in Figure 5.5 suggested that the models used in this study can provide enough confidence to the following simulation results with regard to the combustion process and emissions.

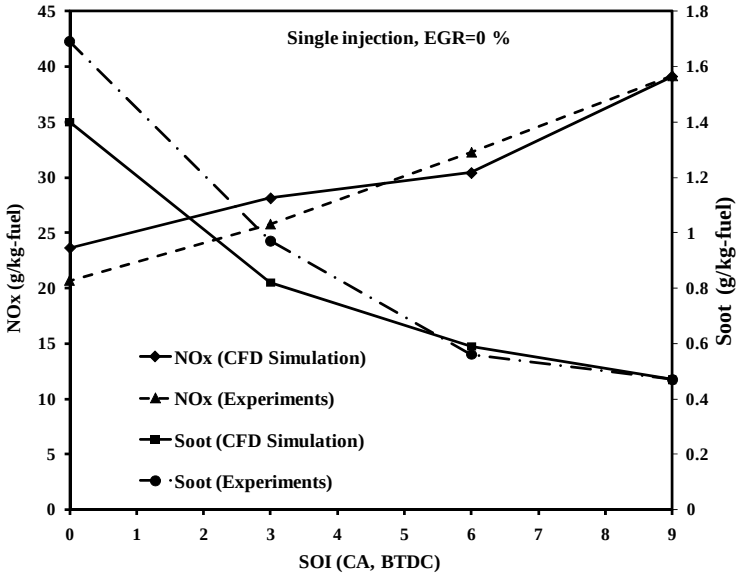

Figure 5.5 – The effect of injection timing on NOx and soot, single injection, EGR=0%

5.2.3. Modeling Methodology

Based the above success of validations with just a single injection, simulation results with split injection and different EGR rate will be presented and discussed in the following sections.

Figure 5.6 gives a summary of the injection strategies used in this study. For all cases, the start of injection is fixed at 9˚ CA BTDC. Totally, there are 12 different injection arrangements for which two injection pulses with variable fuel amount for each pulse (up to 30% for the second pulse) and variable separation/dwell between two pulses (up to 30˚ CA) were considered. For same initial conditions, it should be noted that the inlet pressure and the inlet temperature for 10% EGR rate were kept same as 0% EGR.

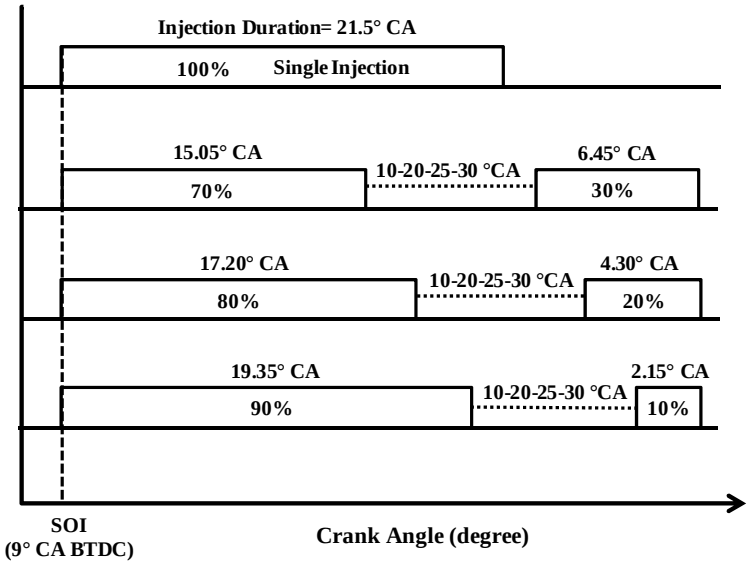

Figure 5.6 – Injection profiles for different strategies used

5.2.4. Results and Analysis

In Figures 5.7 and 5.8, the amount of soot and NOx emission for different split injection cases with 0% and 10% EGR rates are illustrated, respectively.

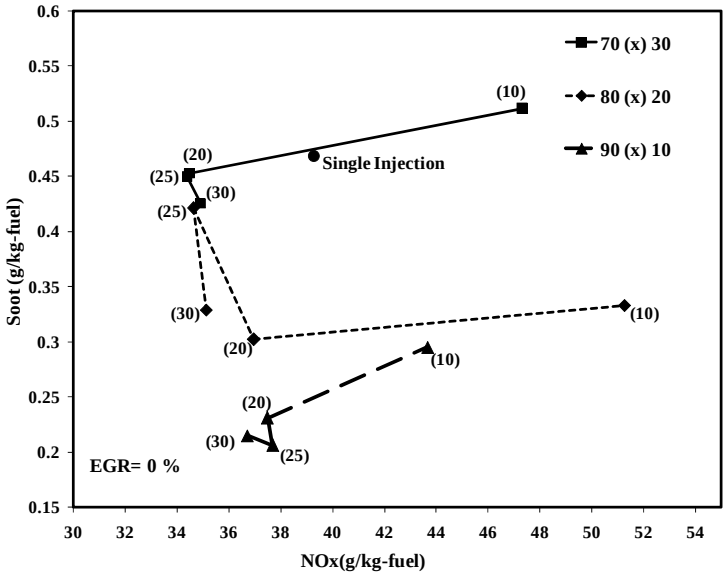

Figure 5.7 – Soot-NOx trade-off, EGR=0%

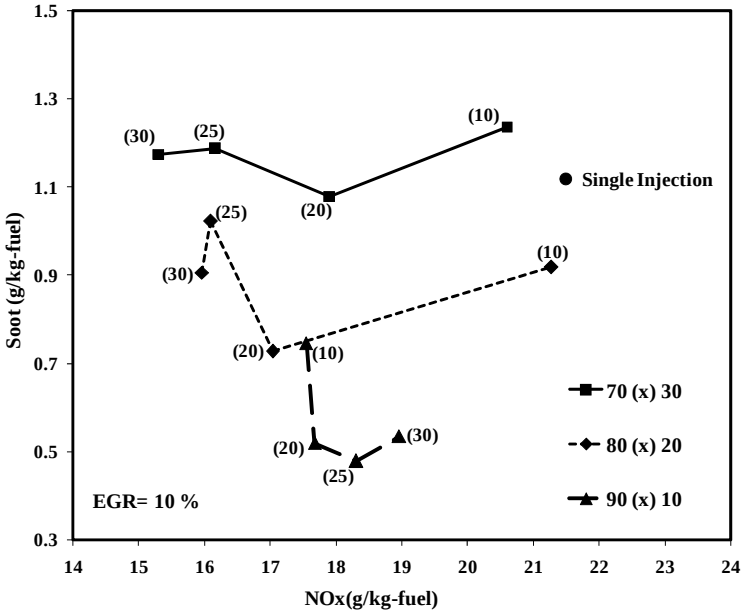

Figure 5.8 – Soot-NOx trade-off, EGR=10%

The labeling scheme for the split injection cases gives the percent of the fuel injected in the first and last pulses, and the dwell between two injections. For instance, 70(10)30 represents 70% fuel injected in the first pulse, 10 crank angle degree dwell between the two injection pulses and 30% fuel in the second pulse.

Basically, in Figure 5.7 and 5.8, it can be seen that the majority of split injection schemes can simultaneously reduce soot and NOx emissions compared to the single injection scheme, though some cases have increased emissions. There are a number of reasons why split injection could be beneficial to overall reduction in soot emissions. While experimental observations have suggested that soot is formed and accumulates at the fuel spray tip of a diesel engine [44, 49], by pulsating the fuel injection, there is substantial decrease in the amount of soot formed because the rich regions (conducive to soot formation) at the tip of the fuel spray are no longer being replenished during the interval between injections. In addition, the use of split injection schemes is an effective means to improve fuel-air mixing and lean out the mixture. Injecting the second pulse

after an optimum delay dwell will tend to generate more turbulence and increase entrainment of the combustible air.

As shown in Figure 5.7, the minimum amount of NOx formation was achieved with the case of 70(25)30, though it is just a little lower than other several operating points. It may be due to the fact that premixed combustion which is the main source of the NOx formation is relatively low in comparison with other cases. Higher amounts of the second injection pulse into the lean and hot combustion zones cause the newly injected fuel to burn rapidly and effectively at high temperature, resulting in high soot oxidation rates. From comparisons of Figure 5.7, it can be seen that the optimum delay dwell between the injection pulses for simultaneous reduction of soot and NOx formation is between 25° and 30° CA for all operating conditions. If considering all data in Figure 5.7 and 5.8, it can be seen that the split injection strategy under 10% EGR conditions can be more beneficial for the substantial reduction of NOx formation. The optimum engine performance for reduction of soot and NOx emissions can be obtained with 20˚ CA delay between injection pulses in the 80(20)20 and 90(20)10 cases, though the lowest total soot is seen with the split injection ratio 90(25)10. In addition, it can be concluded that the delay dwell does not affect soot emission significantly. The combustion of 30% fuel in the second injection pulse only causes a small effect of soot variations compared to the other cases in this injection category i.e. 70(x)30. It is clearly seen in Figure 5.8 that the 90(20)10 case shifts the soot-NOx trade-off to the optimum level.

Figure 5.9 shows the amount of Homogeneity Factor (HF) as a function of crank angle for different split injection cases.

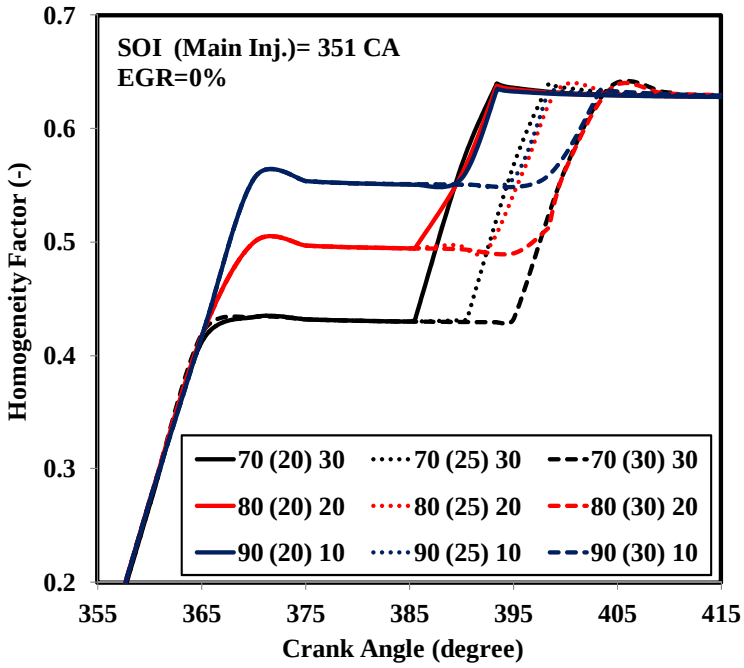

Figure 5.9 – Homogeneity Factor for different injection strategies

As can be seen in Figure 5.9, for different split injection schemes, the amount of homogeneity factor is increasing when more fuel is distributed in the first pulse, however this trend have different effects on soot and NOx emissions. With the use of split injection, combustion of the second pulse injected fuel is delayed by the injection pause which affects on soot and NOx formation. Therefore, careful adjustment must be made for ideal reduction for both NOx and soot emissions.

It can be concluded from Figures 5.7 and 5.9, when the dwell delay between injection pulses is longer than 20˚ CA, it leaves more time for the air-fuel mixing and initial combustion process of first injection pulse and therefore, the increase of Homogeneity Factor takes place at a later stage and it can caused a reduction of NOx formation. However, as the dwell delay between injection pulses becomes small (e.g., 10˚ CA), combustion of first pulse injected fuel has an important effect on NOx production, and it results in more NOx being formed in the earlier combustion stage, and hence more total NOx production.

For further exploring the effects of Homogeneity Factor, the amount of this parameter at 10 CA ATDC is selected here to evaluate its response for different split injection cases, as illustrated in Figures 5.10 and 5.11.

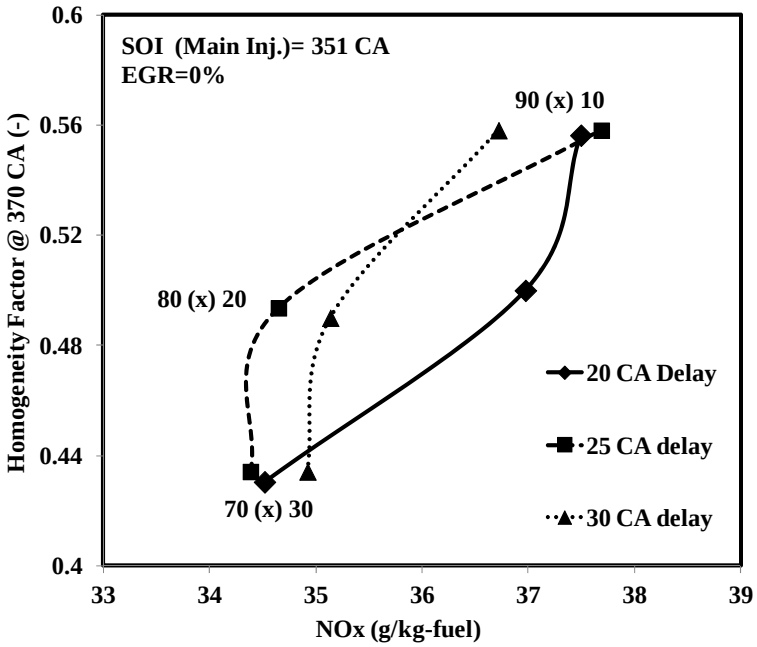

Figure 5.10 – Homogeneity Factor at 10 CA ATDC vs. NOx emission for different split injection cases

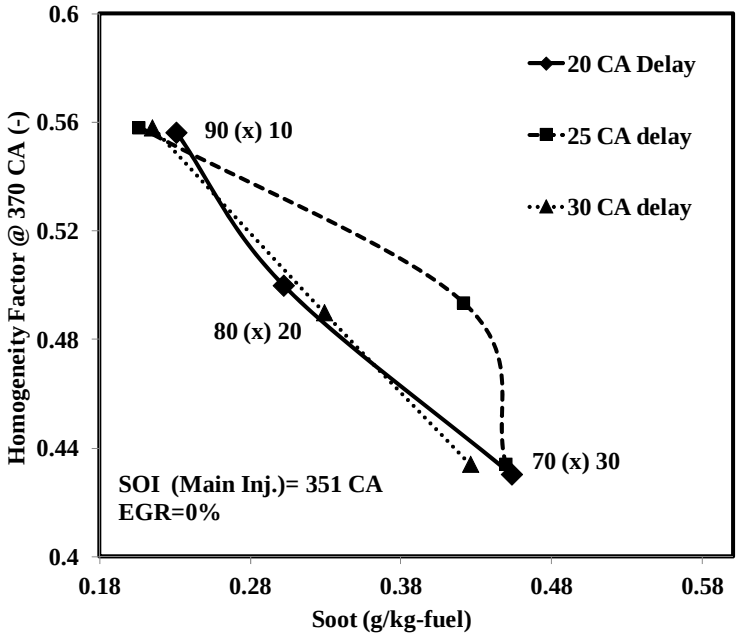

Figure 5.11 – Homogeneity Factor at 10 CA ATDC vs. soot emission for different split injection cases

As can be clearly seen in Figure 5.10 the higher Homogeneity Factor will result in higher NOx emissions. It can be concluded that higher Homogeneity Factor will increase the rate of air-fuel mixing and more complete combustion process which will cause the increase of NOx emission. By comparison between Figure 5.10 and 5.11, the best operating points for simultaneous reduction of NOx and soot emissions can be obtained by the 70(x)30 cases.

Figures 5.12 and 5.13 illustrate the heat release rates for the three split injection cases compared to single injection case in the optimum delay dwell i.e. 20°CA for EGR levels of 0% and 10%, respectively.

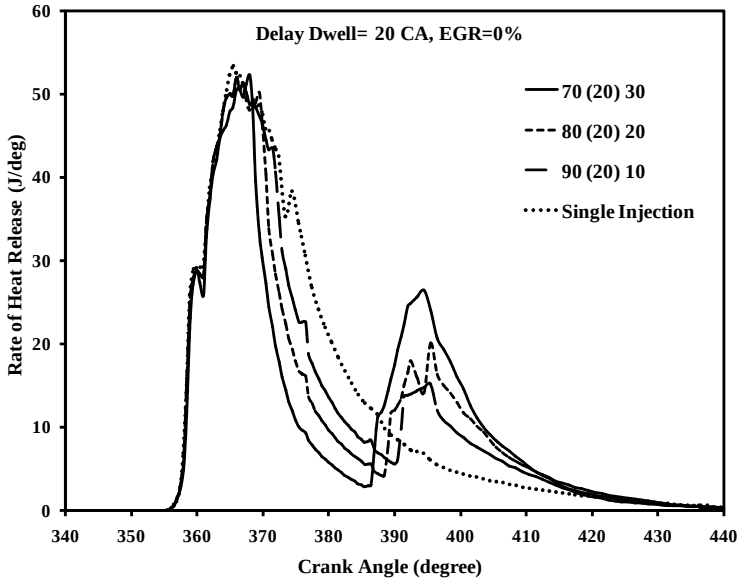

Figure 5.12 – The HRR curve, optimum injection cases compared to single injection case, EGR=0%

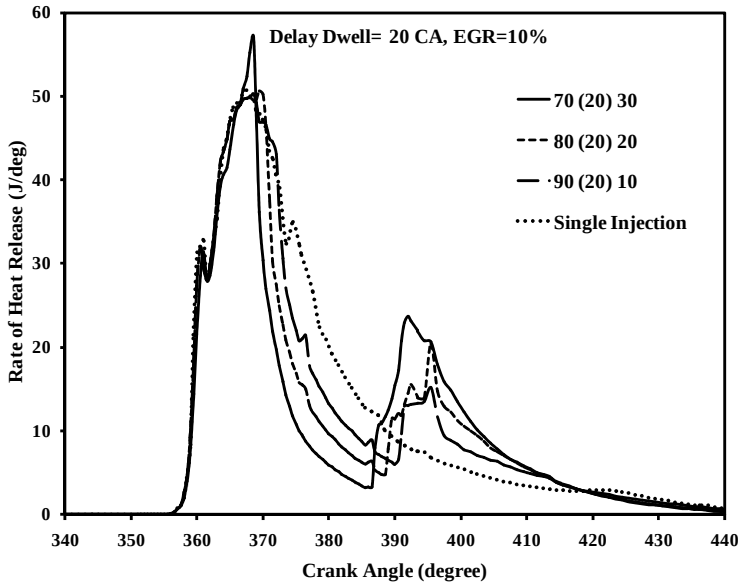

Figure 5.13 – The HRR curve, optimum injection cases compared to single injection case, EGR=10

As shown in Figures 5.12 and 5.13, the heat release curves of split injection are very different from single injection. Between two peaks which should be resulted in by two pulses, there is an obvious valley (around 390˚ CA) which cannot found normally from single injection combustion. The second fuel injection, occurred at the late combustion stage, affects the in-cylinder pressure and temperature that causes second peak in HRR diagram.

Figure 5.14 illustrates the amount of Homogeneity Factor for three optimum injection cases along with their injection profiles.

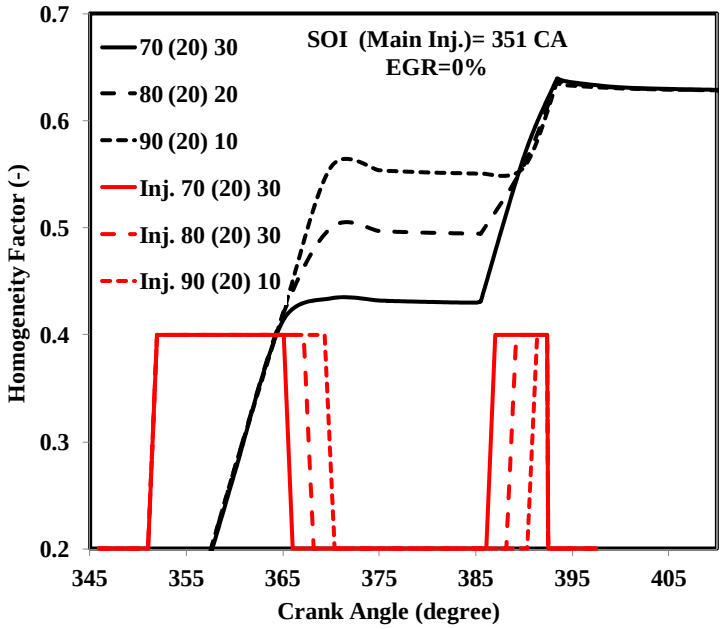

Figure 5.14 – Homogeneity Factor for three optimum injection cases

As mentioned previously, the first injection starts at 351 CA for all injection cases. From Figure 5.14, it can be seen that for the 70 (20) 30 case, which has the higher amount of injected fuel as a second pulse, the Homogeneity Factor keeps increasing quickly after second injection. As a result, for those injection schemes with more portion of post injected fuel, the air-fuel mixing process takes very well during the late compression stroke. However for these strategies, less mixing time can be attainable to achieve a large portion of homogeneous mixture at the late combustion process.

Figure 5.15 and 5.16 indicates the cylinder temperature for the three split injection cases in the optimum delay dwell i.e. 20°CA for EGR levels of 0% and 10%, respectively.

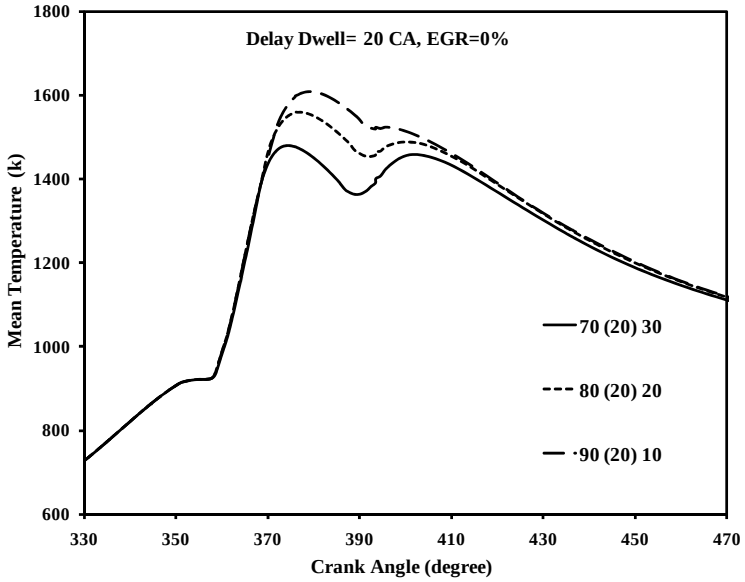

Figure 5.15 – In-cylinder temperature, optimum split injection scheme, EGR=0%

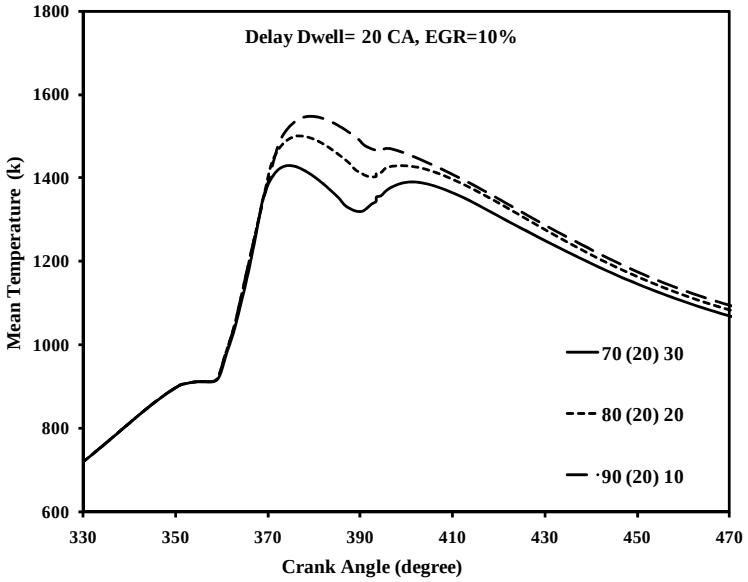

Figure 5.16 – In-cylinder temperature, optimum split injection scheme, EGR=10%

As can be seen in Figure 5.15 and 5.16, for the 70(20)30 case, the first and second peaks are lower than the other cases. Moreover, after the second peak, the cylinder temperature tends to increase more in comparison with the other cases.

Figures 5.17 and 5.18 show ISFC versus NOx curves at 0% and 10 % of EGR. In addition Figure 5.19 illustrates the amount of Homogeneity Factor at 10 CA ATDC for different injection schemes.

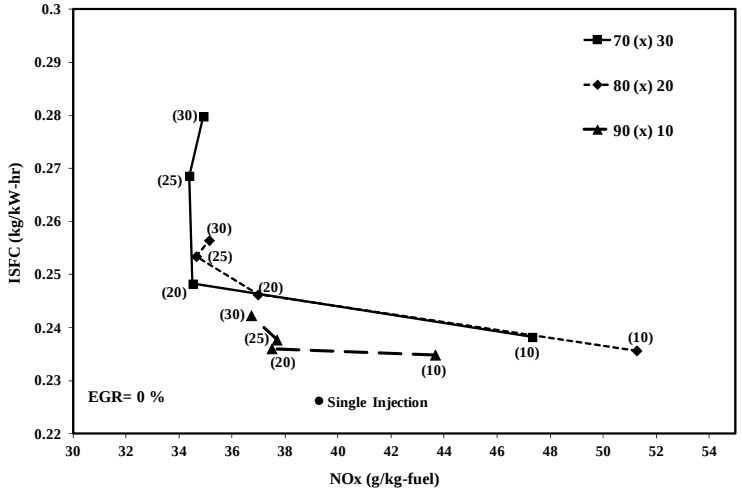

Figure 5.17 – ISFC vs. NOx trade-off, EGR=0%

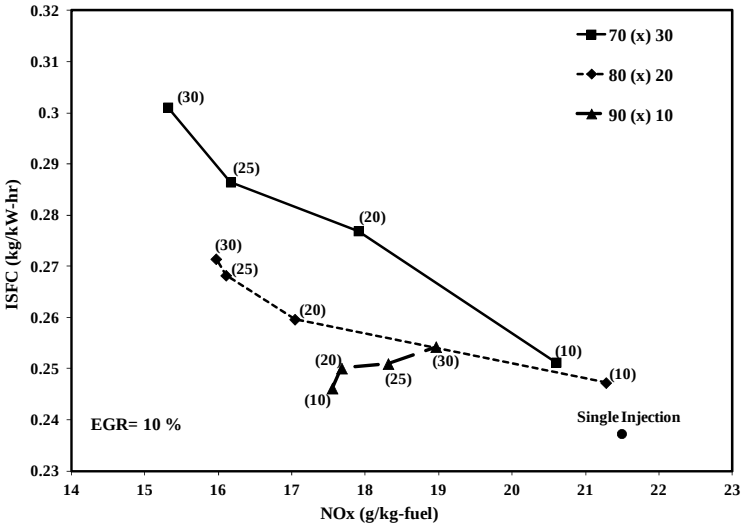

Figure 5.18 – ISFC vs. NOx trade-off, EGR=10%

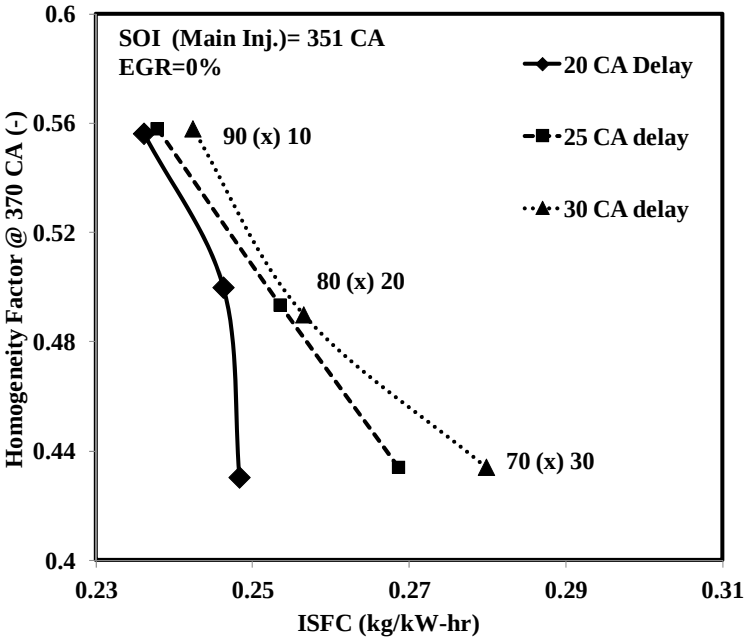

Figure 5.19 –Homogeneity Factor at 10 CA ATDC vs. ISFC for different split injection cases

As shown in Figures 5.17 and 5.18, for the 90(x)10 case the differences between ISFC versus NOx emission is lower than other cases. It can be concluded that the split injection shows minimal effects on ISFC when the secondary injection were relatively small compared to the main injection. In addition, as can be seen the trade-off characteristics for the 90(x)10 case is relatively different for two level of EGR rates. In addition, as shown in Figure 5.19, the higher amount of Homogeneity Factor results in reduction of ISFC. It can be concluded that the higher rate of air-fuel mixing process will improve the combustion process and therefore, the lower amount of ISFC can be expected to be achieved.

Figures 5.20 and 5.21 illustrate IMEP versus NOx curves at 0% and 10% of EGR. As shown in Figure 5.20, in the 70(20)30 case, the optimum value can be obtained with 20˚CA delay between injection pulses. A similar trend can be observed by using two other cases. However, as mentioned above and also shown in Figures 5.20 and 5.21, for the 90(x)10 case the result is relatively different for EGR levels of 0% and

10%. It has been well established that optimum operation point can be achieved with 20˚ CA delay between injection pulses for the three split injection cases.

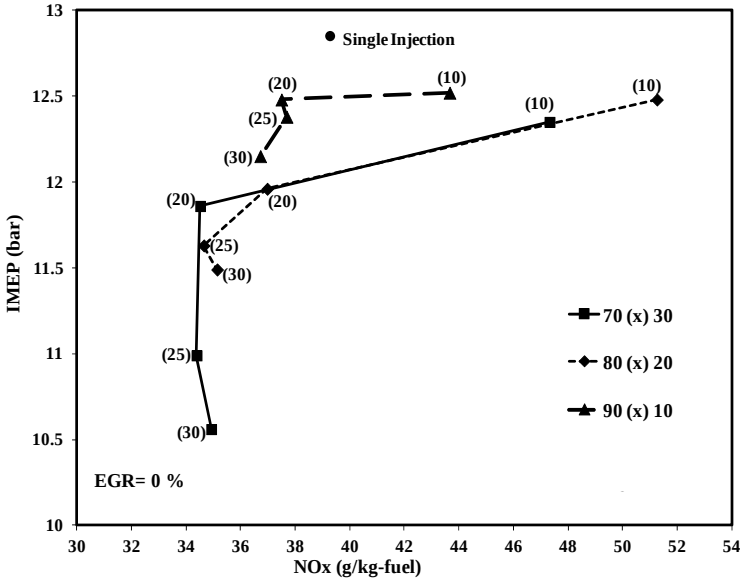

Figure 5.20 – IMEP vs. NOx trade-off, EGR=0%

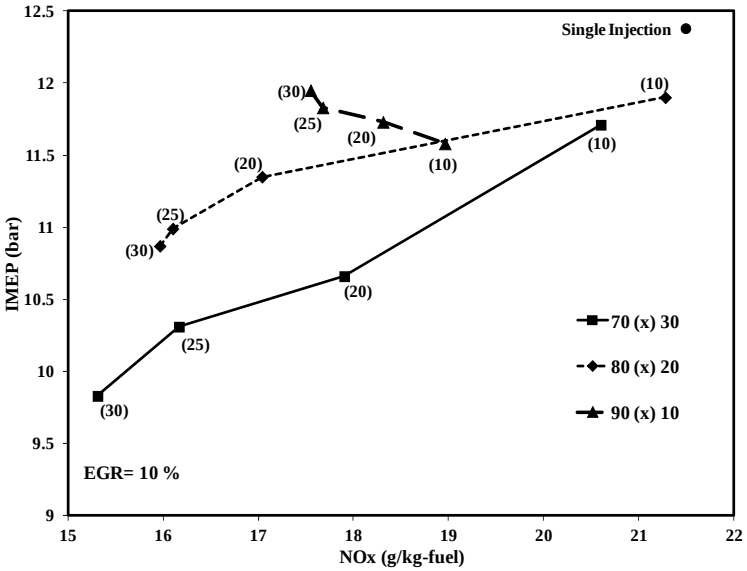

Figure 5.21 – IMEP vs. NOx trade-off, EGR=10%

Figure 5.22 shows the velocity field contours for single injection case in comparison with the three split injection cases in the optimum delay dwell i.e. 20°CA at 360, 385 and 410 CA.

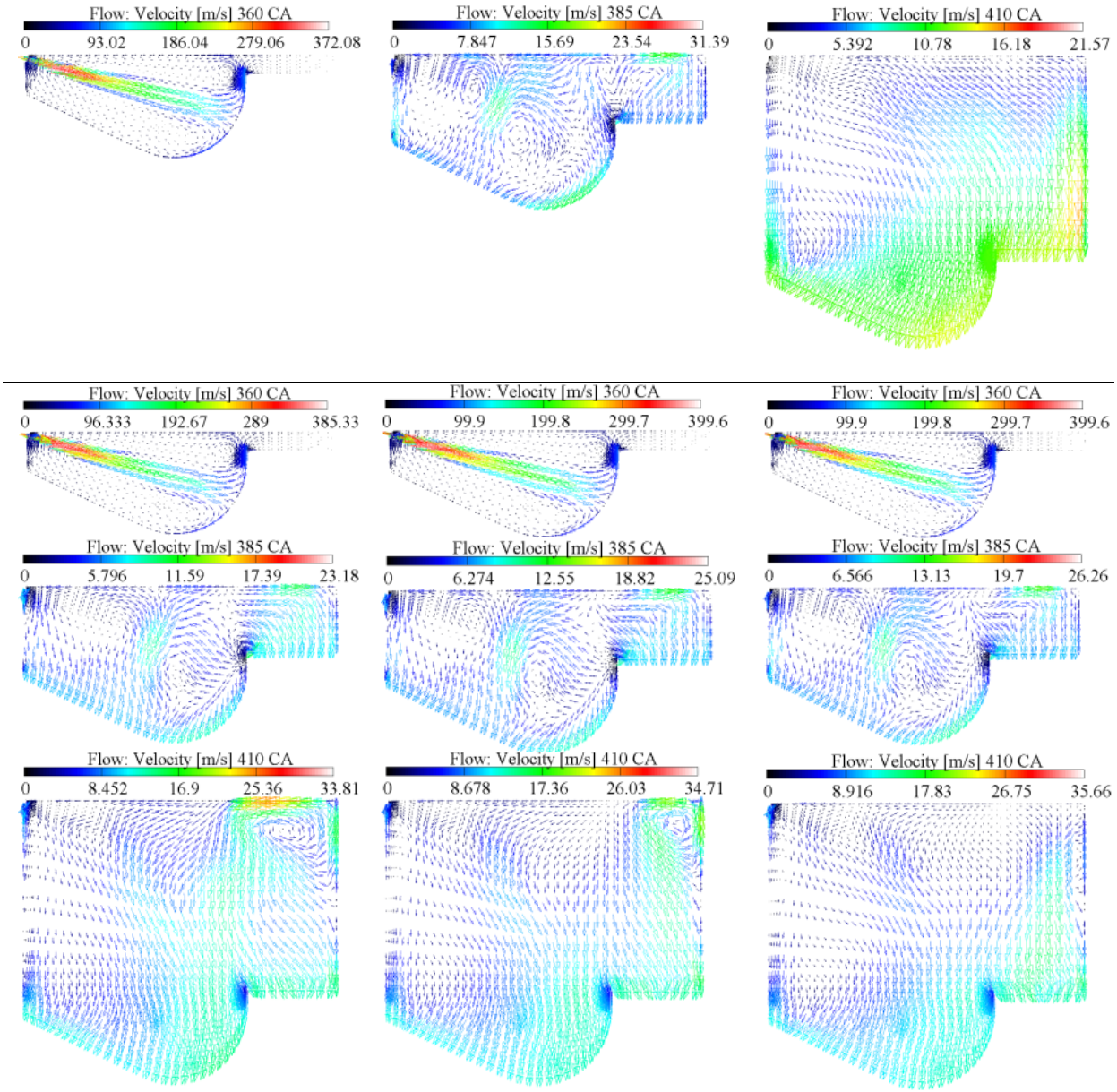

70(20)30 80(20)20 90(20)10

Figure 5.22 – The velocity fields contours, single injection (first row), 70(20)30 (first column), 80(20)20 (second column), 90(20)10 (third column)

As can be seen in Figure 5.22, the velocity field within the cylinder increases dramatically for the three split injection cases in comparison with the single injection case at 410 CA. It can be concluded that injecting fuel in the second pulse in the later stage of combustion duration had a significant effect on flow filed and causes the subsequent effects on soot oxidization and NOx formation.

The evolution of the NOx distribution within the combustion chamber for single injection case in comparison with optimum split injection scheme (80(20)20) is shown in Figure 5.23 at 385, 410 and 420 CA.

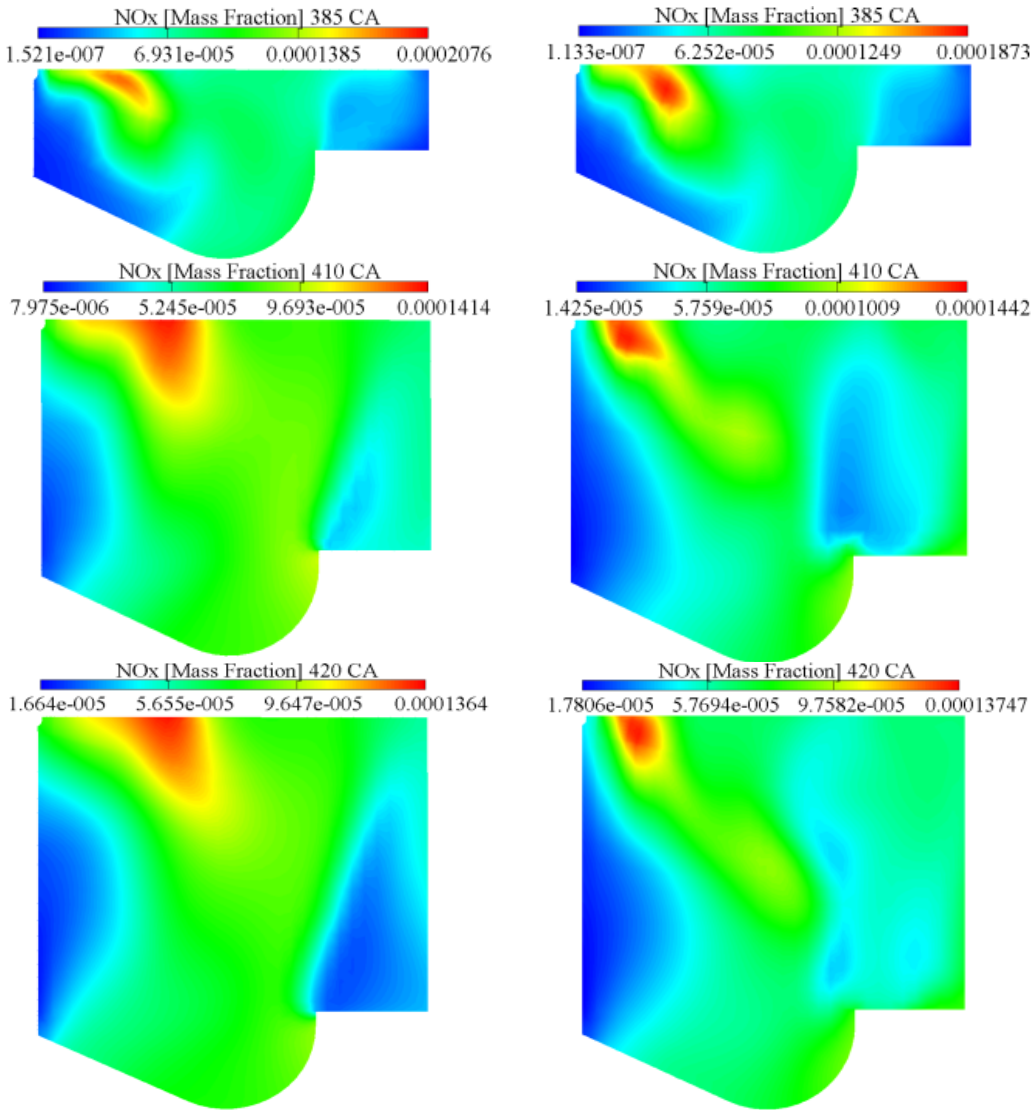

Figure 5.23 – NOx mass fraction contours, single injection (first column) in comparison with optimum split injection scheme (second column)

Figure 5.24 shows the comparison of in-cylinder soot formations for the same operating points.

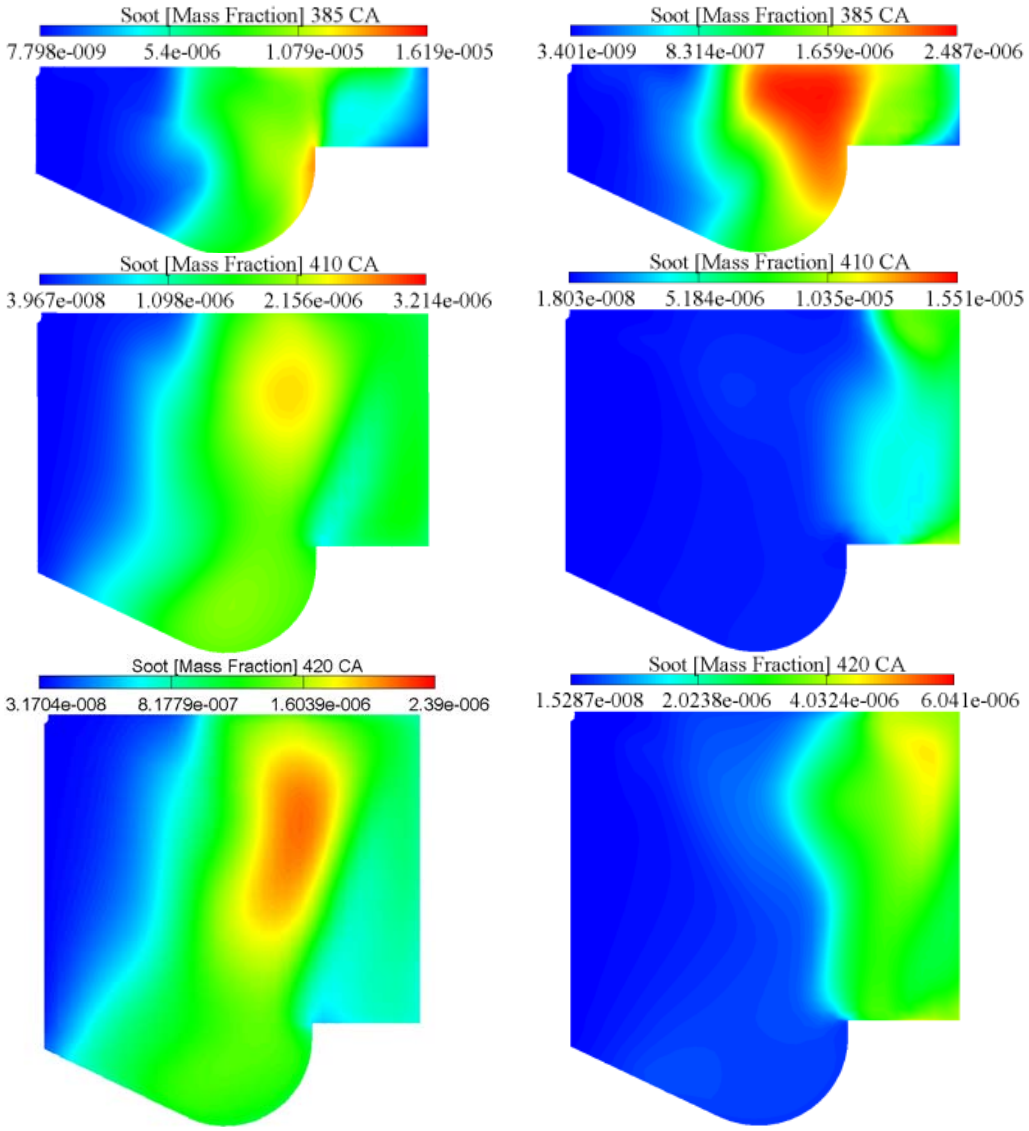

Figure 5.24 – Soot mass fraction contours, single injection (first column) in comparison with optimum split injection scheme (second column)

The local soot-NOx trade-off is evident in these contour plots, as the NOx formation and soot formation occur on opposite sides of the high temperature region. It can be seen that for the 80(20)20 case, NOx and soot mass fractions are lower in comparison with the single injection case. Because of the optimum delay dwell, the second injection pulse, maintains the low NOx and soot emissions until EVO. It can be

concluded that, for the split injection case, the second pulse injected fuel enters into a relatively lean and high temperature region which is remained from the combustion of the first pulse. Soot formation is therefore significantly reduced because the injected fuel is rapidly consumed by combustion before a rich soot region can accumulate. In the single injection case, the soot formed in the later combustion phase is difficult to be oxidized for two reasons. First, it is close to the end of the combustion period, and second, the temperature decreases rapidly in expansion stroke. In the same manner, the soot produced during the main combustion phase will not be oxidized easily for the lower temperature in-cylinder.

The above results explain why split injections can improve the soot-NOx trade-off. It is expected that further emission reduction could be obtained if the injection timing was also varied.

The predicted soot-NOx trade-off using different injection timing for optimum split injection cases are illustrated in Figures 5.25 and 5.26 for EGR levels of 0% and 10%, respectively. Numbers in Figure are the injection timing (ATDC).

It is clearly seen in these two figures that the 80(20)20 case shifts the soot-NOx trade-off to a lower level of NOx emissions with almost no penalty in the soot emission when the same injection timing is used for different injection schemes. In the single injections cases, NOx can be reduces with a corresponding penalty of increased soot with retarding injection timing. This trend is also seen in the split injection schemes. However, with the combination of split injection and retarded injection timing, significant reduction of NOx and soot can be achieved simultaneously.

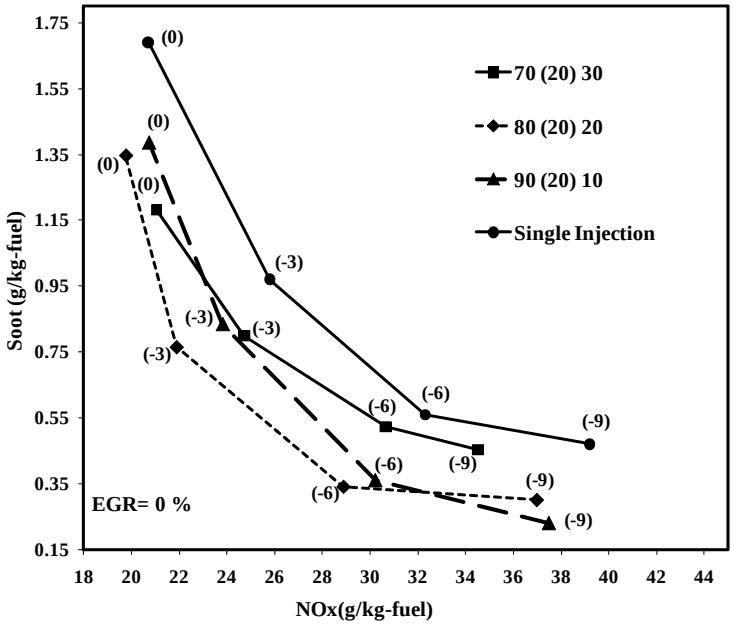

Figure 5.25 – Soot-NOx trade-off for different SOI timing, EGR=0%

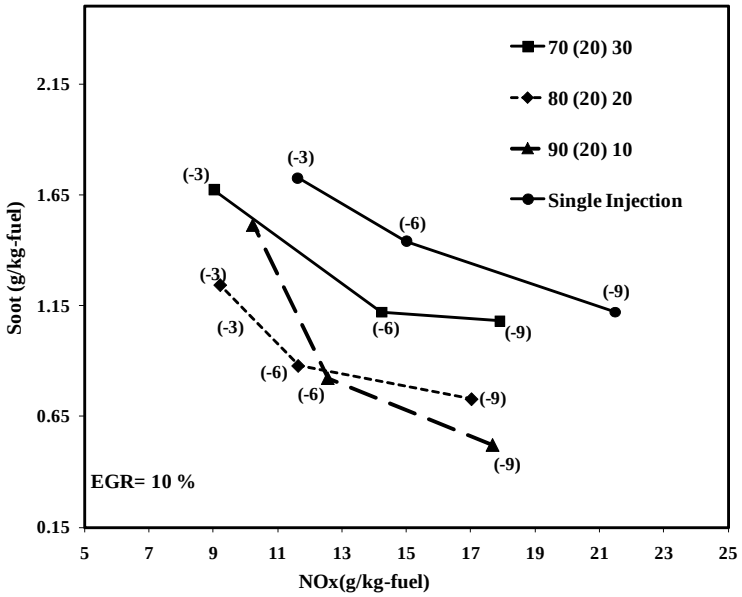

Figure 5.26 – Soot-NOx trade-off for different SOI timing, EGR=10%

5.2.5. Summary

The mechanism of soot and NOx reduction using split injections was studied computationally using a designed set of injection schemes in a Caterpillar 3401 test engine. The simulation was performed from IVC to EVO at 1600 rev/min. For this

purpose, 12 different injection strategies for which two injection pulses with different fuel amount for each pulse (up to 30% for the second pulse) and different separation between two pulses (up to 30˚ CA) were evaluated. From those prediction results, the following conclusions were suggested.

- The computed in-cylinder, soot and NOx emissions were compared with measured data and good agreement between the predicted and experimental values was ensured the accuracy of the numerical predictions collected with the present work.

- Compared to the single injection, split injection was very effective for reducing NOx and Soot emissions. However, the split injection must be optimized for best emission reducing effects by varying the fuel distribution in each pulse and the separation between pulses for each operating condition.

- The optimum separation for simultaneous reduction of soot with low NOx emissions can be obtained by using 20°CA dwell delay between the injection pulses.

- With the combined use of EGR and split injection, NOx and soot were simultaneously reduced with more obvious results.

- When the dwell delay between injection pulses becomes longer, it leaves more time for the air-fuel mixing and initial combustion process of first injection pulse and therefore, the increase of Homogeneity Factor takes place at a later stage and it can caused a reduction of NOx formation. The higher Homogeneity Factor will result in higher rate of air-fuel mixing and more complete

combustion process. However, the careful adjustment must be made for ideal reduction for both NOx and soot emissions.

- It was confirmed that soot emissions can be reduced by split injections and this strategy also allows the injection timing to be retarded to reduce NOx emission. By using an optimum injection schemes with retarded injection timing, both soot and NOx can be reduced simultaneously.

5.3. Pilot Injection

Benefits of split injection for emission reduction were discussed in previous section. In order to fully investigate the potential of multiple injection strategies, the effects of pilot injection followed by various main and post injection schemes are considered in this section.

5.3.1. Modeling Methodology

Totally, 12 different injection arrangements for which multiple injection cases with variable fuel amount for each pulse (up to 30% for the second pulse) and variable separation/dwell between pulses (up to 30˚ CA) have considered in this section. In addition, two more cases (including double and triple injections during main injection) were also evaluated which will be discussed in next section. The injection schemes used in this study are shown schematically in Figure 5.27.

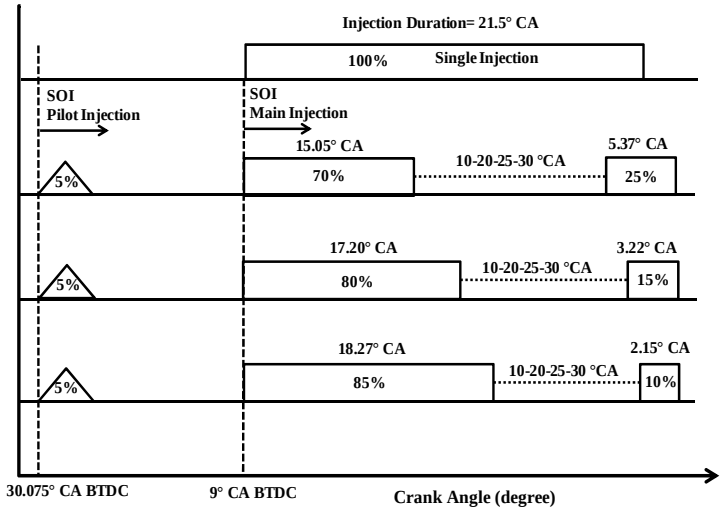

Figure 5.27 – Injection profiles for different multiple injection cases with pilot injection

Table 5.3 shows the parameters which were fixed for all injection cases. The same amount of fuel is injected in all the cases considered. Based on previous research which was done by Mobasheri et al. [135] at this operating points, the optimum separation for simultaneous reduction of soot with low NOx emissions was obtained by using 20°CA dwell delay between the injection pulses for split injection cases without pilot injection.

Table 5.3 – Computational conditions for studied cases

Total Fuel	0.1622 g/cycle
Pilot (SOI)	-30.075˚ ATDC
Pilot duration	1.075˚ CA
Separation*	30˚ CA
Main (SOI)	-9˚ ATDC
Main duration	21.5˚ CA

*The period between end of pilot injection and start of main injection

5.3.2. Results and Analysis

Figures 5.28 and 5.29 show the amount of soot and NOx emissions for different multiple injection cases for EGR levels of 0% and 10%, respectively.

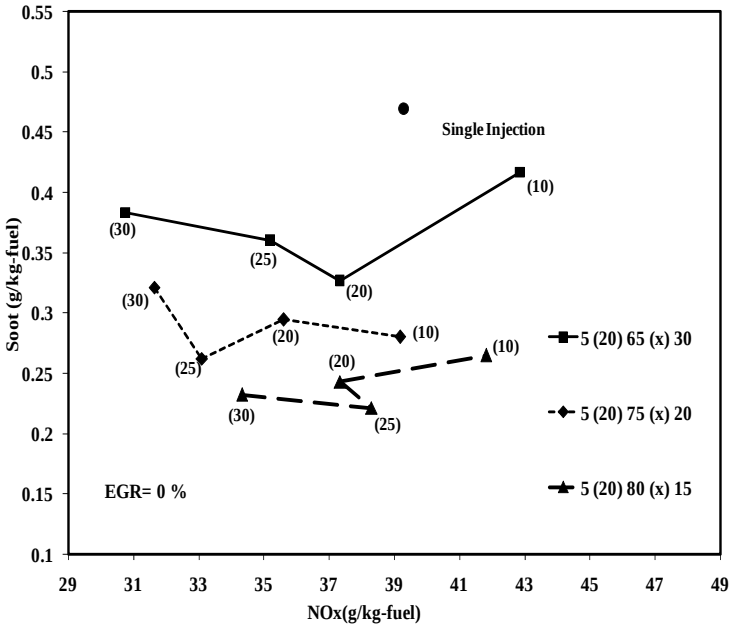

Figure 5.28 – Soot-NOx trade-off, Multiple Injection, EGR=0%

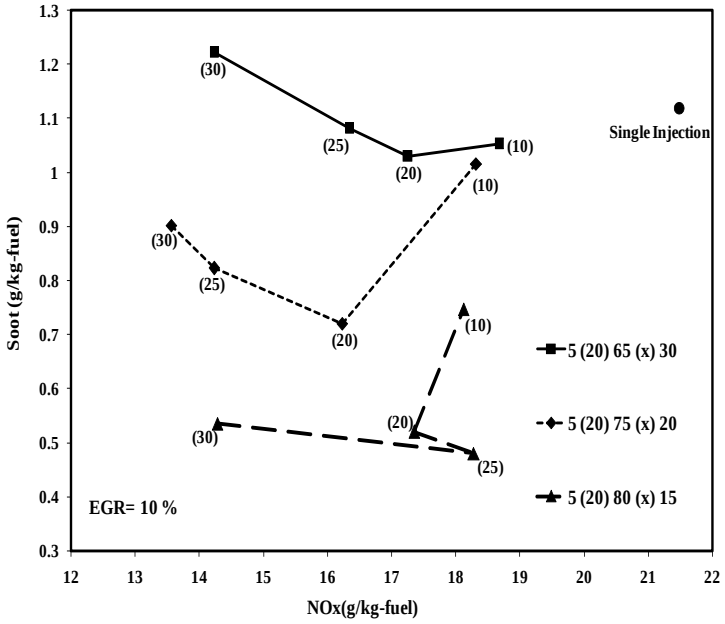

Figure 5.29 – Soot-NOx trade-off, Multiple Injection, EGR=10%

As illustrated in Figures 5.28 and 5.29, for multiple injection schemes both NOx and soot emissions decreased compared to single injection scheme in majority of cases. The pilot injection, which was set at about 30.075˚ CA BTDC, reduces the ignition delay and therefore the amount of premixed combustion, leading to lower temperatures

and NOx emissions. The results of Figure 5.29 confirm EGR's effectiveness at reducing NOx. In addition, Figure 5.29 shows the effectiveness of multiple injections at controlling soot emission under EGR conditions. It can be concluded that by using multiple injections the soot formation is occrued in the multiple regions in the combustion chamber and thus has more area for oxidation. Finally, the fuel that is pulsed into the combustion chamber after main injection ignites rapidly and thus will not contribute significantly to soot formation in high temperature rich regions.

Even though the EGR reduces some of the intake oxygen content, the heat added to the intake air enhances the soot oxidation to some extent which leads to reduction of soot emission. When the percentage of the second pulse injected fuel is larger than 75% of the total fuel, the NOx formation history of the multiple injection has a more impact to simultaneous reduction of soot and NOx emissions. This trend has also observed when 10 % EGR is used. It can be also concluded that the NOx chemistry is sensitive to the early combustion details because these combustion products stay at a high temperature for the longest time, and the combustion region is not cooled by the vaporization of the continuously injected fuel that occurs in the single injection case.

Figures 5.30 and 5.31 show ISFC versus NOx curves at 0% and 10 % of EGR for different multiple injection cases.

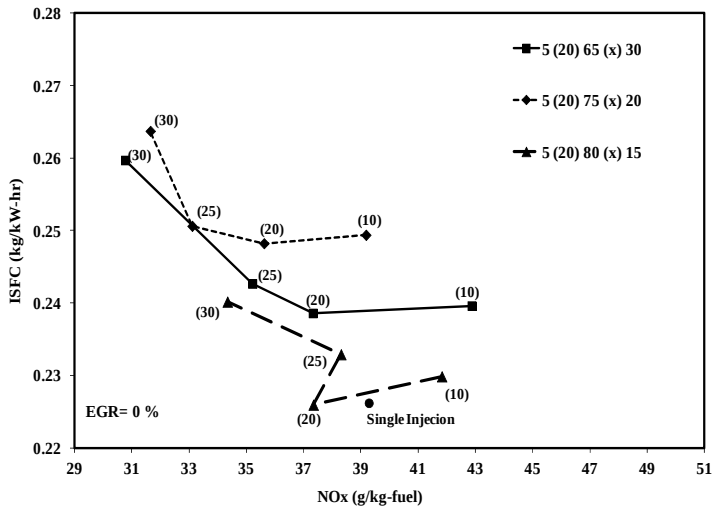

Figure 5.30 – ISFC vs. NOx trade-off, Multiple Injection, EGR=0%

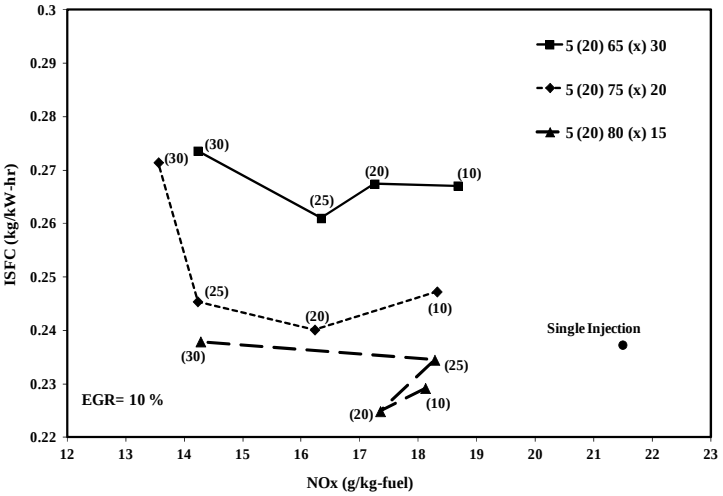

Figure 5.31 – ISFC vs. NOx trade-off, Multiple Injection, EGR=10%

Approximately the same trend of overall reduction of NOx emission and increase of ISFC could be observed in different cases, as illustrated in Figure 5.30 and 5.31, although this trend is kind of different for 25 CA dwell in 5(20)80(x)15 cases. From these results, it can be summarized that the optimum engine performance for reduction of soot and NOx emissions can be obtained with 25˚ CA and 30˚ CA delay between main and post injection pulses in the 5(20)75(25)20 and 5(20)80(30)15 cases, respectively.

Figures 5.32 and 5.33 illustrate the heat release rates for optimum split and multiple injection cases for EGR levels of 0% and 10%, respectively.

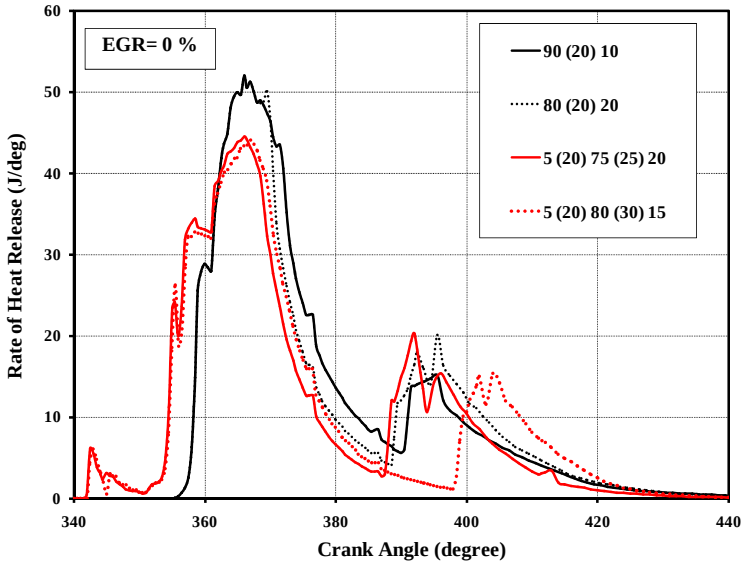

Figure 5.32 – The HRR curve, optimum injection cases, EGR=0%

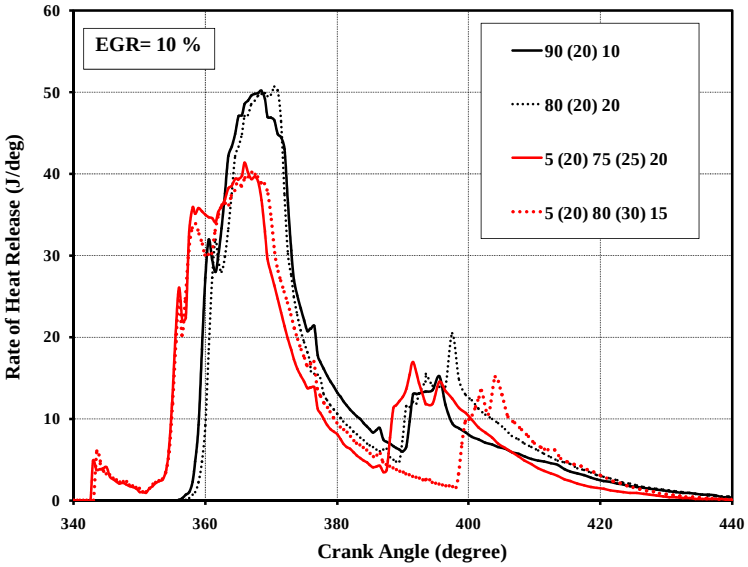

Figure 5.33 – The HRR curve, optimum injection cases, EGR=10%

As shown in Figures 5.32 and 5.33, the second fuel injection, occurred at the late combustion stage, affects the in-cylinder pressure and temperature that causes second peak in HRR diagram. In addition, splitting heat release by using triple injections

allowed reducing heat release maximum value to a lower one than with the split injection. The amount of injected fuel in each pulse and the delay between injections strongly affect the timing and magnitude of the second peak. As illustrated in Figures 5.32 and 5.33, the main combustion event usually has a short auto-ignition delay for multiple injection cases due to the high in-cylinder temperature produced by pre-combustion resulted of pilot injection. It can be seen that the second peak is significantly moved toward the expansion stroke for the 5(20)80(30)15 case. On the other hand, multiple injections is found to reduce NOx emission significantly since it reduces the magnitude of the combustion peak as seen in Figures 5.32 and 5.33.

Figure 5.34 and 5.35 show the cylinder temperature for optimum split and multiple injection cases for EGR levels of 0% and 10%, respectively.

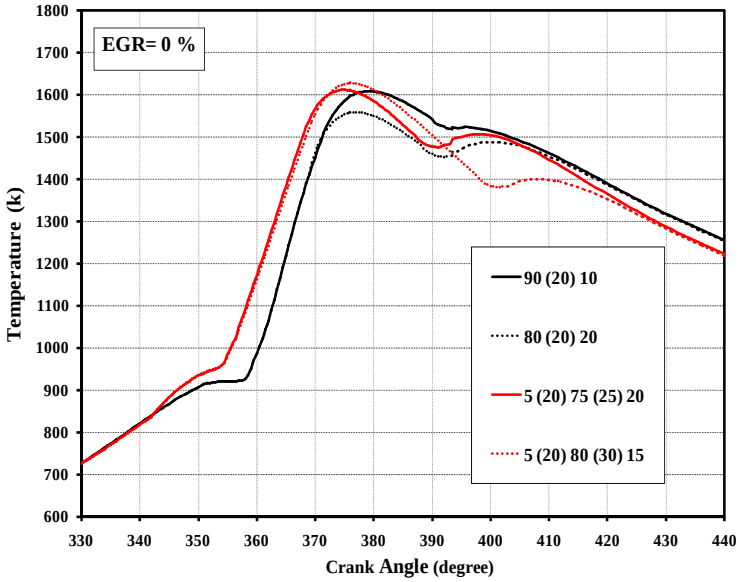

Figure 5.34 – In-cylinder temperature, optimum injection cases, EGR=0%

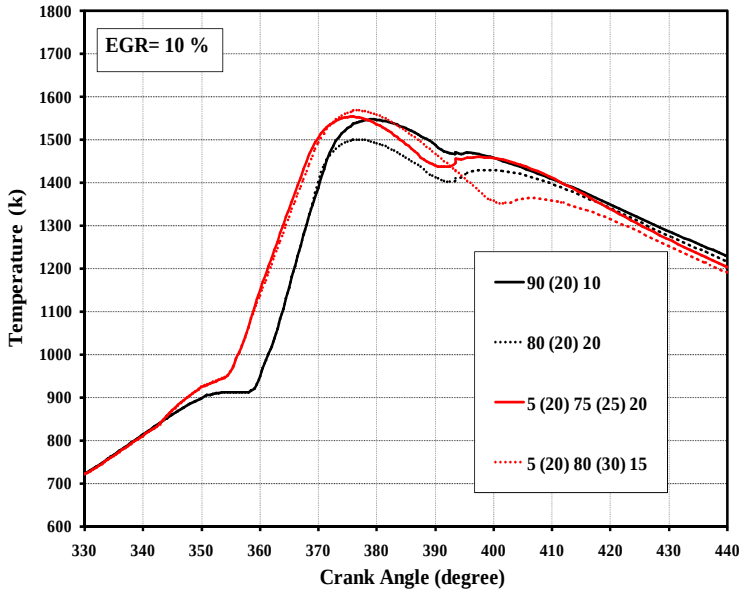

Figure 5.35 – In-cylinder temperature, optimum injection cases, EGR=10%

As can be seen in Figures 5.34 and 5.35, for the 5(20)80(30)15 case, the second peaks are lower than the other cases for both EGR rate. Moreover, for the 70(20)30 case, the first peak are lower than the other cases. In addition, after the second peak, the cylinder temperature tends to increase more in comparison with the other cases.

Figure 5.36 shows the velocity field contours for single injection case in comparison with the three optimum injection cases at 360, 385 and 410 CA.

As can be seen in Figure 5.36, the maximum velocity within the cylinder increases dramatically for the three optimum injection cases in comparison with the single injection case at 410 CA especially for 5(20)80(30)15 case. It can be concluded that multiple injection had a significant effect on flow filed and causes the subsequent effects on soot oxidization and NOx formation.

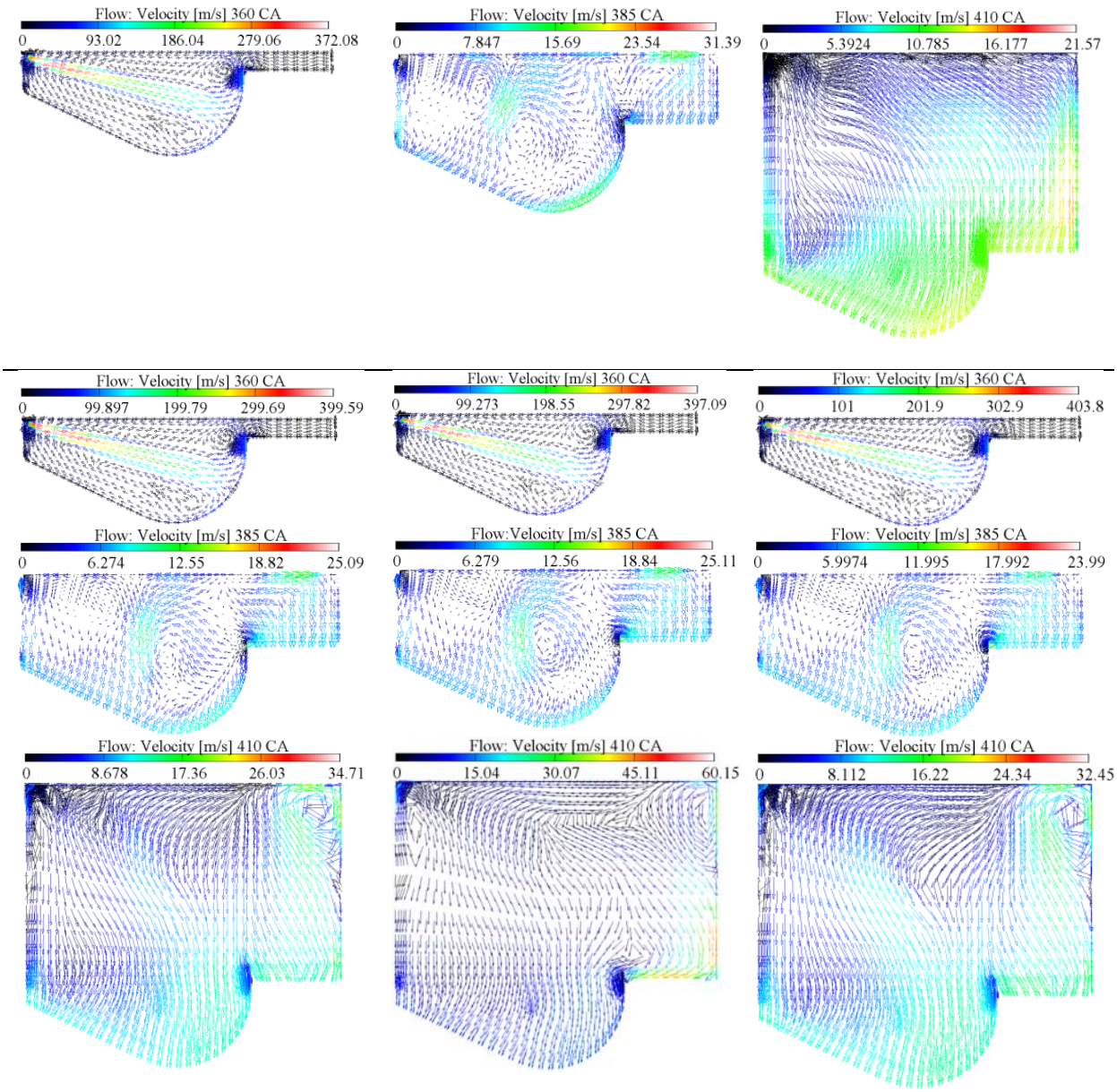

(80) 20 (20) 5 (20) 80 (30) 15 5 (20) 75 (25) 20

Figure 5.36 – The velocity fields contours, Single injection case (first row) in comparison with three optimum injection cases (three columns) at 360, 385 and 410 CA

The NOx distribution for the three optimum injection cases compared to single injection case are shown in Figure 5.37 at 370, 385 and 400 CA. Figure 5.38 shows the comparison of in-cylinder soot formations for the same operating points.

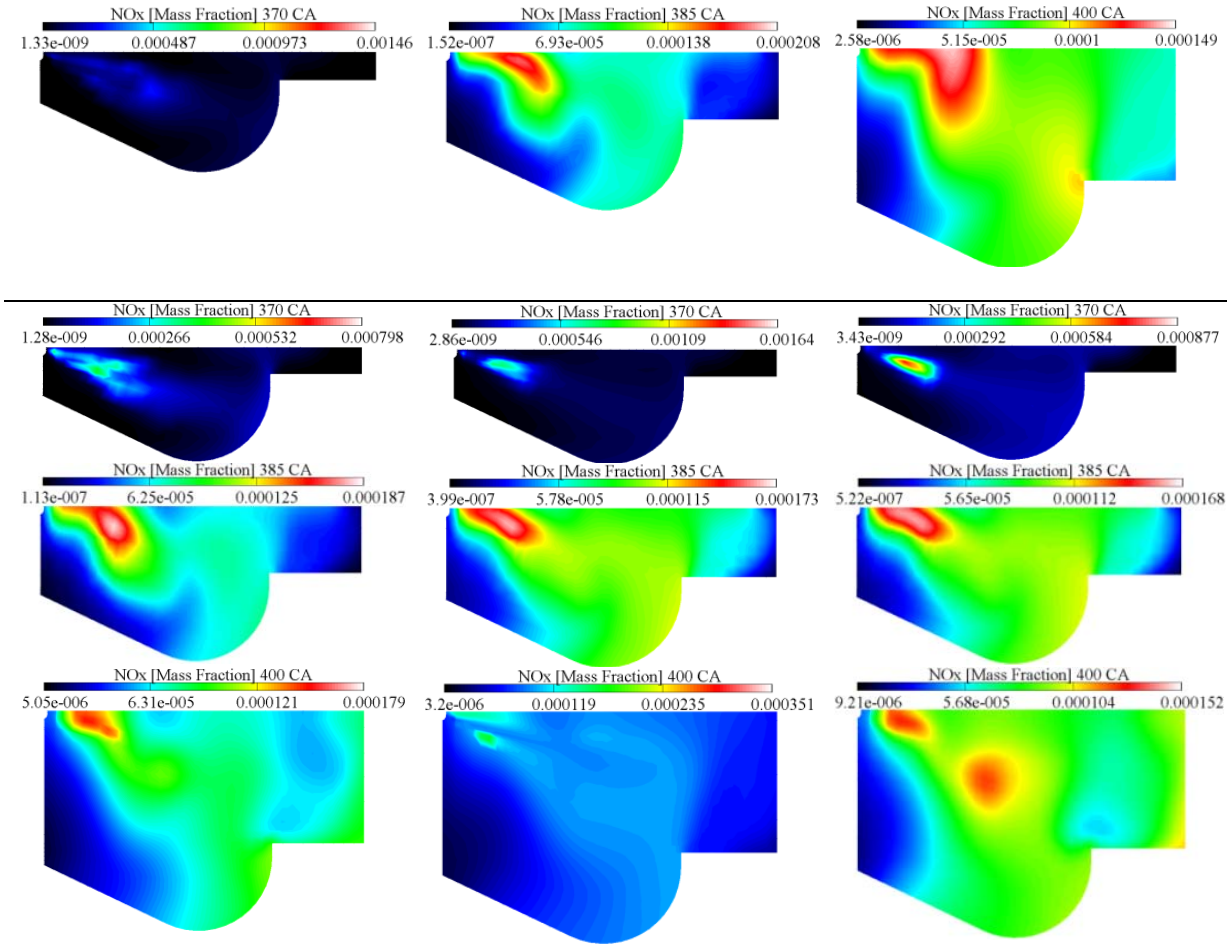

(80) 20 (20) 5 (20) 80 (30) 15 5 (20) 75 (25) 20

Figure 5.37 – NOx mass fraction contours, Single injection (first row) case in comparison with three optimum injection cases (three columns) at 370, 385 and 400 CA

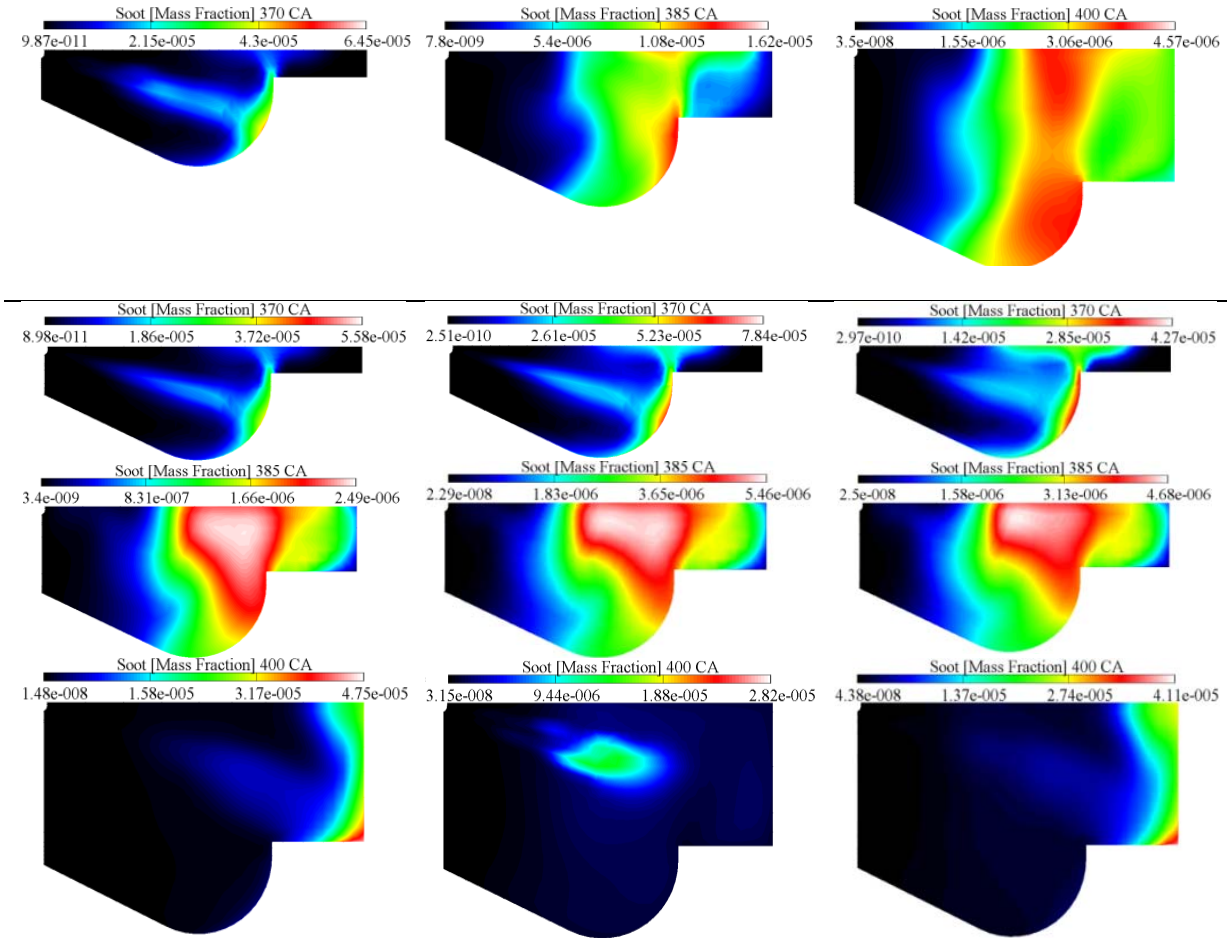

(80) 20 (20) 5 (20) 80 (30) 15 5 (20) 75 (25) 20

Figure 5.38 – Soot mass fraction contours, Single injection case (first row) in comparison with three optimum injection cases (three columns) at 370, 385 and 400 CA

As can be seen in Figure 5.37 and 5.38, the local soot-NOx trade-off is evident in these contour plots, as the NOx formation and soot formation occur on opposite sides of the high temperature region. It is widely reported that the combustion of single injection caused the rapid premixed combustion phases, because most fuel is injected during the ignition delay period under high ambient pressure and temperature conditions and, thus, is combusted immediately. For this reason, undiluted air-fuel mixtures and fuel-rich region exist locally in the combustion chamber, which usually causes the formation of harmful exhaust emissions and combustion noises. In the single injection

case, the soot formed in the later combustion phase is difficult to oxidize for two reasons. First, it is close to the end of the combustion period, and second, the temperature decreases rapidly in expansion stroke. In the same manner, the soot produced during the main combustion phase will not be oxidized easily for the lower temperature in-cylinder. It can be seen that for optimum injection cases, NOx and soot mass fractions are lower in comparison with the single injection case. It can be concluded that, for the split injection case, the second pulse injected fuel enters into a relatively lean and high temperature region which is remained from the combustion of the first pulse. Soot formation is therefore significantly reduced because the injected fuel is rapidly consumed by combustion before a rich soot region can accumulate.

The temperature distributions at two crank angle degrees for three optimum injection cases compared to single injection case are shown in Figure 5.39.

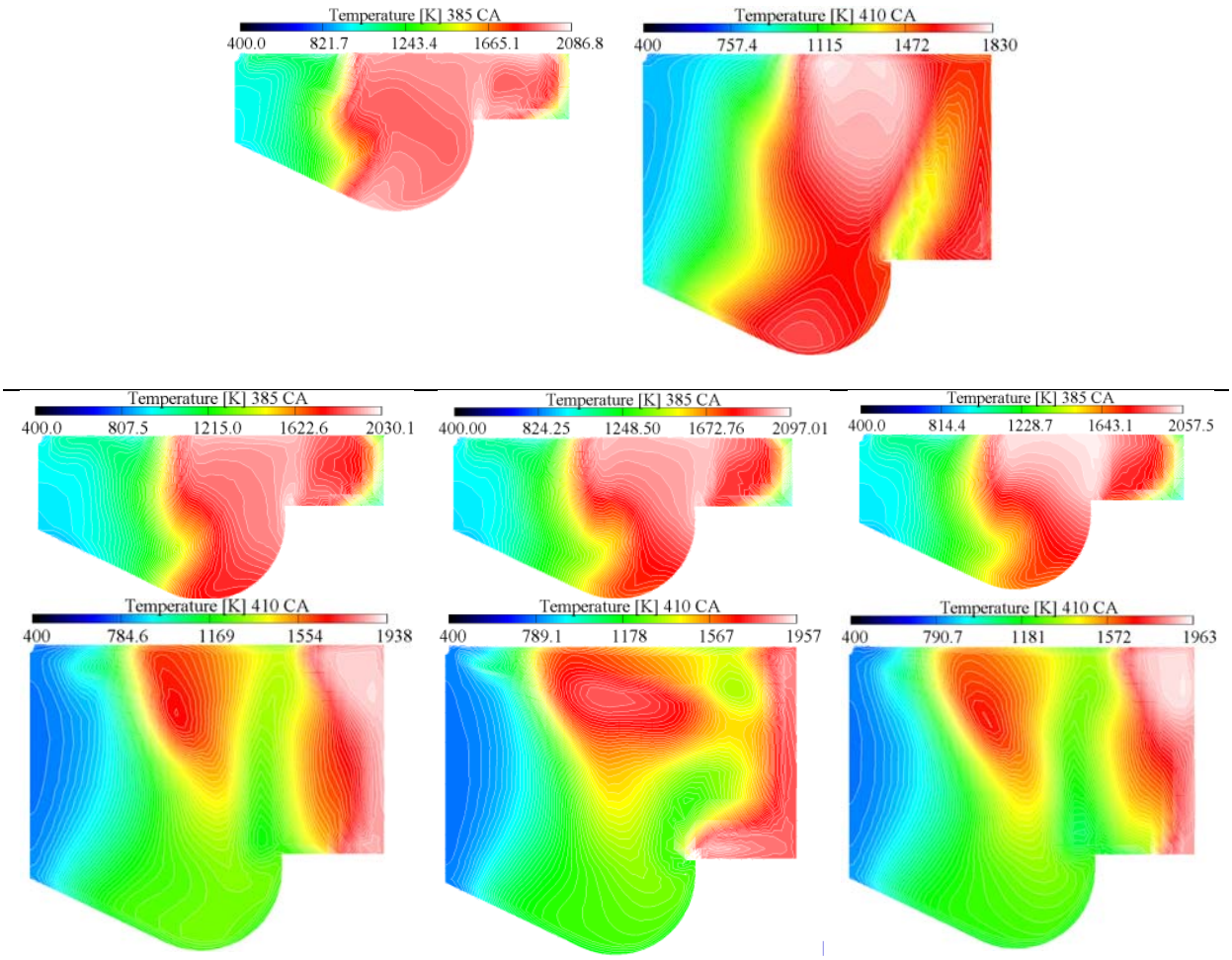

(80) 20 (20) 5 (20) 80 (30) 15 5 (20) 75 (25) 20

Figure 5.39 – Temperature contours, Single injection (first row) case in comparison with three optimum injection cases (three columns) at 385, 400 CA

As can be seen in Figure 5.39, at 410 CA the maximum temperature in optimum cases has a higher amount than single injection case. It can be concluded that injecting adequate fuel in post injection leads to the increase of temperature in late stage of combustion process that allows soot reduction without a NOx penalty rate.

5.3.3. Using Double and Triple Injections During Main Injection

The previous section has shown the potential of pilot and different multiple injection cases to reduce NOx and soot emissions. In this section, the main injection has divided in two and three pulses to explore its effects for more reduction of pollutant

emissions. For this purpose, two more injection schemes, as shown in Figure 5.40, has been proposed and considered based on optimum cases which were obtained in last section.

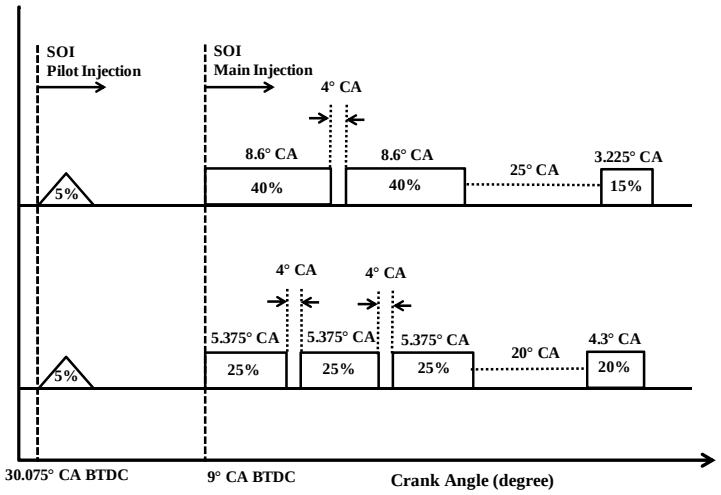

Figure 5.40 – Injection profiles for two multiple injection cases with double and triple main injections

Figure 5.41 shows the heat release rate diagram and temperature curves based on two injection strategies illustrated in Figure 5.40.

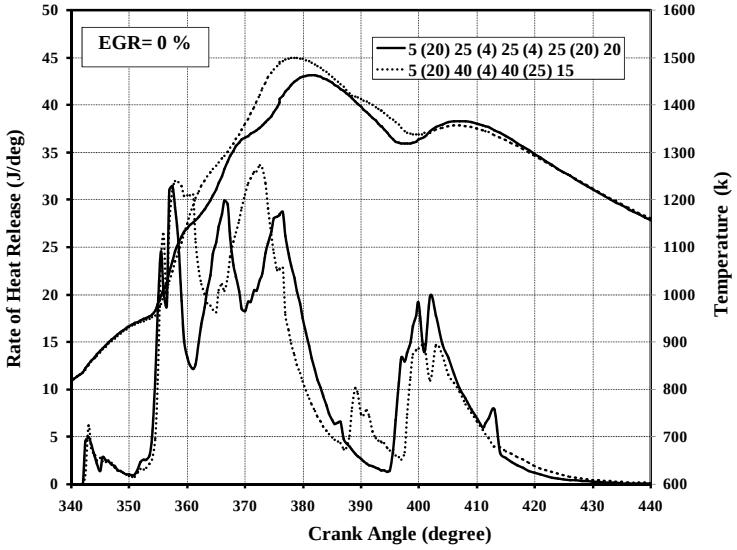

Figure 5.41 - Heat release rate and temperature for optimum multiple injection cases

It can be seen that due to double and triple injection during main injection the peak of HRR and temperature diagram is lower than multiple injection schemes which were previously considered. The amount of ISFC, NOx and Soot emission for these cases are summarized in Table 5.4.

Table 5.4 – Soot, NOx and ISFC for two multiple main injection cases

CASE	Soot (g/kg-fuel)	NOx (g/kg-fuel)	ISFC (kg/kW-hr)
5(20)25(4)25(4)25(20)20	0.242	28.43	0.2574
5(20)40(4)40(25)15	0.2311	30.21	0.2751

As can be seen in Table 5.4, two proposed injection cases can be more beneficial for the substantial reduction of NOx and Soot emissions, however the amount of ISFC in these cases should be considered as a main disadvantage.

The effects of optimum injection strategies on CO emissions are shown in Figure 5.42.

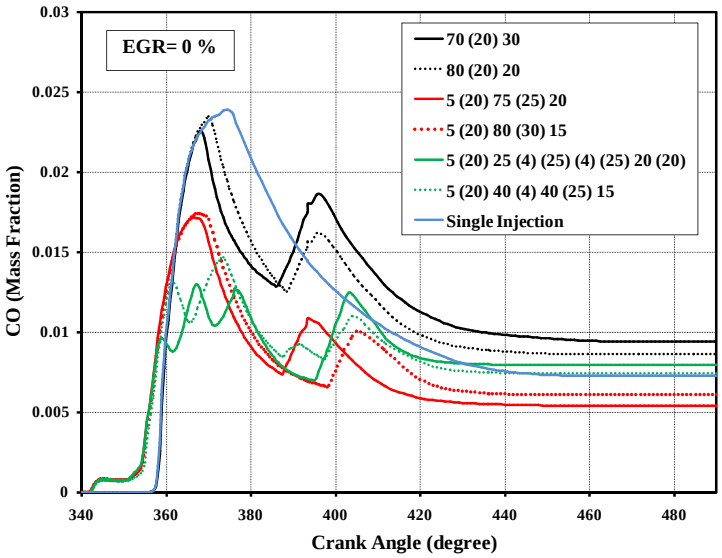

Figure 5.42 - Effects of multiple injection strategy on CO emissions

It can be seen that the concentration of CO emissions for two optimum injection case including 5(20)80(30)15 and 5(20)75(25)20 are generally lower than other cases. The reason for lower CO emissions can be considered to be that spray has relatively

better fuel atomization and air-fuel mixing, as well as a more complete combustion characteristic, which can be explained by the faster evaporation and vaporization of fuel spray droplets.

5.3.4. Summary

The effect of different multiple injection strategies on the improvement of fuel atomization and the reduction of exhaust emission characteristics was analyzed. These results compared with those from the single injection condition in a DI Diesel engine. The conclusions are summarized as follows:

- Investigation on multiple injection strategies showed the soot level can be dramatically reduced if an early pilot injection is combined with a main injection.
- Employing a post-injection combined with a pilot injection results in reduced soot formation from diffusion combustion and enhances the soot oxidation process during the expansion stroke, resulting in decreased soot emissions, while the NOx concentration is maintained in low levels.
- For majority of multiple injection cases, the amount of ISFC is increased compared to the single injection cases. This trend has also observed when 10% EGR is used. It can be concluded that applying multiple injection cases can be used as an effective tool to decrease the amount of soot and NOx emission but a fuel economy penalty is paid and this matter should be considered as a main barrier.

Chapter 6

Included Spray Angle in Conjunction with Multiple Injections

6.1. Background

As described in previous chapter, Mobasheri et al. [135-137] studied the effects of different split injection strategies on combustion process and pollutant formation. Their results showed that soot emissions can be reduced by split injections and this strategy also allows the injection timing to be retarded to reduce NOx emission. By using an optimum injection scheme with retarded injection timing and early pilot injection, both soot and NOx reduced simultaneously. The optimum separation for simultaneous reduction of soot with low NOx emissions was obtained by using 20°CA dwell delay between the main and post injection pulses. The present chapter builds upon the included spray cone angle concept and explores further their use in conjunction with multiple-injection strategies in a heavy duty common-rail DI diesel engine. Different included spray angles in conjunction with various optimum multiple injection strategies

are adopted for this assessment. The results presented in this chapter are partially based on [139, 140].

6.2. Engine Operating Conditions and Model Validation

The experimental data which was obtained from the University of Wisconsin-Madison [138] for a single-cylinder version of a Caterpillar 3401 heavy-duty DI Diesel engine were used in this study, as described in Chapter 5. The engine speed was kept constant for a part load operation at 1600 rev/min. A 60˚ sector mesh of the combustion chamber considering the fuel injector with six holes was used to calculate combustion and emission characteristics. The computational mesh was created using AVL ESE Diesel Tool [73]. The computational grid at top dead centre (TDC) is shown in Figure 6.1.

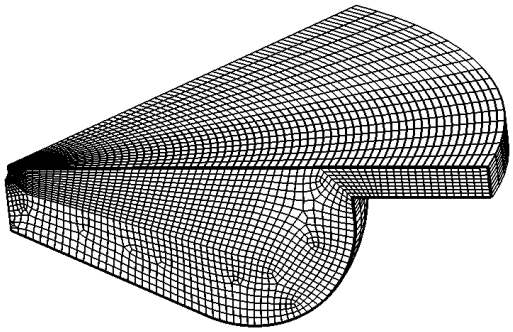

Figure 6.1 – Outline of Computational grids at TDC

Computations were performed from the intake valve close timing until the exhaust valve open timing. The ground of the bowl has been meshed with two continuous layers for a proper calculation of the heat transfer through the piston wall. The final mesh consists of a hexahedral dominated mesh. Number of cells in the mesh was about 34725 and 79311 at BDC and TDC, respectively. The present resolution was found to give adequately grid independent results.

Figure 6.2 shows comparisons between the predicted and measured in-cylinder pressure and heat release rate using the baseline included injection angle (125°). The result is based on the assumption of uniform wall temperature 425 K for the cylinder wall, 525 K for the cylinder head and 525 K for the piston top.

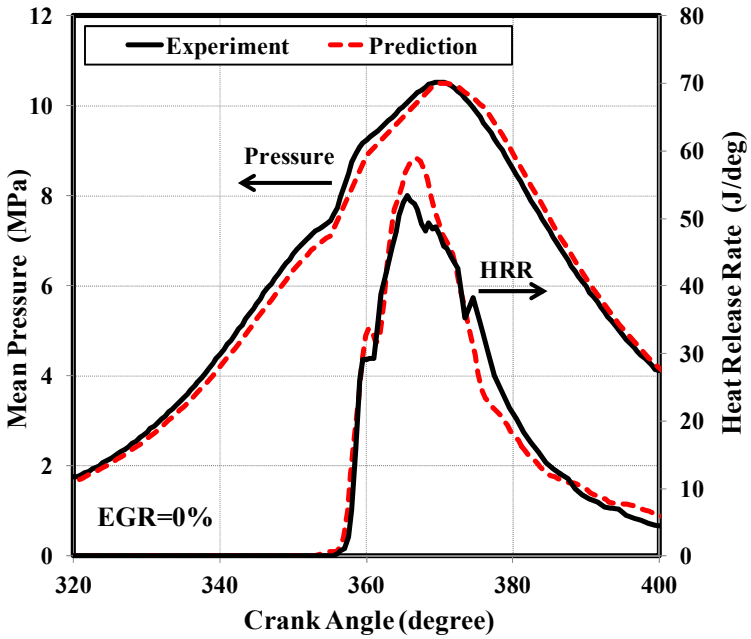

Figure 6.2 – Comparison of calculated and measured cylinder pressure and heat release rate using the baseline injection angle

The present model is seen to perform well for this conventional wide angle injector. In particular, the peak pressure and ignition delay are accurately predicted, although there are discrepancies in magnitudes, as can be seen in Figure 6.2. These discrepancies could be related to experimental uncertainties in input parameters to the computations such as the precise injection duration, start of injection timing and gas temperature at IVC.

The predicted soot and NOx emission were also compared with the measurement, as shown in Table 6.1. As can be seen in Table 6.1, the predictions agree

reasonably well with the measured values. The model also predicts correctly the decrease in NOx and increase in soot emission as EGR is increased.

Table 6.1 – Comparison the predicted and measured NOx and soot emission

Case	EGR= 0%	EGR =10 %
Measured Soot (g/kg-fuel)	0.47	1.12
Calculated Soot (g/kg-fuel)	0.46	1.18
Measured NOx (g/kg-fuel)	39.2	21.5
Calculated NOx (g/kg-fuel)	39.14	21.06

6.3. Effects of Included Spray Angle

In this study, three different types of included spray angles ($\alpha = 145°, 105°, 90°$) were studied to explore further their use in conjunction with various pilot and split pre- and post-TDC injection strategies. The main advantages for narrow included spray angles are the wider injection timing domain without cylinder liner wetting [9]. In order to make a full use of these advantages, effects of different early and post injection timings were chosen to be analyzed in this study.

Figure 6.3 shows a schematic diagram of fuel spray angles were studied in comparison with the baseline spray angle ($\alpha = 125°$).

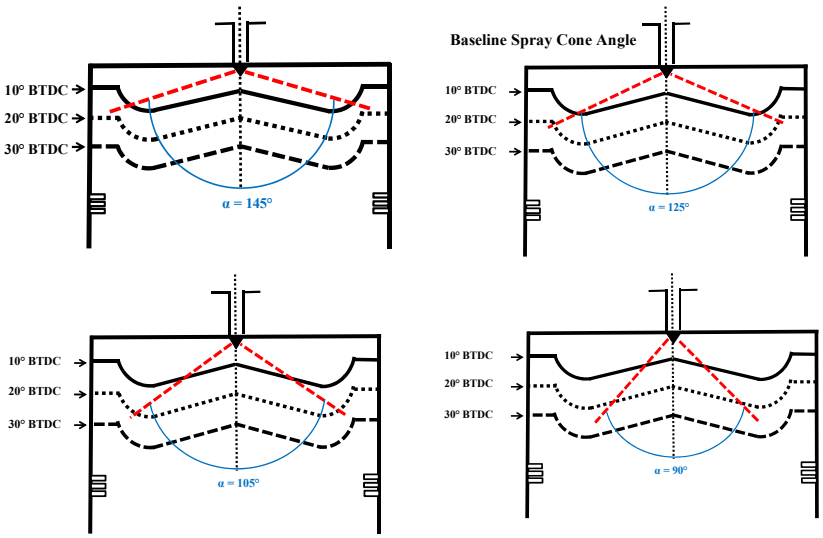

Figure 6.3 – Schematic diagrams of different types of studied included fuel spray angles ($\alpha = 145°, 105°, 90°$) compared to the baseline spray cone angle (125°)

Table 6.2 also shows the injection parameters and conditions which were fixed for all injection cases. It should be stated that all results reported in this study were investigated at a constant fuel injection rate and no model constants were changed during the computations.

Table 6.2 - Computational conditions for studied cases

Number of nozzle holes	6, equally spaced
Nozzle hole diameter	0.26 mm
SOP	30˚, 25˚, 20˚, 15˚ BTDC
Pilot duration	4.3˚ CA
Main (SOI)	9˚ BTDC
Main duration	21.5˚ CA
Spray pattern included angle	145˚, 125˚,105˚,90˚

6.3.1. Effects of Pilot Injection Timing with Various Included Spray Angles

A pilot injection timing sweep at constant injection pressure was performed to determine its effects on engine performance and emissions when different included spray angle have been applied. To study the effect of pilot injection timing, Start Of Pilot (SOP) injection timing was swept from 30° to 15° BTDC. For this purpose, a split injection strategy was employed, where approximately 20% of the fuel was injected in a pilot, while the remaining fuel was injected at a fixed timing of 9° BTDC.

The amount of soot and NOx emission with four types of included injection angles and different pilot injection timings is shown in Figure 6.4. Similarly, Figures 6.5 shows ISFC versus NOx curves for different included spray angles at same operating points.

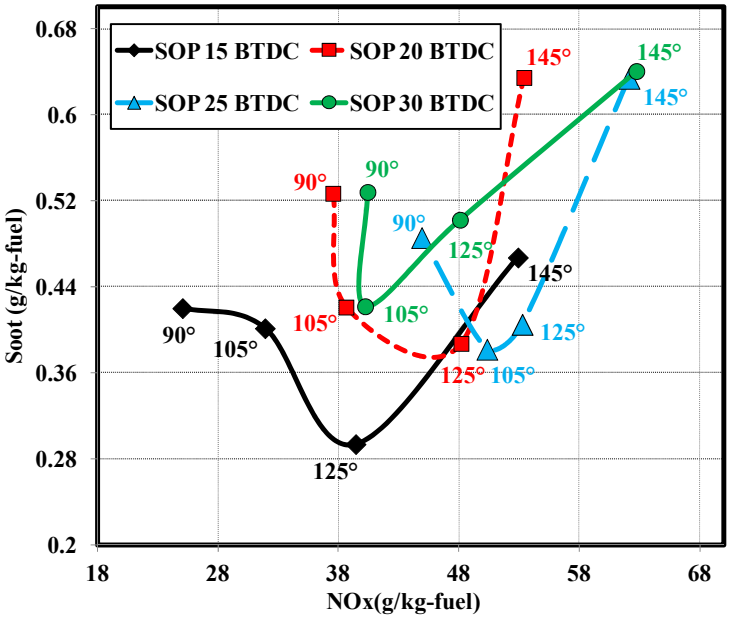

Figure 6.4 – NOx vs. soot trade-off for different included spray angles, as start of pilot varies and main injection timing is fixed at 9° BTDC.

As shown in Figures 6.4 and 6.5, in the case of using 105° included spray angle the best operating points has achieved compared to the conventional injection angle (α =125°). For the conventional wide 125° spray angle with advanced pilot injection timings, some of the spray will miss the piston bowl. It would be expected to have a negative impact on fuel-air mixing compared to the other configurations. As illustrated in Figure 6.5, approximately the same trend of overall reduction of NOx emission and increase of ISFC could be obtained in different cases.

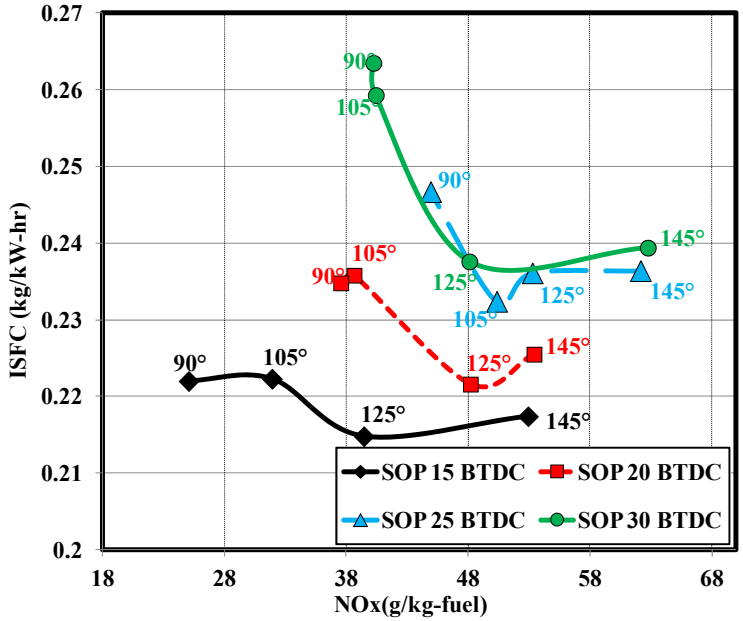

Figure 6.5 – ISFC vs. NOx trade-off for different included spray angles, as start of pilot varies and main injection timing is fixed at 9° BTDC.

Figures 6.6 and 6.7 illustrate the heat release rates and in-cylinder pressure traces for the SOP sweep with 125° and 105° included spray angles, respectively.

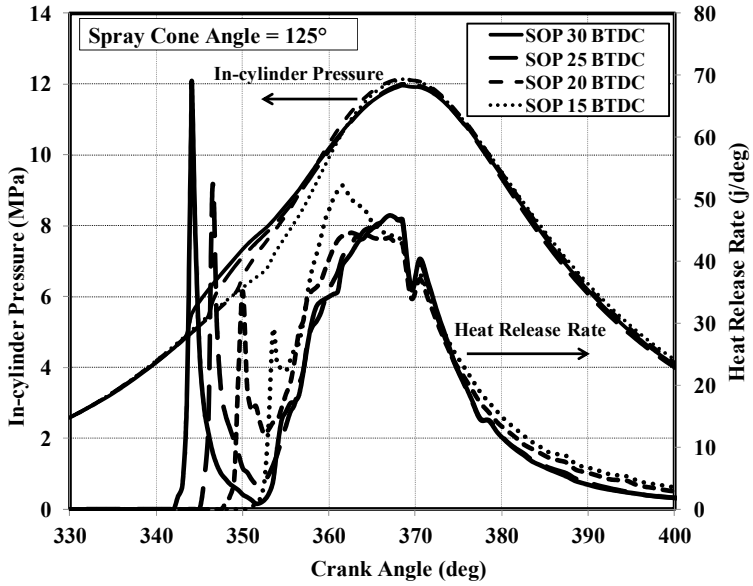

Figure 6.6 – Heat release rate and in-cylinder pressure for 125° included spray angle, as start of pilot (SOP) varies and main injection timing is fixed at 9° BTDC.

As SOP advances, the amount of pre-TDC combustion increases as shown in Figures 6.6 and 6.7. It can be concluded, as SOP is retarded to 15 CA BTDC, the ignition delay becomes shorter due to the higher ambient temperature, results in increased amount of diffusion burn and lower peak heat release rates and thus decrease in amount of NOx emission, as was shown in Figure 6.4. As a result, for earlier SOP timing, a sufficient mixing time is available to achieve a large portion of premixed mixture which produce the higher amount of heat released rate. The more advanced SOP timings produce a more homogeneous, locally fuel-lean in-cylinder mixture at the time of ignition since a sufficient mixing time is available to achieve a large portion of premixed mixture. However, at the most-advanced injection timing, SOP = 30° CA BTDC, the peak value of the HRR trace increases.

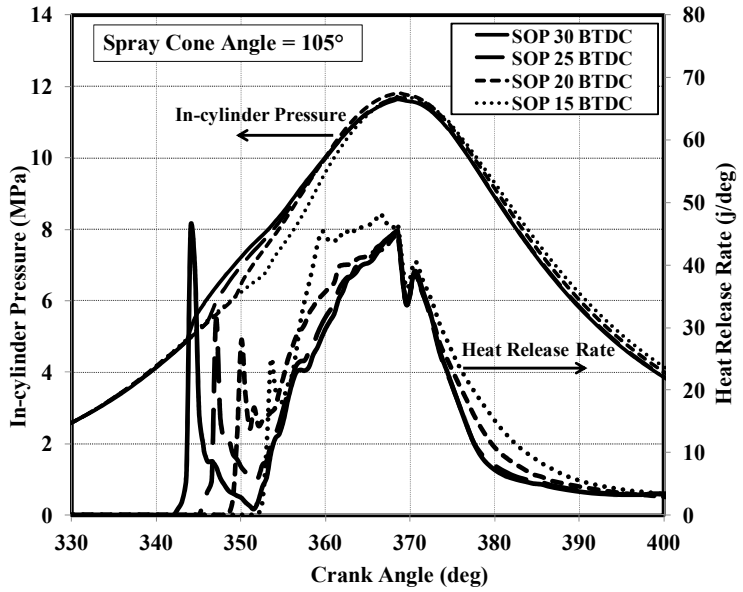

Figure 6.7 – Heat release rate and in-cylinder pressure for 105° included spray angle, as start of pilot (SOP) varies and main injection timing is fixed at 9° BTDC.

As demonstrated in Figure 6.7, the amount of heat release rate in pre-TDC combustion increases as pilot injection timing is advanced; this trend is similar to the observation made for the 125° included spray angle. More importantly, the first peak of

heat release rate for the 105° included spray angle decreases and thus 105° spray angle illustrate the possible benefit of advancing fuel injection for reduction of NOx emission.

6.3.2. Effects of Split Injection Timing with Various Included Spray Angles

Results obtained by Mobasheri et al. [135-137] indicated the effectiveness of multiple injection strategy to reduce NOx and soot emissions. In current section, three different injection arrangements for which split injection cases with variable fuel amount for each pulse (up to 30% for the second pulse) and all with 20˚CA separations have been studied to explore the effects of different split injection cases accompanied with various included injection angles.

Figures 6.8 and 6.9 show the amount of soot and NOx emissions for different multiple injection cases for EGR levels of 0% and 10%, respectively.

The labeling scheme for the multiple injection cases gives the percent of the fuel injected in the first and last pulses, and the dwell between two injections. For instance, 70(20)30 represents 70% fuel injected in the first injection pulse and 20 crank angle degree dwell between pulses, 30% fuel is injected in the second pulse.

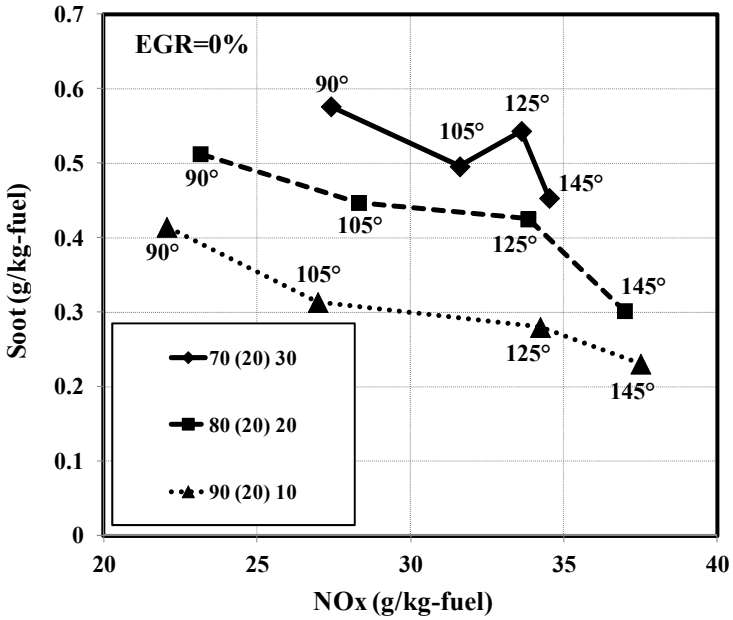

Figure 6.8 – NOx vs. soot trade-off for different multiple injection cases and various included spray angles, EGR=0%

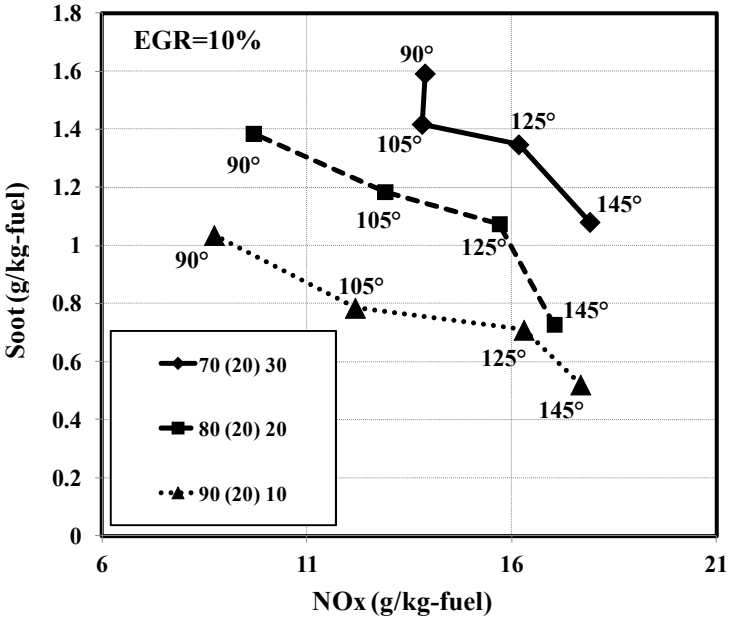

Figure 6.9 – NOx vs. soot trade-off for different multiple injection cases and various included spray angles, EGR=10%

From Figures 6.8 and 6.9, it can be summarized that the optimum engine performance for simultaneous reduction of soot and NOx emissions is achieved with 105˚ included spray angle. As illustrated in Figures 6.8 and 6.9, the wide included spray

angle (145°) shows the highest amount of NOx emission while the conventional included spray angle (125°) show some slightly lower of NOx emission. The narrowest angle of 90° show low NOx over the whole injection strategies, while the amount of soot emission is remarkably increased compared to the other configurations.

Figures 6.10 and 6.11 show ISFC versus NOx curves at 0% and 10 % of EGR using different multiple injection strategies and various included spray angles.

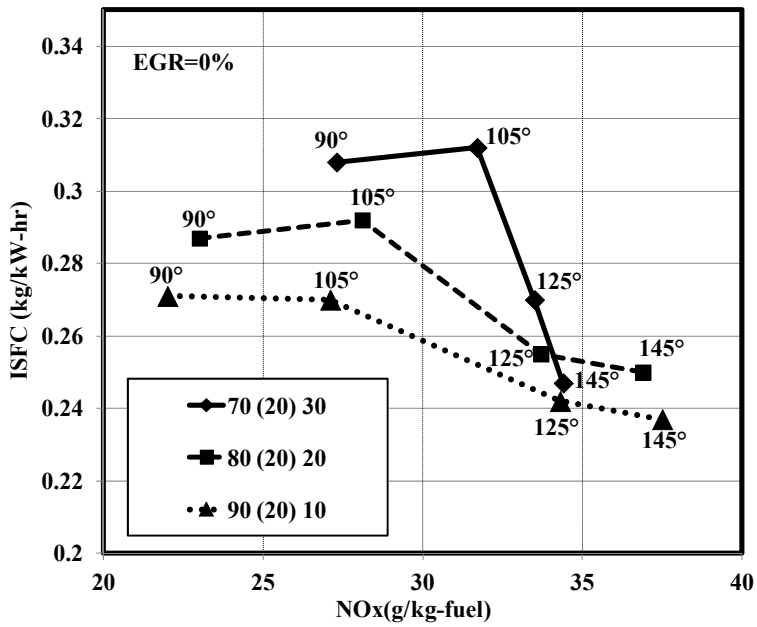

Figure 6.10 – ISFC vs. NOx trade-off for different multiple injection cases and various included spray angles, EGR=0%

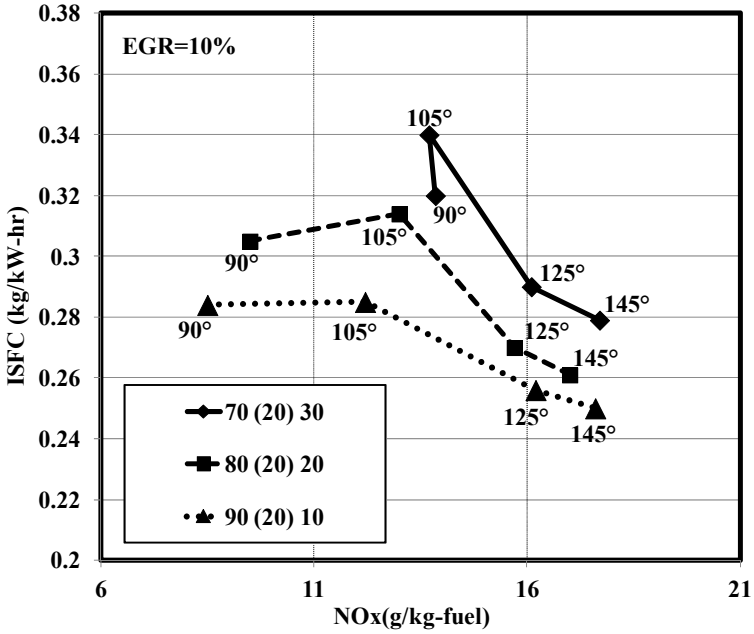

Figure 6.11 – ISFC vs. NOx trade-off for different multiple injection cases and various included spray angles, EGR=10%

It can be seen from Figures 6.10 and 6.11 that the amount of injected fuel in main and post injection pulses strongly affect the timing and magnitude of Indicated specific fuel consumption for different included spray angle configurations. As identified previously, the 105˚ included spray angle offers more advantages to reduce the amount of NOx emission since it allows improved spray targeting into the piston bowl at early timings, however the ISFC levels are slightly increased in this case compared to the conventional included spray angle (125˚).

Figure 6.12 shows the accumulated heat release for different included spray angles using the 90(20)10 injection strategy.

As illustrated in Figure 6.12, for all included spray angles using an optimum split injection strategy i.e. 90(20)10 caused that amount of injected fuel in each pulse and the delay between main and post injection strongly affect the timing and magnitude of the second peak in accumulated heat release traces.

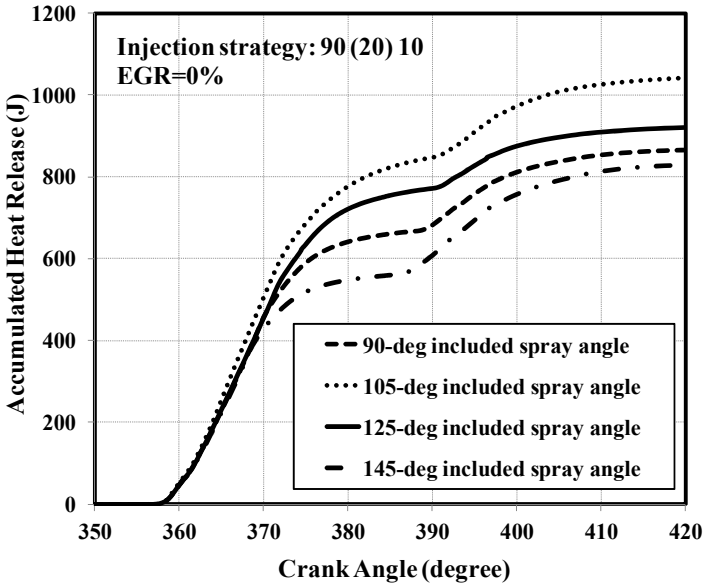

Figure 6.12 – Accumulated heat release for different included spray angles, 90 (20)10, EGR=0%

It can be concluded that in case of using split injection the main combustion event has a short auto-ignition delay due to the high in-cylinder temperature produced by pre-TDC injection pulse. As shown in Figure 6.12 in case of using 105˚ included spray angle the rate of heat released is higher than other cases. It can be concluded that in this case the conditions for a better mixture formation is provided because the spray is impinging close to the piston bowl. A higher level of accumulated heat release indicating a higher global temperature which helps to oxidize the soot in the late combustion stage. However, more decreasing of included angle leads to a reduction of accumulated heat release level, bringing an extra fuel consumption penalty, as described in Figures 6.10 and 6.11.

Figure 6.13 shows distributions of equivalence ratio for conventional included spray angle (125˚) in comparison with the 105˚ included angle for the optimum injection strategy i.e. 90(20)10 at 370, 380 CA.

The results showed in Figure 6.13 confirm that spray targeting is very effective for controlling the in-cylinder mixture distributions especially when it accompanied with a split injection strategies. As illustrated in Figure 6.13, narrow injection angle (105˚ included spray angle) offers more efficient air-mixing process due to better interaction with the combustion chamber and cylinder liner.

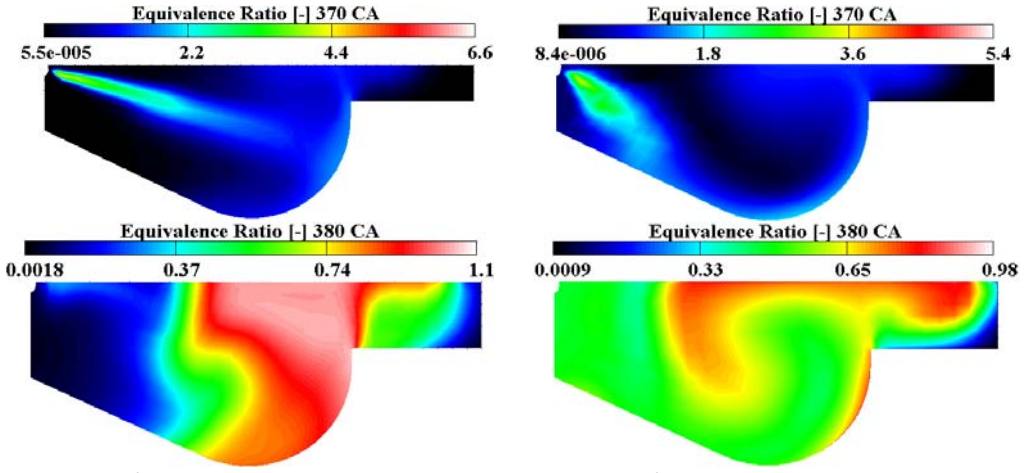

125˚ included spray angle **105˚ included spray angle**

Figure 6.13 – Equivalence ratio at 370 and 380 CA for the optimum injection strategy

Figure 6.14 shows the NOx emission contours for conventional included spray angle (125˚) in comparison with the 105˚ included angle for the optimum injection strategy i.e. 90(20)10 at 370, 380 and 390 CA.

As shown in Figure 6.14, for 105˚ included spray angle the fuel spray impinges at the edge of the piston bowl and a counterclockwise flow motion is generated that pushes mixture toward the center of the piston bowl along the piston bowl surface. As can be seen in Figure 6.14, the most important observation for 125˚ included spray angle is the spray wall impingement due to the wider included spray angle which caused a fuel deposition on the wall. This fuel deposition forms a higher fuel film on the wall surface.

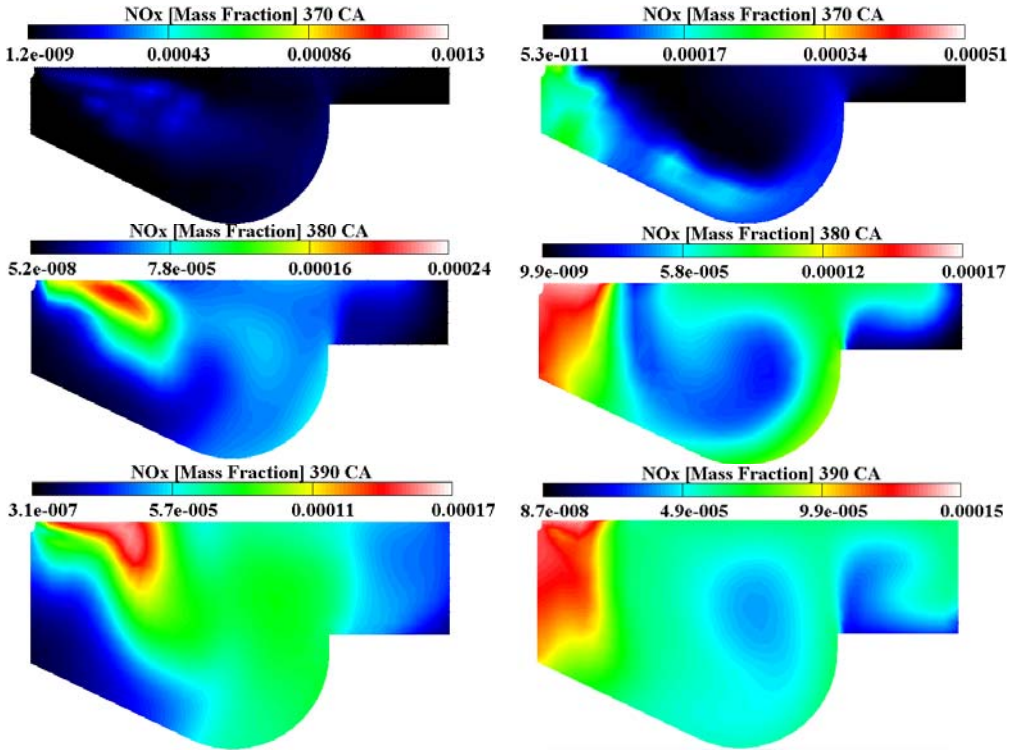

Figure 6.14 – NOx emission at 370, 380 and 390 CA for the optimum injection strategy

The soot distribution for conventional included spray angle (125˚) in comparison with the 105˚ included angle for the optimum injection strategy i.e. 90(20)10 at 370, 380 and 390 CA is shown in Figure 6.15.

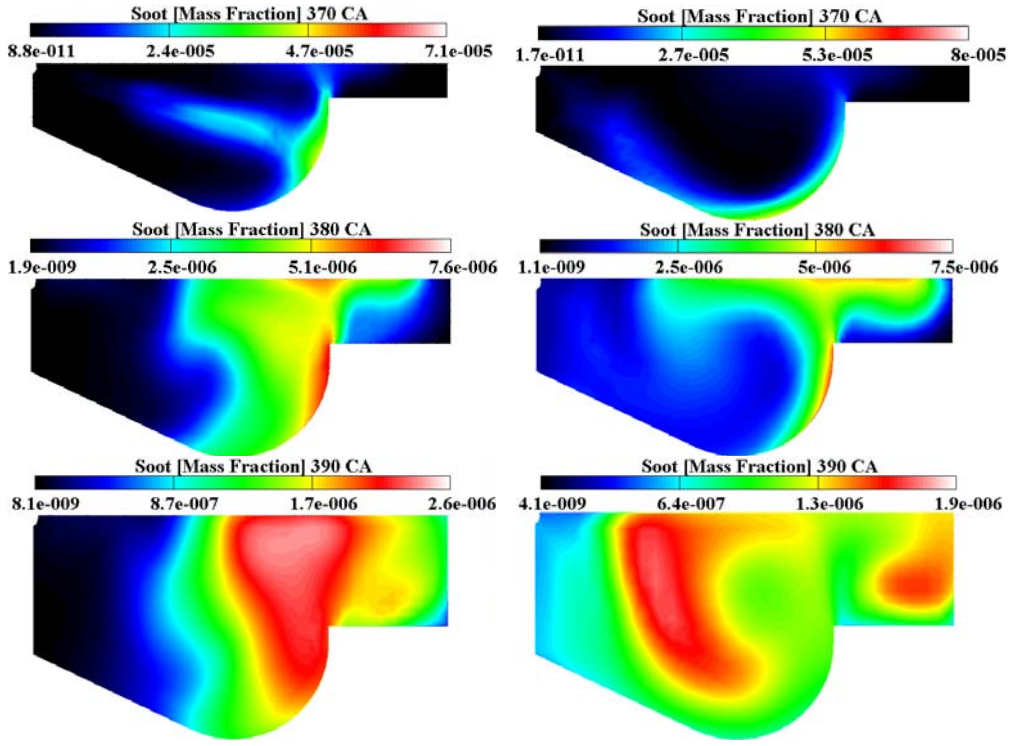

125˚ included spray angle **105˚ included spray angle**

Figure 6.15 – Soot emission at 370, 380 and 390 CA for the optimum injection strategy

The local soot-NOx trade-off is evident in Figures 6.14 and 6.15, as the NOx formation and soot formation occur on opposite sides of the high temperature region. It can be seen that for the 105˚ included spray angle case, NOx and soot mass fractions are lower in comparison with the conventional spray angle. The second fuel injection explains this discrepancy. The second pulse injected fuel enters into a relatively lean and high temperature region which is remained from the combustion of the first pulse. Soot formation is therefore significantly reduced because the injected fuel is rapidly consumed by combustion before a rich soot region can accumulate.

As illustrated in Figure 6.15, the 125˚ included spray angle experiences higher wall interaction compared to 105˚ included spray angle at different position crank angle. This observation suggests that the 125˚ included spray angle produces more soot emission.

Incomplete combustion products such as CO could result from either fuel lean or fuel rich conditions due to insufficient gas temperature to sustain combustion. To illustrate the source of CO emissions, Figure 6.16 shows the predicted distributions of CO emission at 370, 380 and 390 CA.

It can be seen that CO emission reside in the same region as soot and are due to the incomplete combustion of the fuel rich mixture where oxidizer is lacking. Because of fuel impingement and fuel film deposition for the 125˚ included spray angle, a quite rich region is formed in the near wall region due to less air available for mixing. The rich air-fuel mixtures result in CO formation in the near wall region.

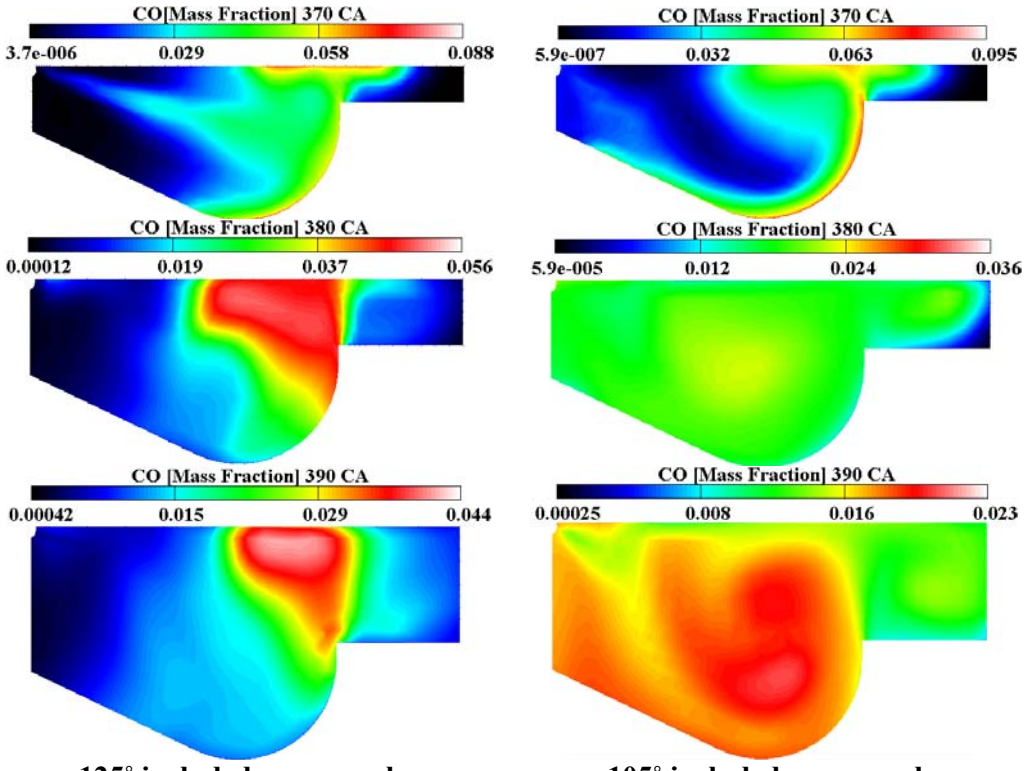

125˚ included spray angle **105˚ included spray angle**

Figure 6.16 – CO emission at 370, 380 and 390 CA for the optimum injection strategy

6.4. Conclusion

The goal of this study was to determine the influence of the different included spray angles on the emissions and combustion efficiency. The model was firstly calibrated against experimental data on a common rail DI Diesel engine. In this study, three different types of included spray angles ($\alpha = 145°, 105°, 90°$) were studied in comparison with the conventional spray injection angle ($\alpha = 125°$). The main findings can be summarized as follows:

- The computed in-cylinder pressure, heat release rate and amount of soot and NOx emissions were compared with measured data and good agreement between the predicted and experimental values was ensured the accuracy of the numerical predictions collected with the present work.

- As SOP advances, a sufficient mixing time is available to achieve a large portion of premixed mixture which produce the higher amount of heat released rate. The more advanced SOP timings produce a more homogeneous, locally fuel-lean in-cylinder mixture at the time of ignition. In spite of this advantage, both NOx and soot levels exceed development goals, thus suggesting that a narrower cone angle is required.

- The results showed that included spray angle can be an important factor influencing the heat release rate. Compared with the conventional included spray angle, $105°$ angle offers more flexibility for simultaneous reduction of NOx and soot emission since it allows improved spray targeting into the piston.

- In the cases of narrower injection angle, it was found that the fuel spray impinges at the edge of the piston bowl and a counterclockwise flow motion is generated that pushes mixture toward the center of the piston bowl along the piston bowl surface.

The optimum engine performance for simultaneous reduction of soot and NOx emissions was achieved with 105˚ included spray angle.

- The results show that spray targeting is very effective for controlling the in-cylinder mixture distributions especially when it accompanied with various injection strategies. It was found that 105° spray cone angle along with an optimized split pre- and post-Top Dead Center (TDC) injection strategy could significantly reduce NOx and soot emissions as compared to the wide spray angle. However, the BSFC levels are slightly increased. In addition, a narrow injection angle offers more efficient air-mixing process due to better interaction with the combustion chamber and cylinder liner.

Chapter 7

Combustion Chamber Geometry

7.1. Background

The combustion chamber geometry development in diesel engines, in order to improve the combustion quality, is an important step along the path to decreasing the engine specific fuel consumption and pollutant emissions. The effect of combustion chamber shape on the engine performance is very complex due to its influence on the flow field and the air-spray interaction. A proper choice of the combustion chamber design allows accelerating the combustion process, decreasing the cycle-to-cycle variations and improving the engine performance. In addition, combustion chamber geometry optimization is a very efficient tool for engine designers since no additional equipment (i.e., cost) is added to the engine. In this chapter, an investigation has been carried out to study the effects of re-entrant combustion chamber geometry on combustion process and pollutant emissions in a high speed direct injection (HSDI) diesel engine. The results of study are partially based on [141, 142].

7.2. Effects of Re-Entrant Combustion Chamber Geometry

In recent years, diesel engines have been widely used not only for commercial vehicles but also for passenger cars. The HSDI diesel engines has gained popularity in automotive applications relatively due to its low fuel consumption, durability, ever increasing power density, and improved drivability. However, the future of this success is threatened by regulations that call for continual pollutant emissions reductions. This has motivated researchers to review the basic strategies for combustion engines.

In current section, an advanced CFD simulation has been implemented with respect to its applicability for modeling a HSDI diesel engine to analyze the effects of re-entrant combustion chamber. For this purpose, 13 different types of combustion chamber configurations have been considered. For all the investigated configurations, bowl volume and squish clearance volume ratio were kept constant so that the compression ratio was the same for all investigated chambers. In addition, the selected operating points was achieved with a same injection profile for all considered cases, to avoid that the effects of changes in chamber geometry be masked by the effect of other engine parameters, e.g. injection timing and etc.

7.2.1. Model Validation

The computational mesh was created using AVL ESE Diesel Tool [73]. Details of the computational mesh used at TDC are shown in Figure 7.1. The computation used a 60˚ degree sector mesh (the diesel injector has 6 Nozzle holes). The ground of the bowl has been meshed with two continuous layers for a proper calculation of the heat transfer through the piston wall. The final mesh consists of a hexahedral dominated mesh. Number of cells in the mesh was about 61043 and 28453 at BDC and TDC,

respectively. The present resolution was found to give adequately grid independent results.

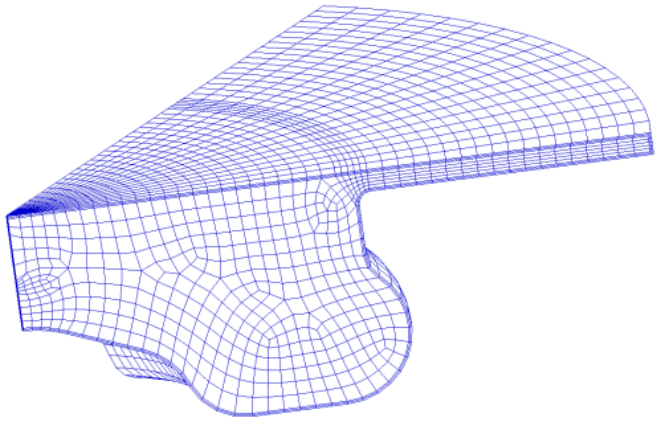

Figure 7.1 – Computational Mesh at TDC

A four cylinders, high speed direct injection (HSDI) diesel engine based on a Ford production engine with a 2nd generation Delphi common rail fuel injection system was modeled in this investigation. The required experimental data for this part of study was achieved from the Brunel University [143, 144]. Table 7.1 shows the overall specifications of the engine. The calculations were carried out for 1600 rev/min.

The specifications of the common rail injection system and the computation and experimental conditions which used for validation are also summarized in Table 7.2.

Table 7.1 – Engine specifications

Engine type	4-valve 2.0 L diesel engine
Number of cylinders	4
Bore	86.00 mm
Stroke	86.00 mm
Compression ratio	18.2:1
Connecting-rod length	160.00 mm
Squish height	0.86 mm
Piston shape	Re-entrant
Intake valve close timing	143˚ CA BTDC
Exhaust valve open timing	131˚ CA ATDC

Table 7.2 - Fuel injection system

Total injected fuel	20.5 mg
Pilot injected fuel	0.5 mg
Pilot injection timing	-30.65 ˚CA ATDC
Pilot injection duration	1.21 ˚CA
Main injection timing	-0.65 ˚CA ATDC
Main injection duration	10.45 ˚CA
Number of Injection Holes	6
Injector Hole Diameter	0.159 mm
Injector cone angle	154˚

Figure 7.2 shows both the computational and experimental in-cylinder pressure traces at 1600 rpm.

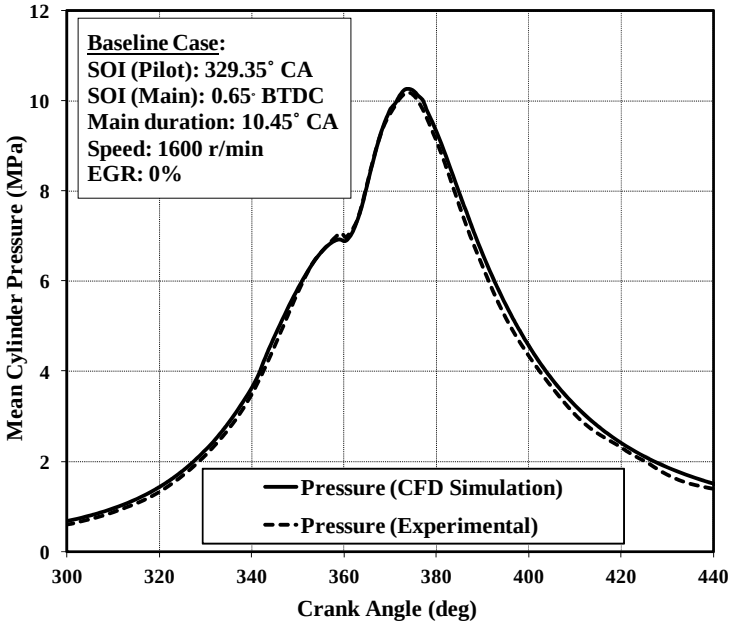

Figure 7.2 – Comparison of computational and experimental in-cylinder pressure trace at 1600 rpm

As illustrated in Figure 7.2, the simulated pressure data are in excellent agreement with the measured values. In particular, the simulation correctly models the time of auto-ignition and the peak pressures in this case. The peak pressure discrepancy between experiment and computation is less than 0.3%.

Figures 7.3 and 7.4 also show comparisons between the predicted and measured engine-out soot and NOx values.

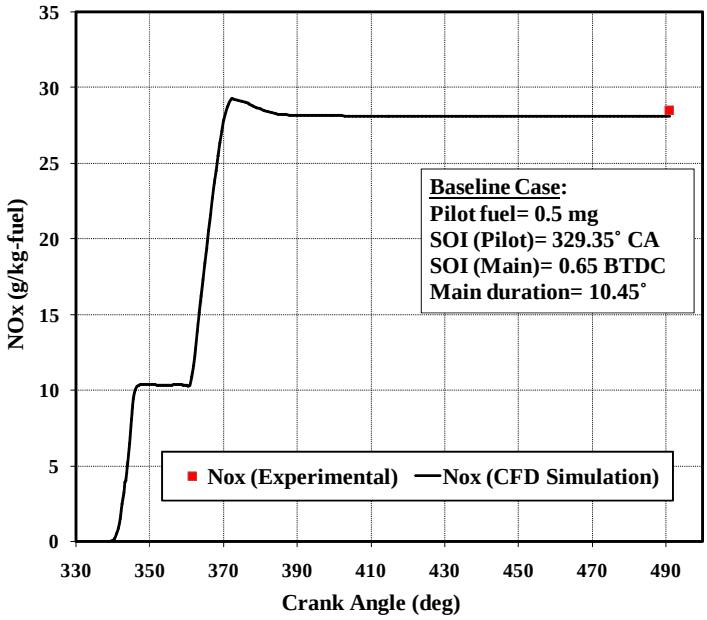

Figure 7.3 – Predicted total in-cylinder and measured engine-out NOx data

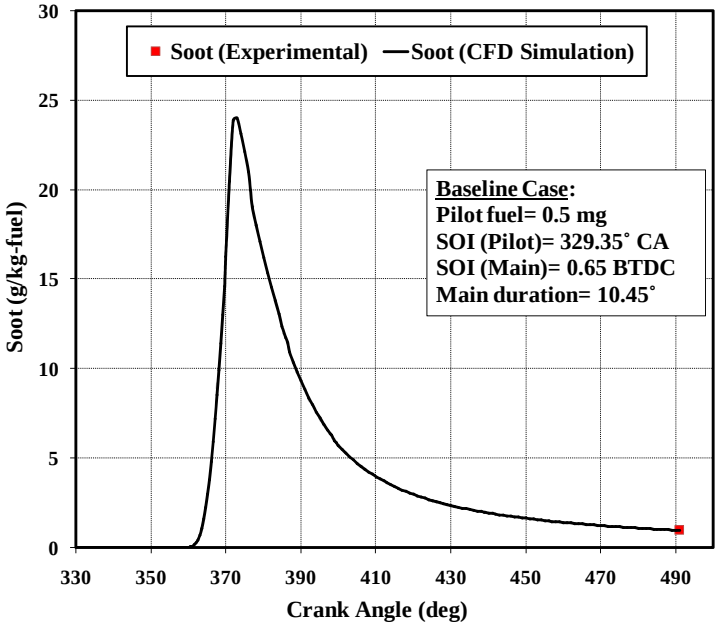

Figure 7.4 – Predicted total in-cylinder and measured engine-out soot data

As shown in Figures 7.3 and 7.4, the NOx and soot formation trends are very well reproduced by the presently adopted modeling approach. It can be seen that the calculated soot emission rapidly increased from the start of the combustion because

combustion occurred in fuel-rich regions. After that, soot is decomposed or oxidized gradually during the expansion stroke.

Based on the confidence obtained by the validation study, the investigation is further extended to analyze the effect of fuel injection timing on engine performance and emissions. For this purpose, three main injection timing, (1) 2.65 BTDC, (2) 0.65 BTDC and (3) 1.35 ATDC, all with 30 crank angle pilot separations were used to evaluate the effect of SOI.

Figures 7.5 and 7.6 show the in-cylinder NOx and soot emissions. The NOx and soot emission obtained for different injection timing is summarized in Table 7.3. It can be seen that the NOx was reduced with the retarding the injection timing, whereas the soot were increased with the retarding injection timing. In addition it can be concluded that the retarded injection timing lead to reduced oxidation of soot because the soot oxidation took place later in the expansion stroke when the gas temperature was lower.

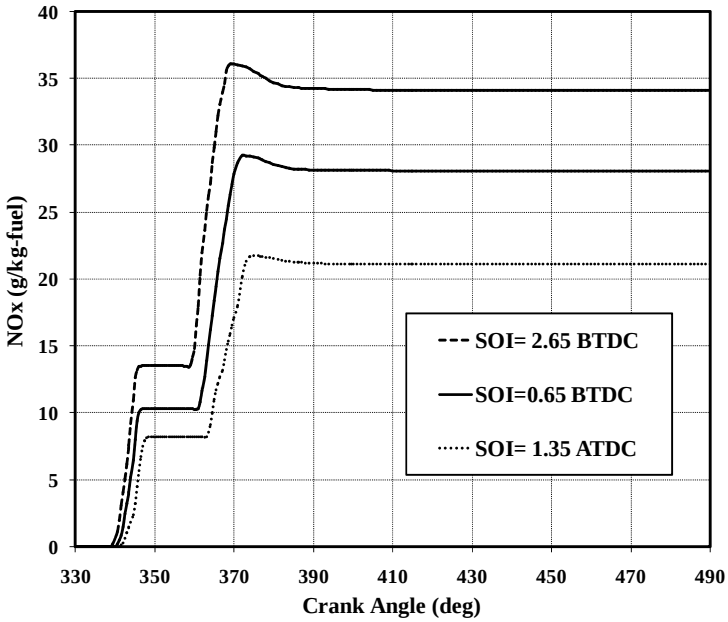

Figure 7.5 – NOx at different injection timings

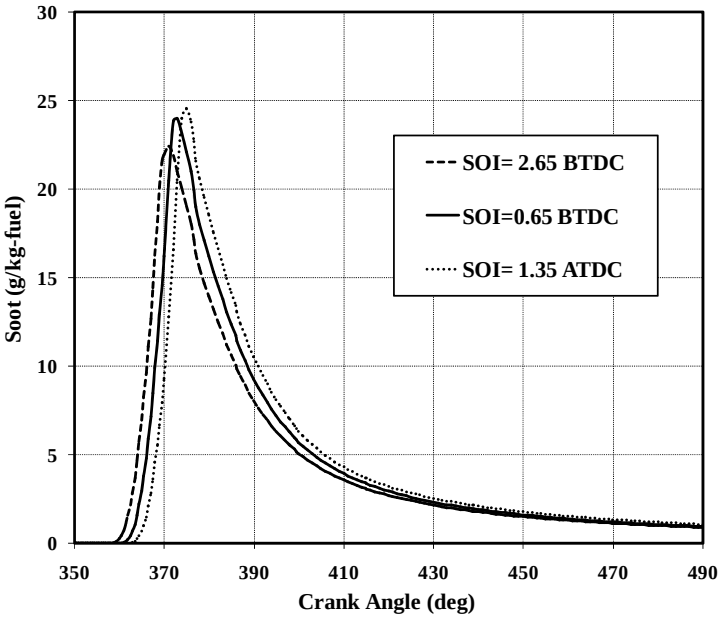

Figure 7.6 – Soot at different injection timings

Table 7.3 – Comparison of fuel injection timing on NOx and soot emissions

Start of main Injection (SOI)	NOx (g/kg-fuel) @ 491˚ CA degree	Soot (g/kg-fuel) @ 491˚ CA degree
2.65 BTDC	34.12	0.89
0.65 BTDC	28.092	0.94
1.35 ATDC	21.12	1.06

The predicted amount of soot and NOx emissions compared to their experimental values at different injection timing is illustrated in Figure 7.7.

Results shown in Figure 7.7 indicate that the optimum operating point to gain the best NOx-soot trade-off could be obtained by injecting fuel at 0.65° BTDC. Moreover, the results confirm that there is a good conformity between the experimental and computational data, and this shows that the models used in this study has sufficient capacity to predict the operating conditions of the engine.

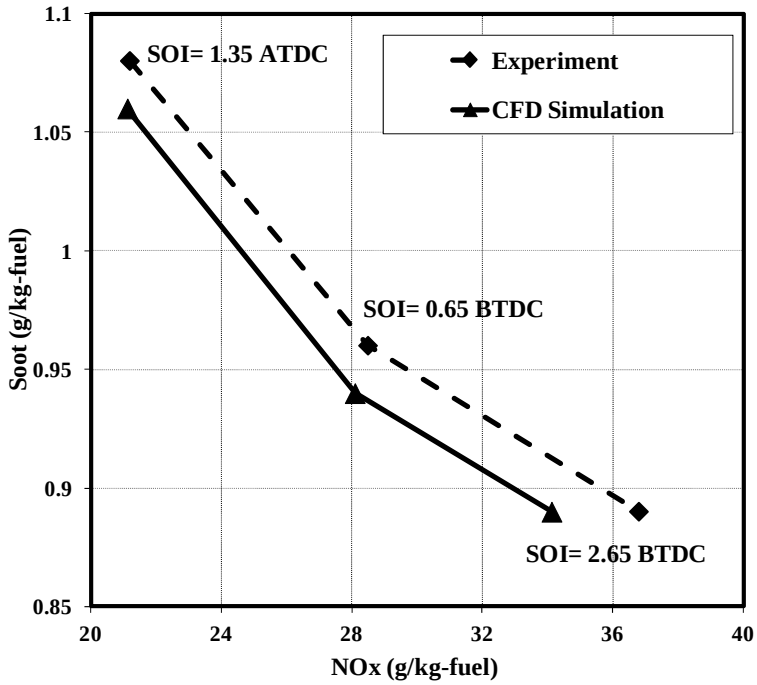

Figure 7.7 – The effect of injection timing on NOx and soot

The evolution of the NOx and soot distribution within the combustion chamber at 380, 400 and 420˚ CA ATDC is shown in Figure 7.8. As can be seen in Figure 7.8, NOx formation starts-off at the locations of the initial combustion onset and then continuously gets formed in fuel lean areas of sufficiently high temperature. In addition, soot is formed at the fuel rich side of the diffusion flame and cumulates at the outer bowl periphery close to the walls due to convective effects and delayed soot oxidation caused by wall cooling effects and lack of oxygen.

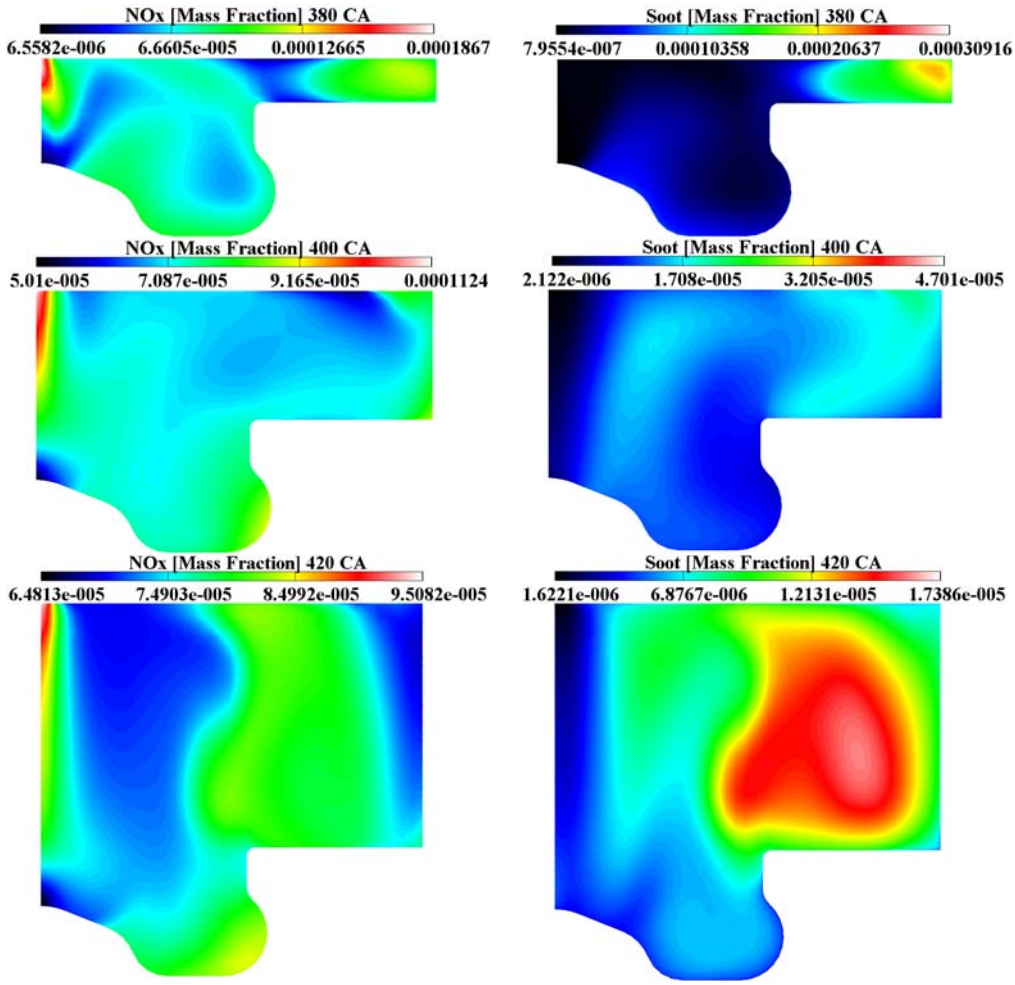

Figure 7.8 – Predicted NOx (first column) and soot (second column) mass fraction contours

Figure 7.9 illustrates some relevant in-cylinder quantities within the cylinder at 20˚ CA ATDC.

From the equivalence ratio contour in Figure 7.9, it can be seen that the injection process has already stopped and no significant amount of newly evaporating fuel is delivered to the in-cylinder charge any more. The evaporated fuel has homogenized, however, still a considerable degree of charge stratification can be observed, with equivalence ratio values up to 1.072 in the fuel rich zones. These have mainly got formed in the piston bowl ground due to the in-cylinder flow motion and the spray/vapor guiding effect of the piston bowl shape. During combustion, the initially fuel rich zones correlate very well with areas of high CO content, whereas the

combustion products in the near stoichiometric and slightly fuel lean areas are mainly consisting of CO_2 and to a less extend of CO.

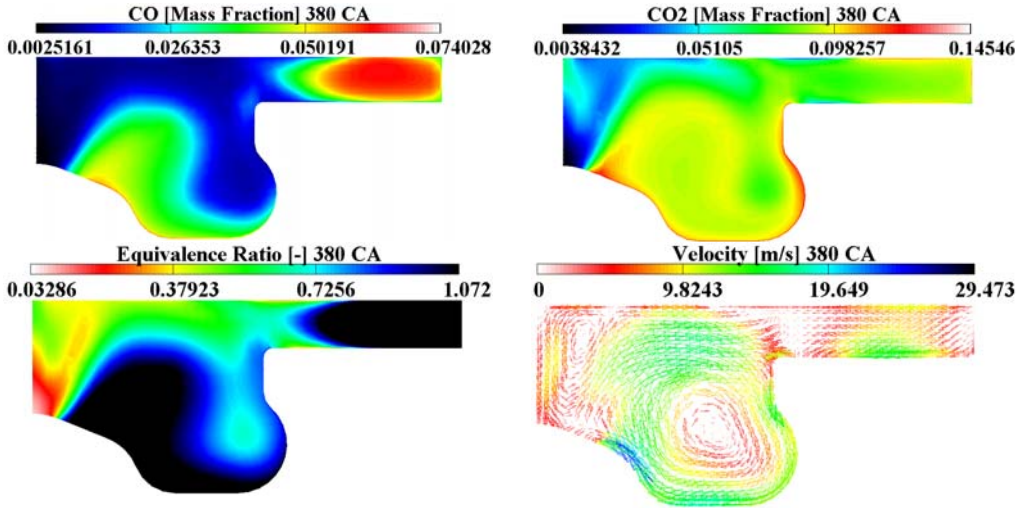

Figure 7.9 – CO (top left), CO_2 (top right),
Equivalence ratio (bottom left) and Velocity (bottom right)
concentration at 20˚ CA ATDC

Generally, there is a good conformity between the experimental and computational data, and this shows that the CFD code has sufficient capacity to predict this operating conditions.

7.2.2. Geometry Parameters

Typically, high-speed direct injection (HSDI) diesel engines use a re-entrant combustion chamber. The re-entrant shape strongly affects the fuel distribution along the combustion chamber wall and air–fuel mixing and therefore affects the emissions and performance. Figure 7.10 shows the schematic diagram of a re-entrant combustion chamber with the different geometry parameters which was analyzed in the present study. In this study, thirteen different geometries have been investigated at a part-load operation condition.

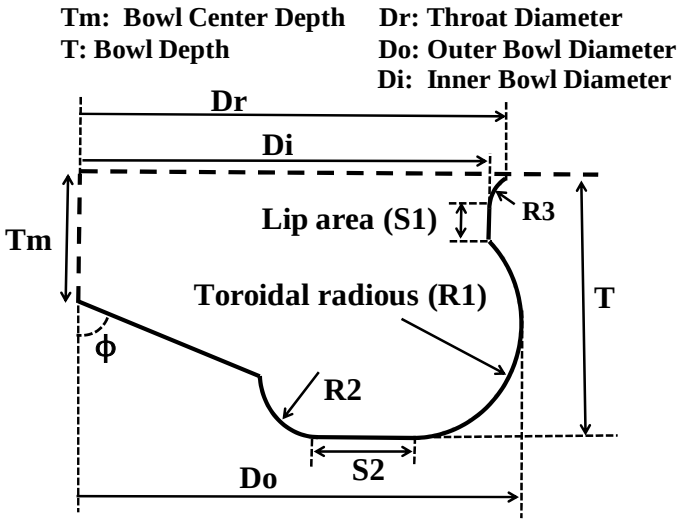

Figure 7.10 - A re-entrant combustion chamber

The geometrical configurations of these models are shown in Figure 7.11. The different parameters varied in the current optimization are listed in Table 7.4, along with each parameter's range.

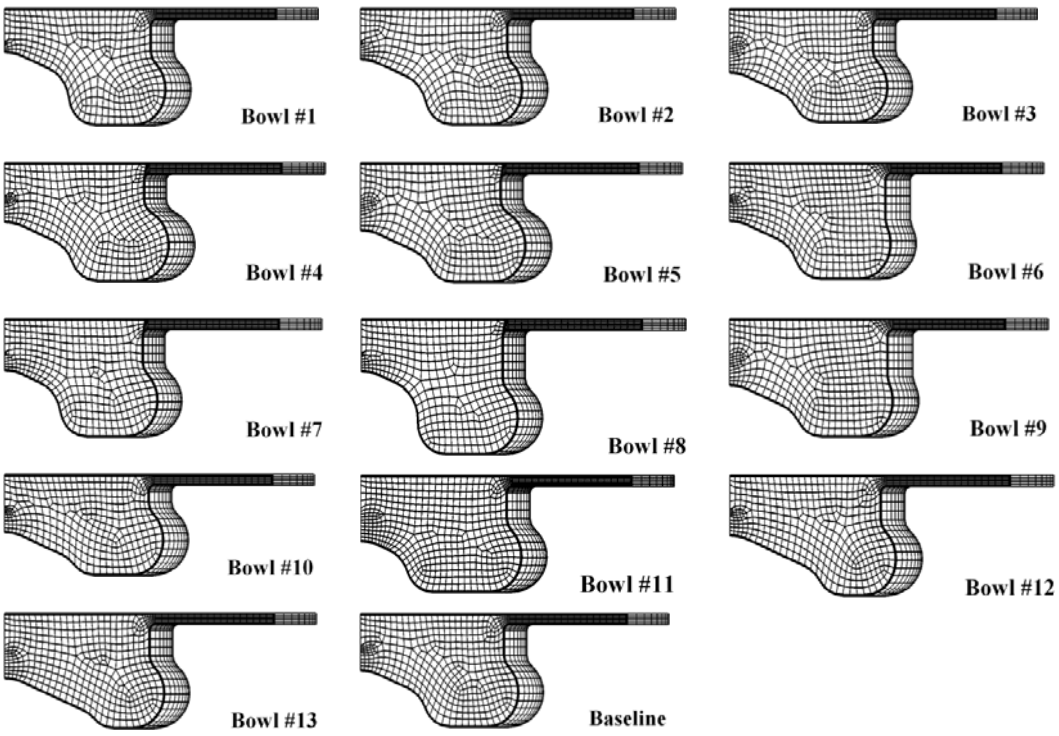

Figure 7.11 – Proposed combustion chamber configurations compared to the baseline case

Table 7.4 – List of optimization parameters and their ranges

Parameters	Range
Tm (mm)	4.52 - 7.52
T (mm)	12.42 - 16.42
Dr (mm)	45.20 - 51.20
Do (mm)	48.20 - 51.20
Di (mm)	43.56 - 49.56
S1 (mm)	1.46 - 5.46
S2 (mm)	3.3 - 9.3

It should be noted that although changes in geometry occur, grid resolution and quality remain unchanged for all investigated cases.

In area of piston design, it is very difficult to change one independent variable without effecting a change in another independent variable. When this is the case, the dependant variables will reflect the net effects of change in both independent variables. For this purpose, in three following sections, the effects of different geometry parameters has been classified and studied based on three categories including piston bowl depth, piston bowl width as well as piston bottom surface and lip area.

7.2.3. Piston Bowl Depth

One of the most dominant physical characteristics of the combustion chamber geometry is piston bowl depth. The effect of this parameter are presented and discussed in the following section.

In Figure 7.12, the NOx emission is plotted as a function of piston bowl depth. For this investigation the bowl depth and bowl center depth was changed from 12.42 to 16.42 mm and 4.52 to 7.52, respectively.

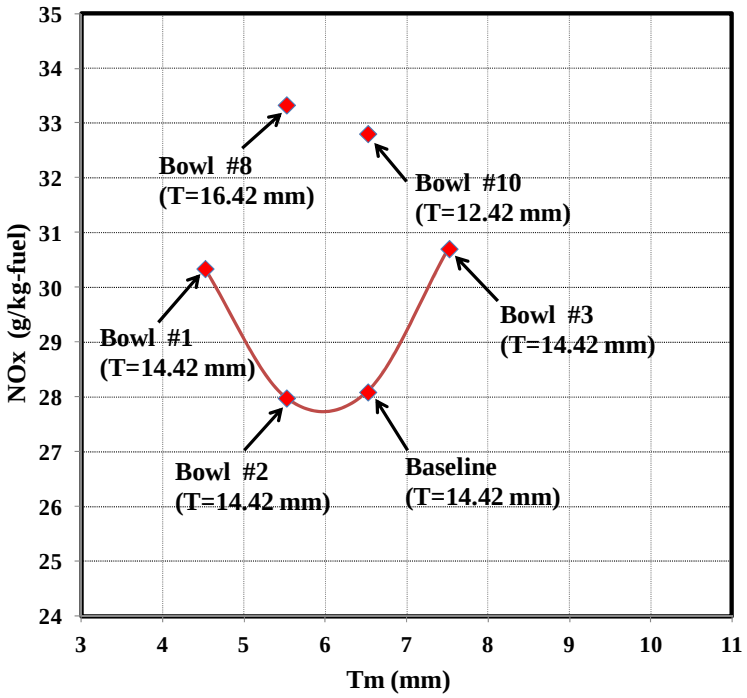

Figure 7.12 – Piston bowl depth effects on NOx emissions

As shown in Figure 7.12, the Bowl #8 and Bowl #10 produce the highest NOx emission compared to other cases. A slightly better operating condition has been obtained with Bowl #2 which has the same bowl depth as baseline case while its bowl depth center is lower than baseline case.

Figure 7.13 plots the soot emissions of various models as a function of piston bowl depth. Similarly, Figure 7.14 shows the effect of piston bowl depth on Indicated specific fuel consumption.

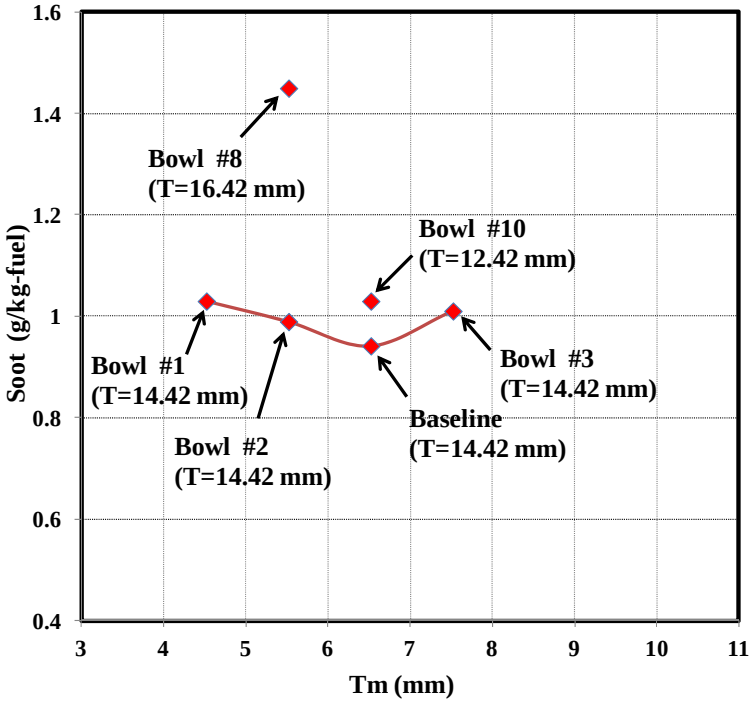

Figure 7.13 – Piston bowl depth effects on soot emissions

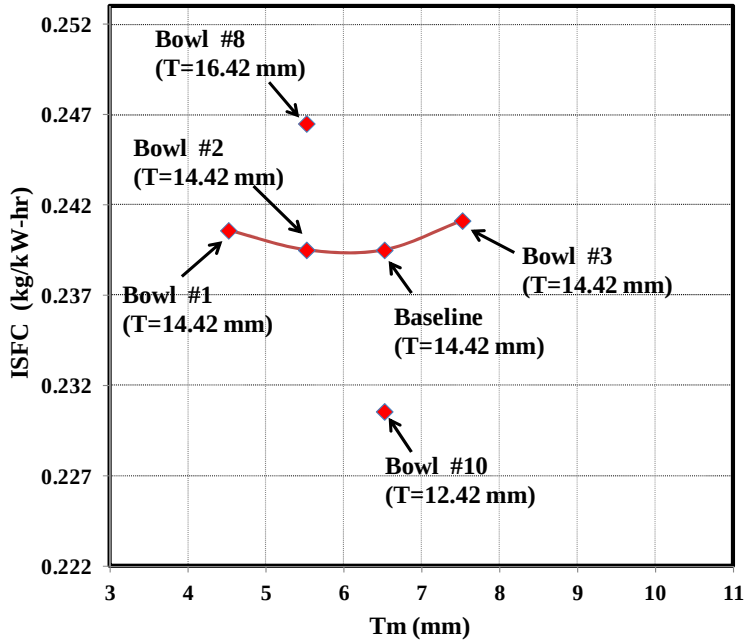

Figure 7.14 – Piston depth effects on ISFC

As can be seen in Figure 7.13, the soot emission still appears to decrease with increasing piston center depth. In addition, as illustrated in Figure 7.14, the higher fuel

consumption rate could be observed when the bowl depth is increased to 16.42 mm (Bowl #8). In contrast, the best ISFC rate is achieved when the bowl depth is decreased to 12.42 mm while the bowl center depth (Tm) was the same to baseline case. It can be concluded that a deep bowl depth combined with a shallow bowl center depth is disastrous for fuel economy.

7.2.4. Piston Bowl Width

In Figure 7.15, the NOx is plotted as a function of piston width. In this section, three geometrical parameters including bowl diameter, inner bowl diameter and outer bowl diameter have been considered to evaluate their effects on engine performance and amount of pollutants emissions. Figures 7.16 shows soot emissions as a function of piston bowl width.

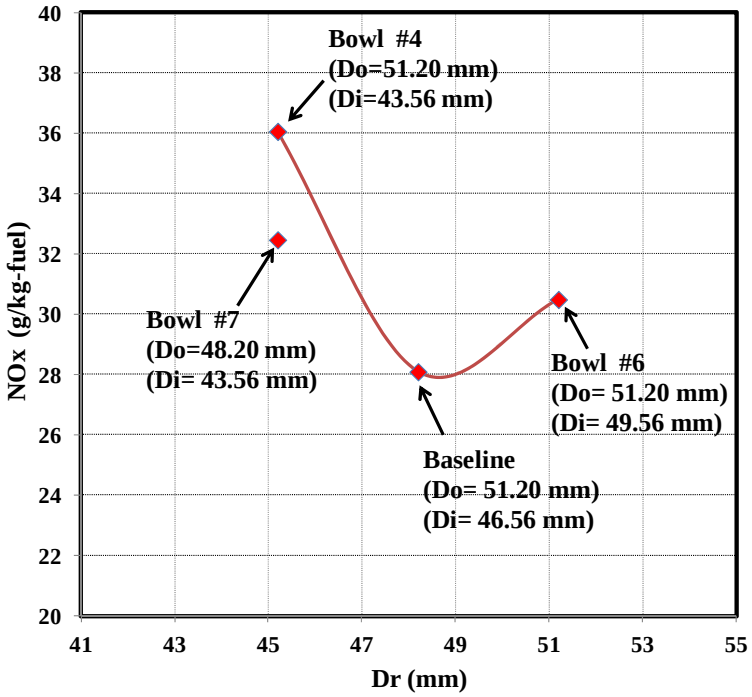

Figure 7.15 – Piston bowl width effects on NOx emission

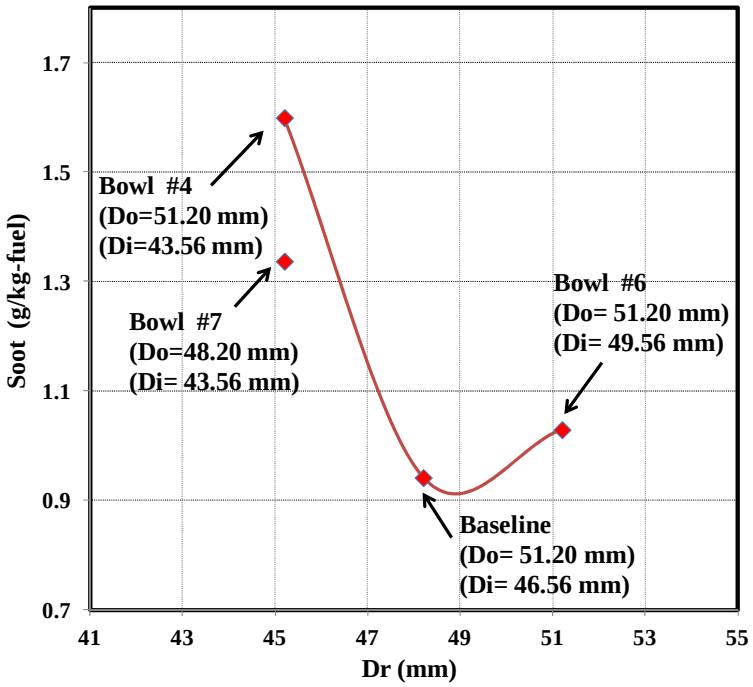

Figure 7.16 – Piston bowl width effects on soot emissions

According to Figures 7.15 and 7.16, increasing the bowl diameter till 48.2 mm decreases the amount of NOx and soot emissions. After this point, the reverse trend has observed. It can be concluded, the narrower width have a higher unburned fuel air mixture region, and thus would have higher soot emissions. But with slightly wider combustion chamber the optimum operating point could be obtained.

Figure 7.17 shows the effect of piston depth on Indicated specific fuel consumption. As illustrated in Figure 7.17, the bowl #6 has the worst results, which indicates the wider bowls did not improve the fuel consumption.

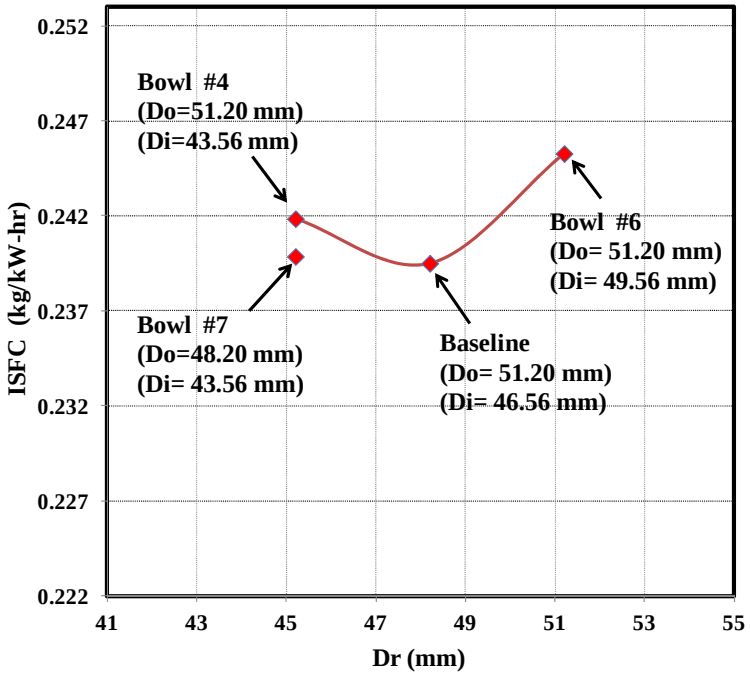

Figure 7.17 – Piston bowl width effects on ISFC

7.2.5. Piston Bottom Surface and Lip Area

Another important parameter which has influence on design on re-entrant combustion chamber is bottom surface of the piston and also lip area of the bowl. In this section the influence of these parameters are discussed. For this purpose, 5 different sketch of combustion chamber has simulated and analyzed compared to baseline case.

Figures 7.18 and 7.19 show NOx and soot emissions as a function of piston bottom surface and lip area.

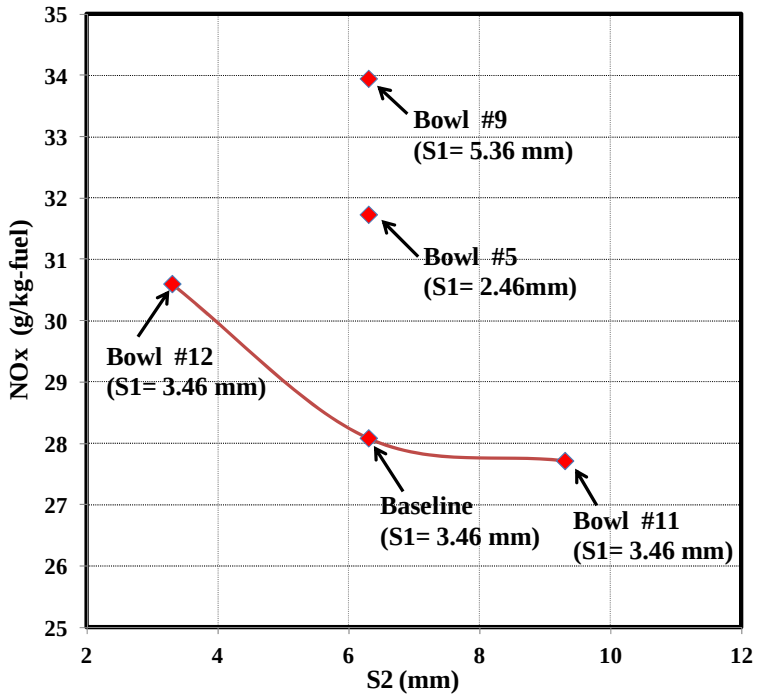

Figure 7.18 – Piston bottom surface and lip area effects on NOx emissions

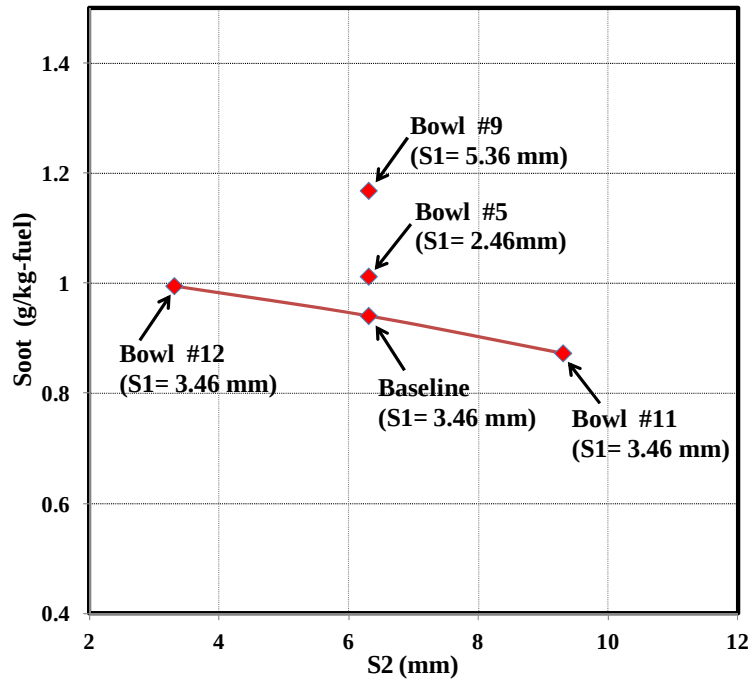

Figure 7.19 – Piston bottom surface and lip area effects on soot emissions

As illustrated in Figure 7.18 and 7.19, the worst operating point have been obtained by using Bowl #9 which has the highest lip area compared to other cases. It

can be concluded that in the bowl with higher lip area, the spray impinges on the wall a little earlier than in the bowl with smaller lip area. Therefore the amount of fuel inside the bowl is larger than in the bowl with smaller lip area and this causes higher soot and NOx emissions.

The ISFC rate is plotted as a function of piston bottom surface and outer surface distance in Figure 7.20.

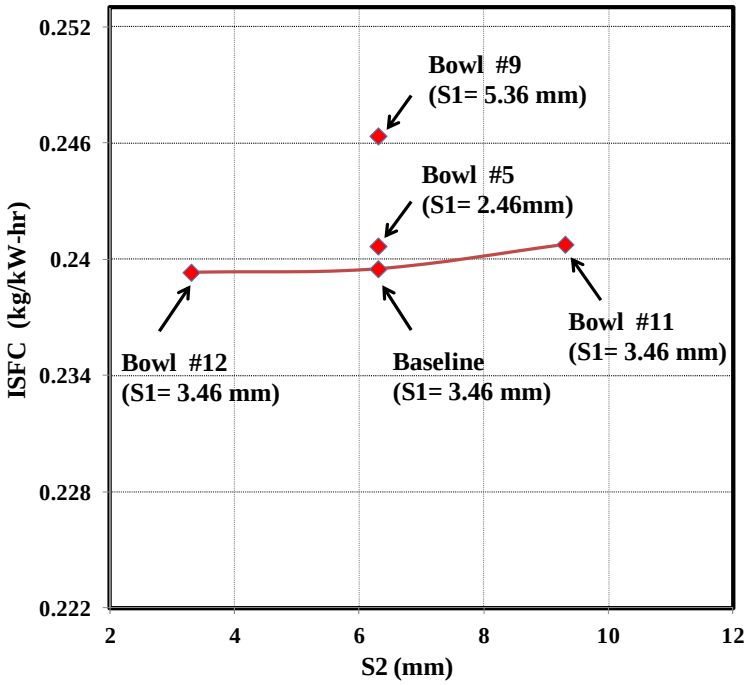

Figure 7.20 – Piston bottom surface effects on ISFC

As can be seen in Figure 7.20, Bowl #11 there appears to be a linear relationship between ISFC and piston bottom surface. As the piston bottom surface increases, the ISFC has a slight increasing when the lip area remains constant.

Figures 7.21 and 7.22 summarize the amount of CO emission and NOx–soot trade-off for all investigated cases, respectively.

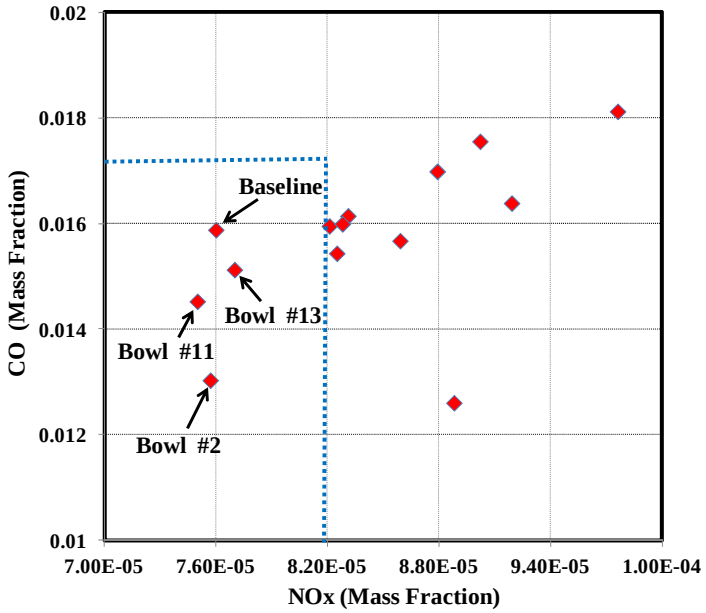

Figure 7.21 – NOx vs. CO for all studied cases

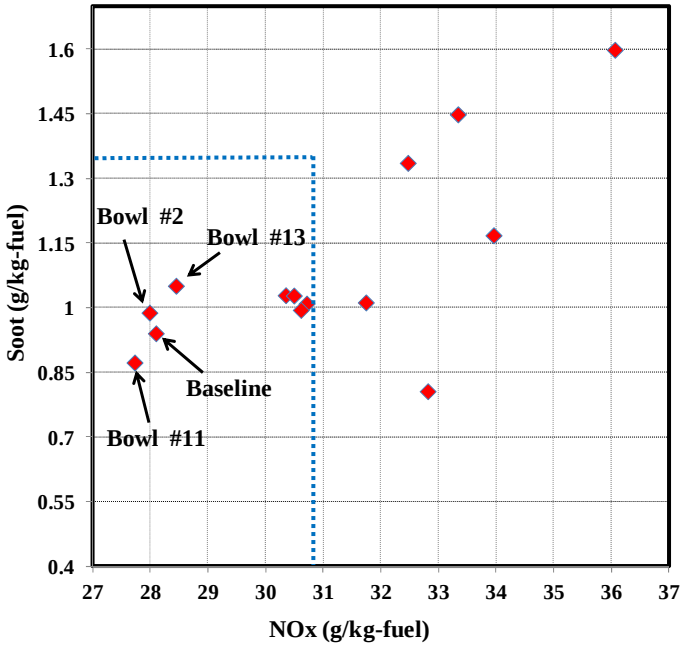

Figure 7.22 – NOx vs. Soot for all studied cases

As shown in Figure 7.21, the two cases including the Bowl#11 and Bowl#12 have lower CO emissions compared to the baseline case. In addition, the Bowl #11 produced the best-soot trade-off point, as illustrated in Figure 7.22.

7.2.6. Optimum Geometries

Based on results which have been obtained in previous sections, two configurations have been selected to analyze in more detail.

Figure 7.23 shows a comparison of pressure traces, heat release rates, and emissions between the baseline case and two optimum cases (Bowl #2 and #11).

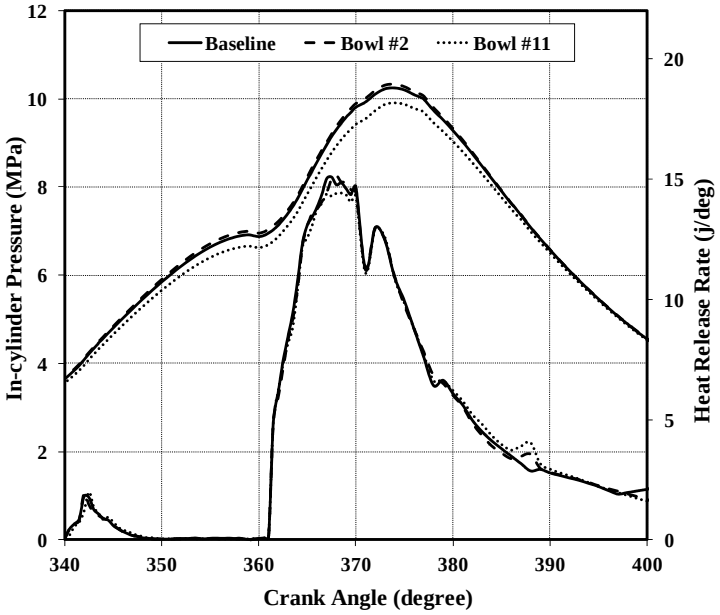

Figure 7.23 – In-cylinder pressure and heat release rate, baseline case vs. with two optimum cases

In Figure 7.23, except for Bow #11, the in-cylinder pressure and heat release rates are rather similar for the two other cases. Recall that the compression ratio was held constant for all geometries considered.

Figure 7.24 presents the history of the overall turbulent kinetic energy (TKE) in the combustion chamber for the optimum cases compared to the baseline cases.

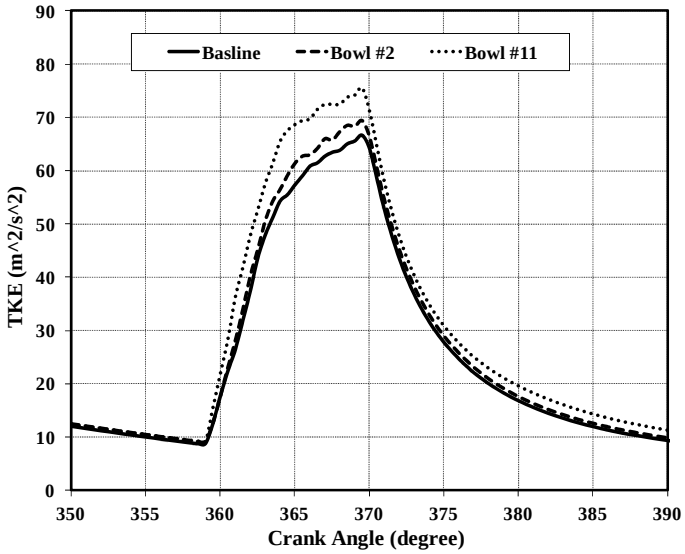

Figure 7.24 – Turbulent Kinetic Energy, baseline case vs. with two optimum cases

As shown in Figure 7.24, after main fuel injection, the optimum cases' TKE raises to a level higher than that of the baseline case. This is mainly due to the much higher mixing rate of the optimum models.

Figure 7.25 illustrates the velocity field contours for two optimum cases compared with the baseline case at 360, 385 and 410 CA.

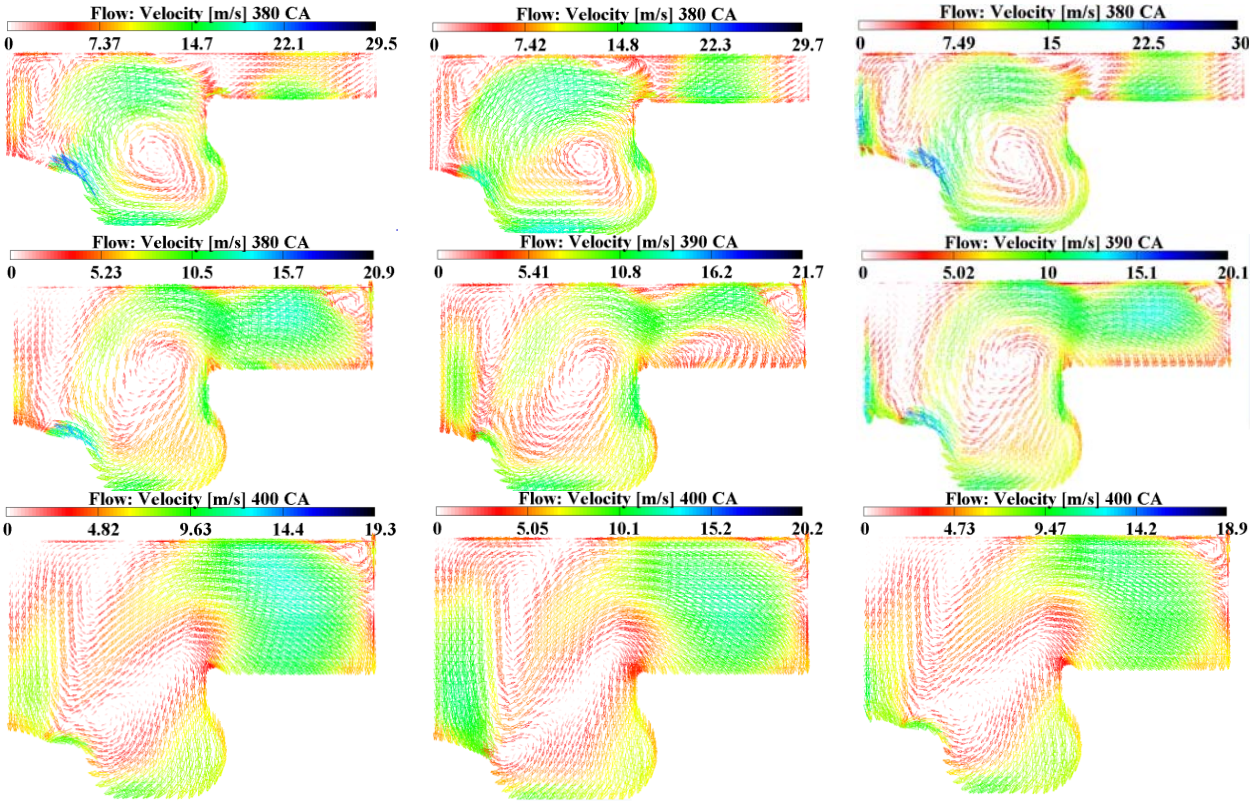

Baseline Bowl # 11 Bowl # 2

Figure 7.25 – The velocity fields contours, baseline case in comparison with two optimum cases

As shown in Figure 7.25, the velocity field within the cylinder increases for with Bowl #2 cases in comparison with the baseline case at 410 CA.

The evolution of the NOx distribution within the combustion chamber for the baseline case in comparison with optimum cases is shown in Figure 7.26 at 380, 390 and 400 CA. Figure 7.27 shows the comparison of in-cylinder soot formations for the same operating points.

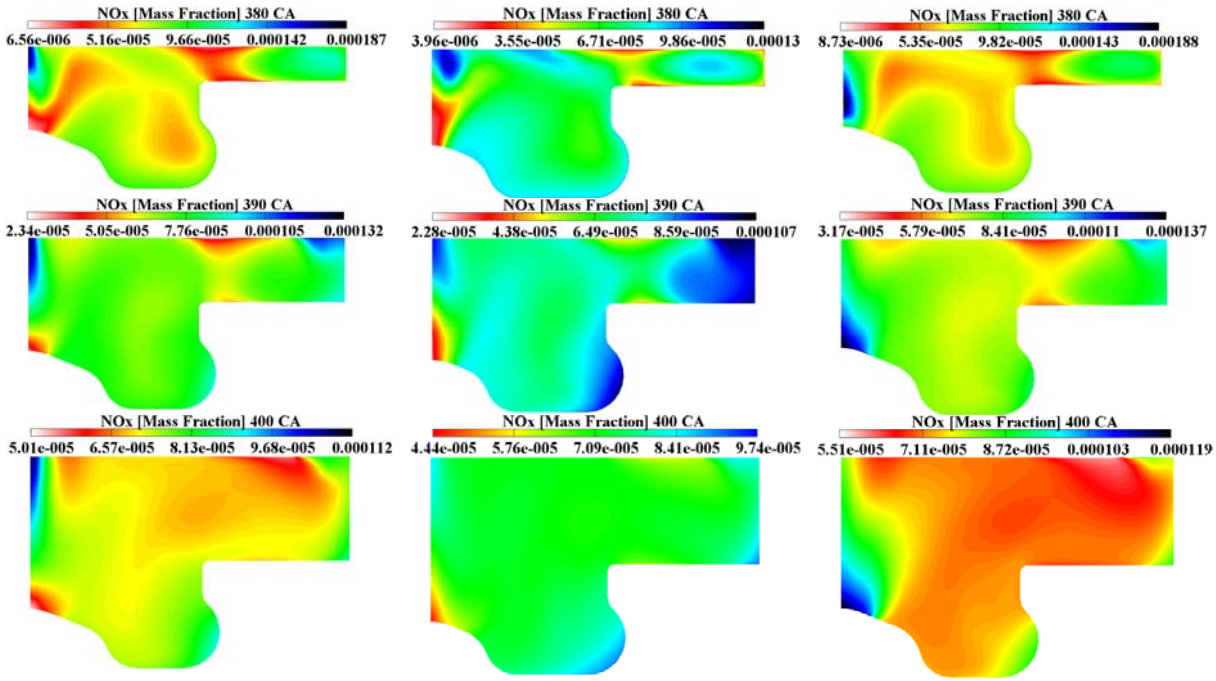

Baseline **Bowl # 11** **Bowl # 2**

Figure 7.26 – The NOx contours, baseline case in comparison with two optimum cases

The local soot-NOx trade-off is evident in these contour plots, as the NOx formation and soot formation occur on opposite sides of the high temperature region. It can be seen that for the Bowl #11 case, has the lowest amount of NOx and soot mass fractions in comparison with other cases. It can be concluded that for this case, which has a larger piston bottom surface than baseline case and Bowl #2, stronger squish flow has formed during the spray development and this increases the spray mixing with higher amount of velocity vectors.

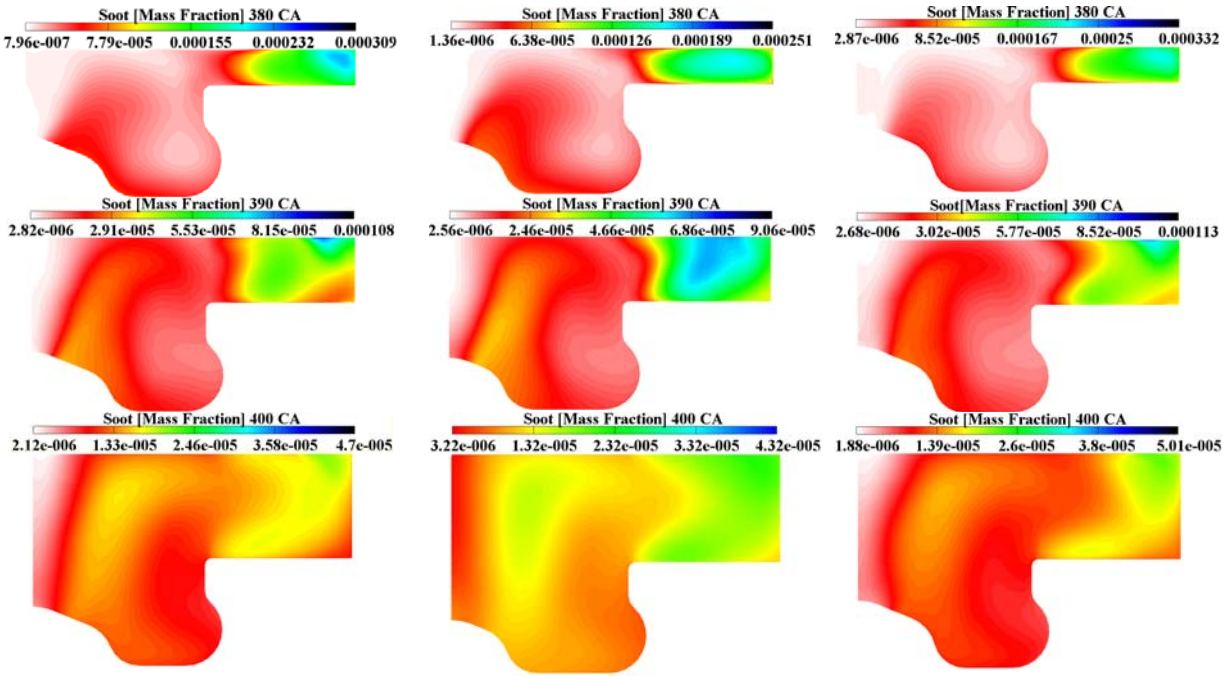

Baseline **Bowl # 11** **Bowl # 2**

Figure 7.27 – The soot contours, baseline case in comparison with two optimum cases

The evolution of the CO emission for the baseline case compared with two other cases is illustrated in Figure 7.28 at 380, 390 and 400 CA.

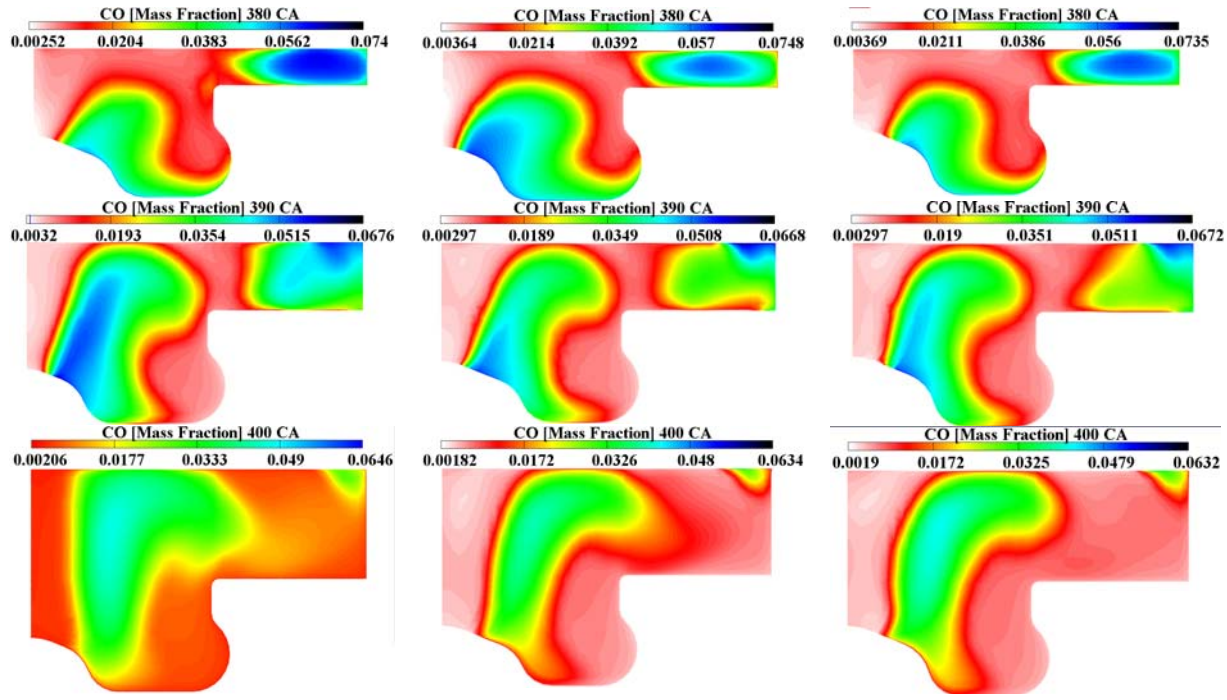

Baseline Bowl # 11 Bowl # 2

Figure 7.28 – The CO contours, baseline case in comparison with two optimum cases

As shown in Figure 7.28, from 390 CA, the CO emissions distribution for Bowl #11 and Bowl #2 configurations is obviously smaller than baseline configuration. It can be concluded the later combustion in the exhaust stroke caused this reduction although the burning velocity in the cylinder is nearly similar for three configurations at this position.

7.3. Effects of Pilot Injection

In order to further investigate the optimum geometries, the baseline pilot injection timings has been varied to evaluate its effects on amount of pollutant emissions and engine performance. For this purpose, the main injection was set at -0.65° CA ATDC and three pilot injection cases, with SOI -35°, -25° and -20° CA ATDC are considered compared to the baseline injection case.

In Figure 7.29, the injection schemes used are illustrated schematically compared to the baseline injection case. It should be stated that the same amount of fuel is injected in all the studied cases.

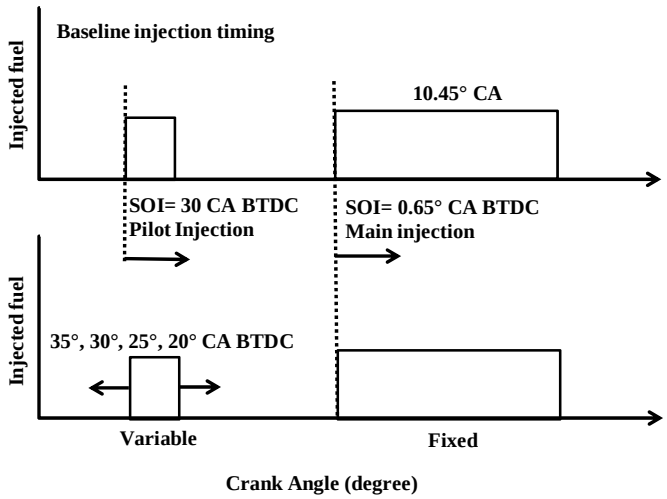

Figure 7.29 – Different pilot injection profiles compared to the baseline injection case

Figures 7.30, 7.31 and 7.32 show the amount of NOx, soot and ISFC for different considered cases, respectively.

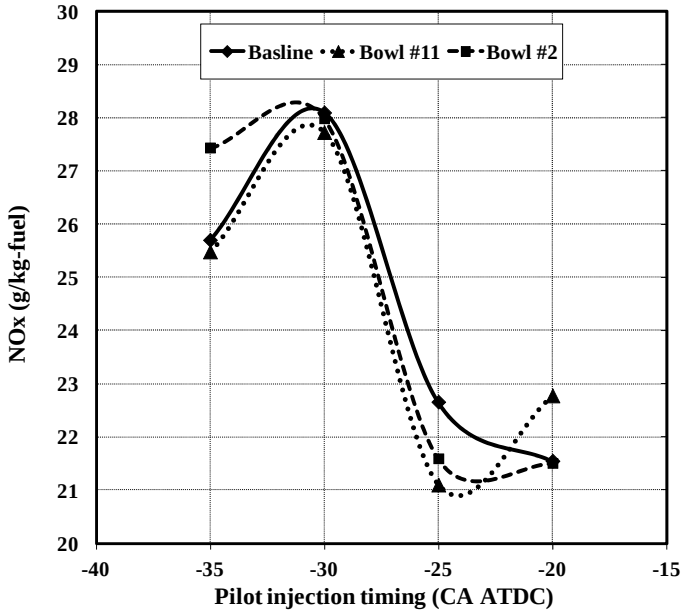

Figure 7.30 – NOx at different pilot injection timings for two optimum cases vs. the baseline case

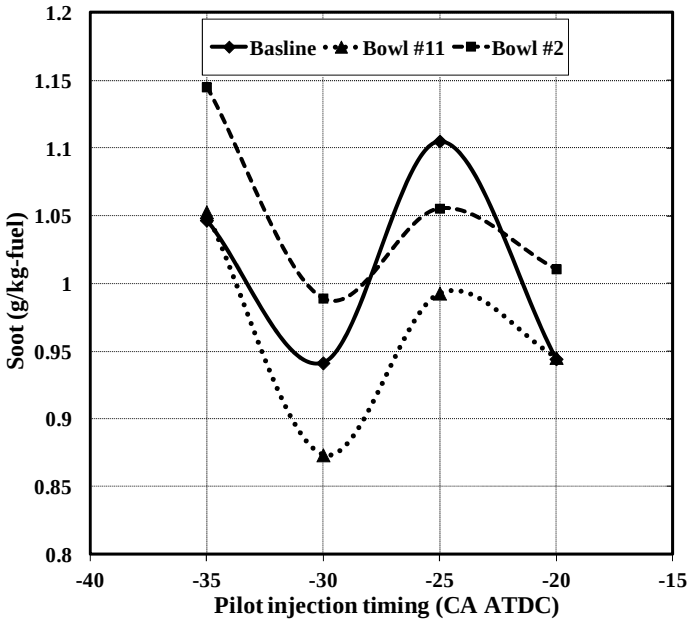

Figure 7.31 – Soot at different pilot injection timings for two optimum cases vs. the baseline case

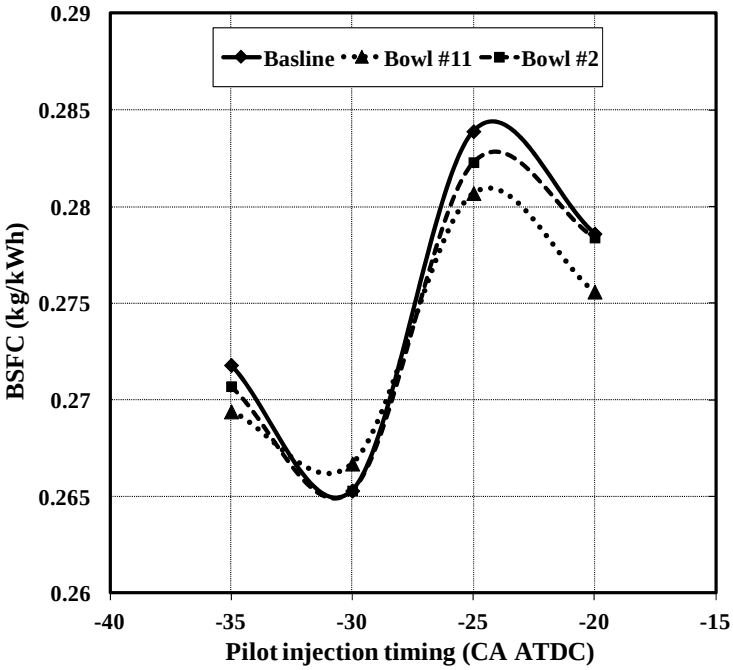

Figure 7.32 – ISFC at different pilot injection timings for two optimum cases vs. the baseline case

It can be concluded, as start of pilot injection (SOP) timing is advanced to -25 CA BTDC, the ignition delay becomes shorter due to the higher ambient temperature, results in increased amount of diffusion burn and lower peak heat release rates and thus decrease in amount of NOx emission, as shown in Figure 7.30. As a result, for earlier SOP timing, a sufficient mixing time is available to achieve a large portion of premixed mixture which produce the higher amount of heat released rate. The more advanced SOP timings produce a more homogeneous, locally fuel-lean in-cylinder mixture at the time of ignition since a sufficient mixing time is available to achieve a large portion of premixed mixture. However, at the more-advanced injection timing, the peak value of the NOx level increases.

In addition, the results in Figures 7.30 and 7.32 demonstrate the NOx emissions could decreased when the pilot injection timing is advanced to -25° CA BTDC while ISFC showed a slight increasing from 0.267 kg/kWh to 0.282 kg/kWh. It can also be

concluded, for the baseline combustion chamber with advanced pilot injection timings, some of the spray will miss the piston bowl. It would be expected to have a negative impact on fuel-air mixing compared to the other configurations. As illustrated in Figures 7.30 and 7.32, approximately the same trend of overall reduction of NOx emission and increase of ISFC could be obtained in different cases. In addition, since the soot oxidation was actively generated at higher combustion temperatures therefore, the amount of soot slightly increased as the injection timing was retarded.

7.4. Summary

A CFD Simulation was conducted to analyze the effects of combustion chamber geometry and pilot injection timing for optimization of engine performance and amount of pollutant emissions in a high speed direct injection (HSDI) diesel engine. The computed in-cylinder pressure, soot and NOx were firstly compared with experimental data and good agreement between the predicted and experimental values was ensured the accuracy of the numerical predictions collected with the present work. To study the effects of combustion chamber geometry, thirteen different configurations were selected and analyzed compared to the original piston bowl geometry. The results showed that for shallower bowls, decreasing the bowl depth shows a higher amount of NOx emissions and a deep bowl depth combined with a shallow bowl center depth is disastrous for fuel economy. It was also found that the narrower width of combustion chamber has a higher unburned fuel air mixture region, and thus would have higher soot emissions but with slightly wider combustion chamber the optimum operating point could be obtained.

Chapter 8

Conclusions and Recommendations

8.1. Introduction

This chapter summarizes the main contributions of this dissertation, by including the most important findings of the studies introduced in the previous chapters. Possible future work that may improve the results of the current study is also proposed. The results of this thesis have been published in [135-137, 139-142].

8.2. Conclusions

In first part of this study, an advanced CFD simulation was performed to demonstrate the emission reduction capability of the combined effects of multiple injection and EGR on a Direct Injection (DI) diesel Engine (Caterpillar 3401). The main objection of this part was to gain a detailed understanding of the mechanisms through which fuel injection interacts with other engine parameters and influences diesel combustion and emissions, and hence to attempt to generalize the adoption of multiple injection strategies with regards to improving diesel engine performance. For this

purpose, 12 different injection strategies were evaluated at two EGR rates. In addition, a modified parameter called "Homogeneity Factor of in-cylinder charge" (HF) was proposed and applied as a new measure to investigate the air-fuel mixing and combustion process. From those prediction results, the following conclusions were suggested.

- Compared to the single injection, split injection was very effective for reducing NOx and soot emissions. However, the split injection must be optimized for best emission reducing effects by varying the fuel distribution in each pulse and the separation between pulses for each operating condition.

- It was confirmed that soot emissions can be reduced by split injections and this strategy also allows the injection timing to be retarded to reduce NOx emission. By using an optimum injection schemes with retarded injection timing, both soot and NOx can be reduced simultaneously.

- The optimum separation for simultaneous reduction of soot with low NOx emissions can be obtained by using 20°CA dwell delay between the injection pulses.

- When the dwell delay between injection pulses becomes longer, it leaves more time for the air-fuel mixing and initial combustion process of first injection pulse and therefore, the increase of Homogeneity Factor takes place at a later stage and it can caused a reduction of NOx formation. The higher Homogeneity Factor will result in higher rate of air-fuel mixing and more complete combustion process. However, the careful adjustment must be made for ideal reduction for both NOx and soot emissions.

- With the combined use of EGR and split injection, NOx and soot were simultaneously reduced with more obvious results.

After locating the optimum point for different split injection cases, it was found that further advantages of multiple injections could be obtained if the split injection cases combined with a pilot injection. Totally, three factors were considered for the injection optimization, which included EGR rate, the separation between main injection and post injection and the amount of injected fuel in each pulse. Moreover, two more cases (including double and triple injections during main injection) were also considered. The main results which achieved by this part of study are summarized as follows:

- Investigation on multiple injection strategies showed the soot level can be dramatically reduced if an early pilot injection is combined with a main injection.

- Employing a post-injection combined with a pilot injection results in reduced soot formation from diffusion combustion and enhances the soot oxidation process during the expansion stroke, resulting in decreased soot emissions, while the NOx concentration is maintained in low levels.

- For majority of multiple injection cases, the amount of ISFC is increased compared to the single injection cases. This trend has also observed when 10% EGR is used. It can be concluded that applying multiple injection cases can be used as an effective tool to decrease the amount of soot and NOx emission but a fuel economy penalty is paid and this matter should be considered as a main barrier.

In next part of this study, a 3D CFD study was performed to determine the influence of the different included spray angles on the emissions and combustion

efficiency. The model was firstly calibrated against experimental data on a common rail DI Diesel engine. In this study, three different types of included spray angles ($\alpha = 145°, 105°, 90°$) were studied in comparison with the conventional spray injection angle ($\alpha = 125°$). The main findings can be summarized as follows:

- As SOP advances, a sufficient mixing time is available to achieve a large portion of premixed mixture which produce the higher amount of heat released rate. The more advanced SOP timings produce a more homogeneous, locally fuel-lean in-cylinder mixture at the time of ignition. In spite of this advantage, both NOx and soot levels exceed development goals, thus suggesting that a narrower cone angle is required.

- The results showed that included spray angle can be an important factor influencing the heat release rate. Compared with the conventional included spray angle, $105°$ angle offers more flexibility for simultaneous reduction of NOx and soot emission since it allows improved spray targeting into the piston.

- In the cases of narrower injection angle, it was found that the fuel spray impinges at the edge of the piston bowl and a counterclockwise flow motion is generated that pushes mixture toward the center of the piston bowl along the piston bowl surface. The optimum engine performance for simultaneous reduction of soot and NOx emissions was achieved with 105° included spray angle.

- The results showed that spray targeting is very effective for controlling the in-cylinder mixture distributions especially when it accompanied with various injection strategies. It was found that 105° spray cone angle along with an optimized split pre- and post-Top Dead Center (TDC) injection strategy could significantly reduce NOx and soot emissions, as compared to the wide spray angle. However, the BSFC levels

are slightly increased. In addition, a narrow injection angle offers more efficient air-mixing process due to better interaction with the combustion chamber and cylinder liner.

In next part of this research, an advanced CFD investigation was carried out to analyze the effect of re-entrant combustion chamber geometry on mixture formation, combustion process and engine performance. A four cylinders, high speed direct injection (HSDI) diesel engine based on a Ford production engine with a 2nd generation Delphi common rail fuel injection system was modeled in this investigation. The computed in-cylinder pressure, soot and NOx were firstly compared with experimental data and good agreement between the predicted and experimental values was ensured the accuracy of the numerical predictions collected with the present work. To study the effects of combustion chamber geometry, thirteen different configurations were selected and analyzed compared to the original piston bowl geometry. The results showed that for shallower bowls, decreasing the bowl depth shows a higher amount of NOx emissions and a deep bowl depth combined with a shallow bowl center depth is disastrous for fuel economy. It was also found that the narrower width of combustion chamber has a higher unburned fuel air mixture region, and thus would have higher soot emissions but with slightly larger piston surface area the optimum operating point could be obtained.

8.3. Suggestion for Future Studies

As mentioned earlier in chapter 2, the effect of swirl ratio on combustion characteristics is closely related to the engine operating conditions, such as injection pressure and dwell between injections. Thus, it would be interesting to optimize the engine operating parameters for each different swirl ratio with much higher EGR rates

and longer dwells. This might provide a deeper understanding of swirl effects on engine performance and amount of pollutant emission.

In addition, the optimization work at different loads and speeds might be able to find interesting strategies for improving emission and fuel economy.

REFRENCES

1. Heywood, J. B., *Internal Combustion Engine Fundamentals*, McGraw-Hill Publishing Company, New York, 1988.

2. Liu, Y., "Diesel Engine Modeling and Optimization for Emission Reduction", Ph.D. Thesis, University of Wisconsin-Madison, 2005.

3. Rakowski, S., Eckert, P. and Witt, A., "*Engine Combustion"*, *Combustion Engines Development*, Springer Berlin Heidelberg. p. 119-168, 2012.

4. Flaig, U., Polach, W., and Ziegler, G., "Common Rail System (CR-System) for Passenger Car DI Diesel Engines; Experiences with Applications for Series Production Projects", SAE Technical Paper 1999-01-0191, 1999.

5. Badami, M., Nuccio, P., and Trucco, G., "Influence of Injection Pressure on the Performance of a DI Diesel Engine with a Common Rail Fuel Injection System" SAE Technical Paper 1999-01-0193, 1999.

6. Shimazaki, N., Hatanaka, H., Yokota, K., and Nakahira, T., "A study of Diesel Combustion Process Under the Condition of EGR and High-Pressure Fuel Injection with Gas Sampling Method", SAE Technical Paper 960030, 1996.

7. Shundoh, S., Kakegawa, T., Tsujimura, K., and Kobayashi, S., "The Effect of Injection Parameters and Swirl on Diesel Combustion with High Pressure Fuel Injection", SAE Technical Paper 910489, 1991.

8. Pierpont, D. and Reitz, R. D., "Effects of Injection Pressure and Nozzle Geometry on D.I. Diesel Emissions and Performance", SAE Technical Paper 950604, 1995.

9. Onishi, S., Jo, S., Shoda, K., Jo, P. and Kato, S., “Active Thermo-Atmosphere Combustion (ATAC) - A New Combustion Process for Internal Combustion Engines”, SAE Technical Paper 790501, 1979.

10. Noguchi, M., Tanaka, Y., Tanaka, T., and Takeuchi, Y., “A Study on Gasoline Engine Combustion by Observation of Intermediate Reactive Products during Combustion”, SAE Technical Paper 790840, 1979.

11. Murase, E. and Hanada, K., “Control of the Start of HCCI Combustion by Pulsed Flame Jet”, SAE Technical Paper 2002-01-2867, 2002.

12. Liu, C. and G.A. Karim, “A simulation of the combustion of hydrogen in HCCI engines using a 3D model with detailed chemical kinetics. International Journal of Hydrogen Energy”, 33(14): p. 3863-3875, 2008.

13. Kono, S., Nagao, A., and Motooka, H., “Prediction of ln-Cylinder Flow and Spray Formation Effects on Combustion in Direct Injection Diesel Engines”, SAE Technical Paper 850108, 1985.

14. Shimada, T., Sakai, K., and Kurihara, S., “Variable Swirl Inlet System and Its Effect on Diesel Performance and Emissions”, SAE Technical Paper 861185, 1986.

15. Rao, K., Winterbone, D., and Clough, E., “Influence of Swirl on High Pressure Injection in Hydra Diesel Engine”, SAE Technical Paper 930978, 1993.

16. Micklow, G.J., Gong, W-D., “Intake and in-cylinder flowfield modelling of a four-valve diesel engine”, Proceedings of the Institution of Mechanical Engineers, Part D: Journal of Automobile Engineering, 221: 1425-1440, 2007.

17. Shi, Y., Ge, H-W. and Reitz, R.D., “*Scaling Laws for Diesel Combustion Systems”*, *Computational Optimization of Internal Combustion Engines*, Springer London. p. 147-176, 2012.

18. Shi, Y., Ge, H-W. and Reitz, R.D., *"Fundamental", Computational Optimization of Internal Combustion Engines*, Springer London. p. 15-73, 2012.

19. Iyer, C. and Yi, J., "3D CFD Upfront Optimization of the In-Cylinder Flow of the 3.5L V6 EcoBoost Engine", SAE Technical Paper 2009-01-1492, 2009.

20. Arcoumanis, C., Bicen, A. F., and Whitelaw, J. H., "Squish and Swirl-Squish Interaction in Motored Model Engines", ASME Journal of Fluids Engineering, Vol. 105, p. 105, 1983.

21. Espey, C., Pinson, J., and Litzinger, T., "Swirl Effects on Mixing and Flame Evolution in a Research DI Diesel Engine", SAE Technical Paper 902076, 1990.

22. Ogawa, H., Matsui, Y., Kimura, S., and Kawashima, J., "Three-Dimensional Computation of the Effects of the Swirl Ratio in Direct-Injection Diesel Engines on NOx and Soot Emissions", SAE Technical Paper 961125, 1996.

23. Fuchs, T. and Rutland, C., "Intake Flow Effects on Combustion and Emissions in a Diesel Engine" SAE Technical Paper 980508, 1998.

24. Jung, M., Ford, R., Glover, K., Collings, N. et al., "Parameterization and Transient Validation of a Variable Geometry Turbocharger for Mean-Value Modeling at Low and Medium Speed-Load Points", SAE Technical Paper 2002-01-2729, 2002.

25. Liu, Z., *"Overview of heavy-duty diesel engines", Advanced direct injection combustion engine technologies and development*, Woodhead Publishing Limited, p. 269-288, 2010.

26. Bai, L. and Yang, M., "Coordinated Control of EGR and VNT in Turbocharged Diesel Engine Based on Intake Air Mass Observer", SAE Technical Paper 2002-01-1292, 2002.

27. Arnold, S., Groskreutz, M., Shahed, S., and Slupski, K., “Advanced Variable Geometry Turbocharger for Diesel Engine Applications”, SAE Technical Paper 2002-01-0161, 2002.

28. Uchida, N., Daisho, Y., Saito, T., and Sugano, H., “Combined Effects of EGR and Supercharging on Diesel Combustion and Emissions”, SAE Technical Paper 930601, 1993.

29. Tanin, K.V., Wickman, D. D., Montgomery, D. T., Das, S., and Reitz, R. D., “The Influence of Boost Pressure on Emission and Fuel Consumption of a Heavy-Duty Single-Cylinder D.I. Diesel Engine”, SAE Technical Paper 1999-01-0840, 1999.

30. Zhang, L., Takatsuki, T., and Yokota, K., “An observation and Analysis of the Combustion Under Supercharging on a DI Diesel Engine”, SAE Technical Paper 940844, 1994.

31. Ramos, J. I., *Internal Combustion Engine Modeling*, Hemisphere Publishing Corporation, New York, 1989.

32. Williams, F.A., *Combustion Theory*, The Benjamin/Cummings Publishing Company, 1985.

33. Ladommatos, N., Abdelhalim, S., Zhao, H., and Hu, Z., “The Dilution, Chemical, and Thermal Effects of Exhaust Gas Recirculation on Disesel Engine Emissions - Part 4: Effects of Carbon Dioxide and Water Vapour”, SAE Technical Paper 971660, 1997.

34. Hentschel, W. and Richter, J., “Time-Resolved Analysis of Soot Formation and Oxidation in a Direct-Injection Diesel Engine for Different EGR-Rates by an Extinction Method”, SAE Technical Paper 952517, 1995.

35. Ladommatos, N., Abdelhalim, S., Zhao, H., and Hu., Z., “Effects of EGR on Heat Release in Diesel Combustion”, SAE Technical Paper 980184, 1998.

36. Dürnholz, M., Eifler, G., and Endres, H., “Exhaust-Gas Recirculation - A Measure to Reduce Exhaust Emissions of DI Diesel Engines”, SAE Technical Paper 920725, 1992.

37. Ladommatos, N., Balian, R., Horrocks, R., and Cooper, L., “The Effect of Exhaust Gas Recirculation on Combustion and NOx Emissions in a High-Speed Direct-injection Diesel Engine”, SAE Technical Paper 960840, 1996.

38. Arcoumanis, C., Nagwaney, A., Hentschel, W., and Ropke, S., “Effect of EGR on Spray Development, Combustion and Emissions in a 1.9L Direct-Injection Diesel Engine”, SAE Technical Paper 952356, 1995.

39. Mattarelli, E., Bianchi, G., and Ivaldi, D., “Experimental and Numerical Investigation on the EGR System of a New Automotive Diesel Engine”, SAE Technical Paper 2000-01-0224, 2000.

40. Yamaki, Y., Mori, K., Kamikubo, H., Kohketsu, S. et al., “Application of Common Rail Fuel Injection System to a Heavy Duty Diesel Engine”, SAE Technical Paper 942294, 1994.

41. Minami, T., Takeuchi, K., and Shimazaki, N., “Reduction of Diesel Engine NOx Using Pilot Injection”, SAE Technical Paper 950611, 1995.

42. Zhang, L., “A Study of Pilot Injection in a DI Diesel Engine”, SAE Technical Paper 1999-01-3493, 1999.

43. Nehmer, D. and Reitz, R., “Measurement of the Effect of Injection Rate and Split Injections on Diesel Engine Soot and NOx Emissions”, SAE Technical Paper 940668, 1994.

44. Mendez, S. and Thirouard, B., “Using Multiple Injection Strategies in Diesel Combustion: Potential to Improve Emissions, Noise and Fuel Economy Trade-Off in Low CR Engines”, SAE Int. J. Fuels Lubr. 1(1):662-674, 2009.

45. Tow, T., Pierpont, D., and Reitz, R., “Reducing Particulate and NOx Emissions by Using Multiple Injections in a Heavy Duty D.I. Diesel Engine”, SAE Technical Paper 940897, 1994.

46. Han, Z., Uludogan, A., Hampson, G., and Reitz, R., “Mechanism of Soot and NOx Emission Reduction Using Multiple-injection in a Diesel Engine”, SAE Technical Paper 960633, 1996.

47. Dürnholz, M., Endres, H., and Frisse, P., “Preinjection A Measure to Optimize the Emission Behavior of DI-Diesel Engine”, SAE Technical Paper 940674, 1994.

48. Ricaud, J.C., Lavoisier, F., “Optimizing the Multiple Injection Settings on an HSDI Diesel Engine”, THIESEL 2002 conference, 2002.

49. Dronniou, N., Lejeune, M., Balloul, I., and Higelin, P., "Combination of High EGR Rates and Multiple Injection Strategies to Reduce Pollutant Emissions," SAE Technical Paper 2005-01-3726, 2005

50. Mikulic, L., Kühn, M., Schommers, J., and Willig, E., "Exhaust-Emission Optimization of DI-Diesel Passenger Car Engine with High-Pressure Fuel Injection and EGR," SAE Technical Paper 931035, 1993.

51. Uchida, N., Shimokawa, K., Kudo, Y., and Shimoda, M., “Combustion Optimization by Means of Common Rail Injection System for Heavy-Duty Diesel Engines”, SAE Technical Paper 982679, 1998.

52. Fang, T., Coverdill, R. E., Lee, C-F. F. and White, R. A., “Effects of injection angles on combustion processes using multiple injection strategies in an HSDI diesel engine”, Fuel, Volume 87, Issues 15-16, 3232-3239, 2008.

53. Akagawa, H., Miyamoto, T., Harada, A., Sasaki, S. et al., “Approaches to Solve Problems of the Premixed Lean Diesel Combustion”, SAE Technical Paper 1999-01-0183, 1999.

54. Walter, B. and Gatellier, B., “Development of the High Power NADI™ Concept Using Dual Mode Diesel Combustion to Achieve Zero NOx and Particulate Emissions”, SAE Technical Paper 2002-01-1744, 2002.

55. Yokota, H., Kudo, Y., Nakajima, H., Kakegawa, T. et al., “A New Concept for Low Emission Diesel Combustion”, SAE Technical Paper 970891, 1997.

56. Hasegawa, R. and Yanagihara, H., “HCCI Combustion in DI Diesel Engine”, SAE Technical Paper 2003-01-0745, 2003.

57. De Risi, A., Donabeo., T., Laforgia., D., “An Innovative methodology to improve the design and the performance of direct injection diesel engine” International Journal of Engine Research, 5 (5), pp. 425-441, 2005.

58. Middlemiss, I., “Characteristics of the Perkins ‘Squish Lip’ Direct Injection Combustion System”, SAE Technical Paper 780113, 1978.

59. Saito, T., Daisho, Y., Uchida, N., and Ikeya, N., “Effects of Combustion Chamber Geometry on Diesel Combustion”, SAE Technical Paper 861186, 1986.

60. Sakata, I., Ishisaka, K., Yanagihara, H., Sami, H. et al., “Development of TOYOTA Reflex Burn (TRB) System in DI Diesel”, SAE Technical Paper 900658, 1990.

61. Corcione, F., Prati, M., Vaglieco, B., and Valentino, G., “Improvement of Combustion System of a Small D.I. Diesel Engine for Low Exhaust Emissions”, SAE Technical Paper 910481, 1991.

62. Zhang, L., Ueda, T., Takatsuki, T., and Yokota, K., “A Study of the Effects of Chamber Geometries on Flame Behavior in a DI Diesel Engine”, SAE Technical Paper 952515, 1995.

63. Zolver, M., Griard, C., and Henriot, S., “3D Modeling Applied to the Development of a DI Diesel Engine: Effect of Piston Bowl Shape”, SAE Technical Paper 971599, 1997.
64. Bianchi, G., Pelloni, P., Corcione, F., Mattarelli, E. et al., “Numerical Study of the Combustion Chamber Shape for Common Rail H.S.D.I. Diesel Engines”, SAE Technical Paper 2000-01-1179, 2000.
65. Shi, Y., Ge, H-W. and Reitz, R.D., “*Introduction”, Computational Optimization of Internal Combustion Engines*, Springer London. p. 1-14, 2012.
66. Amsden AA, Ramshaw JD, O’Rourke PJ, Dukowicz JK, Butler TD, KIVA: a computer program for two- and three-dimensional fluid flows with chemical reactions and fuel sprays. Los Alamos National Laboratory Report No. LA-10245-MS, 1985.
67. Reitz, R.D., Rutland, C.J., “Development and Testing of Diesel Engine CFD Models”, Prog Energy Combust Sci 21:173–196, 1995.
68. Kong, S., Marriott, C., Reitz, R.D., and Christensen, M., “Modeling and Experiments of HCCI Engine Combustion Using Detailed Chemical Kinetics with Multidimensional CFD”, SAE Technical Paper 2001-01-1026, 2001.
69. Otto, F., Kruger, Ch., “*Three-Dimensional Flow Fields”, Combustion Engines Development*, Springer Berlin Heidelberg. p. 443-482, 2012.
70. OpenFOAM User Guide. http://www.openfoam.com/docs/user/, Accessed in 2010.
71. Star-CD Version 3.20 User Guide. CD-adapco Group, 2004.
72. FLUENT 6.3 user’s guide. Fluent Inc. 2006.
73. ICE Physics & Chemistry, AVL FIRE User Manual v.2009. 1, 2009.

74. VECTIS 3.8 User's Manual. Ricardo Consulting Engineers Ltd. 2006.

75. Senecal PK (2000) Numerical optimization using the gen4 micro-genetic algorithm code, user manual. Engine Research Center, University of Wisconsin-Madison.

76. Senecal, P., Richards, K., Pomraning, E., Yang, T. et al., "A New Parallel Cut-Cell Cartesian CFD Code for Rapid Grid Generation Applied to In-Cylinder Diesel Engine Simulations," SAE Technical Paper 2007-01-0159, 2007.

77. Liang, L., Naik, C., Puduppakkam, K., Wang, C. et al., "Efficient Simulation of Diesel Engine Combustion Using Realistic Chemical Kinetics in CFD", SAE Technical Paper 2010-01-0178, 2010.

78. Naik, C., Puduppakkam, K., Wang, C., Kottalam, J. et al., "Applying Detailed Kinetics to Realistic Engine Simulation: the Surrogate Blend Optimizer and Mechanism Reduction Strategies", SAE Int. J. Engines 3(1):241-259, 2010.

79. Puduppakkam, K., Liang, L., Shelburn, A., Naik, C. et al., "Predicting Emissions Using CFD Simulations of an E30 Gasoline Surrogate in an HCCI Engine with Detailed Chemical Kinetics", SAE Technical Paper 2010-01-0362, 2010.

80. Ge, H., Shi, Y., Reitz, R., Wickman, D. et al., "Engine Development Using Multi-dimensional CFD and Computer Optimization", SAE Technical Paper 2010-01-0360, 2010.

81. Ge, H.W., Shi, Y., Reitz, R.D., Willems, W., "Optimization of a high-speed direct-injection diesel engine at low-load operation using computational fluid dynamics with detailed chemistry and a multi-objective genetic algorithm", Proc Inst Mech Eng D: J Auto Eng 224:547–563., 2010.

82. Kong, S.C., Reitz, R.D., “Multidimensional modeling of diesel ignition and combustion using multistep kinetics models”, J Eng Gas Turb Power 115:781–789, 1993.
83. Bergin, M., Hessel, R., and Reitz, R., “Optimization of a Large Diesel Engine via Spin Spray Combustion”, SAE Technical Paper 2005-01-0916, 2005.

84. Shi, Y., Reitz, R.D., “Optimization study of the effects of bowl geometry, spray targeting and swirl ratio for a heavy-duty diesel engine operated at low- and high-load”, Int J Engine Res9:325–346, 2008.

85. Munnannur A, “Droplet Collision Modeling in Multi-Dimensional Engine Spray Computations”, PhD Thesis, University of Wisconsin-Madison, 2007.

86. Abani, N., Munnannur, A., Reitz, R.D., “Reduction of Numerical Parameter Dependencies in Diesel Spray Models”, J Eng Gas Turb Power 130:032809, 2008.

87. Abani, N., Reitz, R.D., “Diesel engine emissions and combustion predictions using advanced mixing models applicable to fuel sprays”, Combust Theory Modeling 14:715–746, 2010.

88. Abani, N., Kokjohn, S., Park, S., Bergin, M. et al., “An Improved Spray Model for Reducing Numerical Parameter Dependencies in Diesel Engine CFD Simulations”, SAE Technical Paper 2008-01-0970, 2008.

89. Babajimopoulos, A., Assanis, D.N., Flowers, D.L., Aceves, S.M., Hessel, R.P. “A fully coupled computational fluid dynamics and multi-zone model with detailed chemical kinetics for the simulation of premixed charge compression ignition engines”, Int J Engine Res 6:497–512, 2005.

90. Goldin, G.M., Ren, Z., Zahirovic, S., “A cell agglomeration algorithm for accelerating detailed chemistry in CFD”, Combust Theory Modelling 13:721–739, 2009.

91. Lu, T.F., Law, C.K., “A directed relation graph method for mechanism reduction”, Proc Combust Inst 30:1333–1341, 2005.
92. Pepiot-Desjardins, P., Pitsch, H., “An efficient error-propagation-based reduction method for large chemical kinetic mechanisms”, Combust Flame 154:67–81, 2008.

93. Sun, W., Chen, Z., Gou, X., Ju, Y., “A path flux analysis method for the reduction of detailed chemical kinetic mechanisms”, Combust Flame 157:1298–1307, 2010.

94. Liang, L., Stevens, J.G., Farrell, J.T., “A dynamic adaptive chemistry scheme for reactive flow computations”, Proc Combust Inst 32:527–534, 2009.

95. Shi, Y., Liang, L., Ge, H.W., Reitz, R.D. “Acceleration of the chemistry solver for modeling DI engine combustion using dynamic adaptive chemistry (DAC) schemes”, Combust Theory Model 14:69–89, 2010.

96. Zheng, J., “A Study of Homogeneous Ignition and Combustion Processes in CI, SI and HCCI Engine Systems”, PhD Thesis, Drexel University, 2005.

97. Baumgarten, C., *Mixture formation in internal combustion engines, heat and mass transfers in sprays*, Springer Berlin Heidelberg, 2006.

98. Arcoumanis, C., Gavaises M., “Linking the nozzle flow with spray characteristics in a diesel fuel injection system”, Atomization and Sprays 8:179–197, 1998.

99. Baddock, C., Untersuchungen zum Einfluss der Kavitation auf den primaren Strahlzerfall bei der dieselmotorischen Einspritzung, Dissertation, Universitat Darmstadt, Shaker, 1999.

100. Von Kuensberg Sarre, C., Kong, S., and Reitz, R., “Modeling the Effects of Injector Nozzle Geometry on Diesel Sprays”, SAE Technical Paper 1999-01-0912, 1999.

101. Curran, H.J., Gaffuri, P., Pitz, W.J., Westbrook, C.K., “A comprehensive modeling study of n-Heptane oxidation”, Comb Flame 114:149–177, 1998.

102. Dec, J., “A Conceptual Model of DI Diesel Combustion Based on Laser-Sheet Imaging”, SAE Technical Paper 970873, 1997.

103. Flynn, P., Durrett, R., Hunter, G., zur Loye, A. et al., “Diesel Combustion: An Integrated View Combining Laser Diagnostics, Chemical Kinetics, And Empirical Validation”, SAE Technical Paper 1999-01-0509, 1999.

104. Siebers, D. and Higgins, B., “Flame Lift-Off on Direct-Injection Diesel Sprays Under Quiescent Conditions”, SAE Technical Paper 2001-01-0530, 2001.

105. Glassman, I., “Soot formation in combustion processes”, Proc. of the 22nd international symposium on combustion, The Combustion Institute, pp 295–311, 1998.

106. Eckert, P. and Rakowski, S., “*Pollutant Formation”, Combustion Engines Development*, Springer Berlin Heidelberg. p. 193-223, 2012.

107. Nandha, K. and Abraham, J., “Dependence of Fuel-Air Mixing Characteristics on Injection Timing in an Early-Injection Diesel Engine”, SAE Technical Paper 2002-01-0944, 2002.

108. Peng, Z., Liu, B., Tian, L., and Lu, L., “Analysis of Homogeneity Factor for Diesel PCCI Combustion Control”, SAE Technical Paper 2011-01-1832, 2011.

109. Tatschl, R., “3D-CFD Simulation of IC-Engine Flow, Mixture Formation and Combustion with AVL FIRE”, *Combustion Engines Development*, Springer Berlin Heidelberg. p. 601-630, 2012.

110. Basara, B., “An eddy viscosity transport model based on elliptic relaxation approach”, AIAA J 44(7):1686–1690, 2006.

111. Popovac, M., Hanjalic, K., “Compound wall treatment for RANS computation of complex turbulent flows”, Proceedings of third MIT conference on computational fluid and solid mechanics, vol 1. Elsevier, Amsterdam, pp 802–806, 2005.

112. Reitz, R. D. “Modeling Atomization Processes in High-Pressure Vaporizing Sprays”, Atomization and Spray Technology, Vol. 3: 309-337, 1987.

113. Corcione, F. E, Allocca, L., Pelloni, P., Bianchi, G. M., and Luppino, F., ”Modeling atomization and drop breakup of high-pressure Diesel Sprays”, ASME Journal of Engineering for Gas Turbine and Power, Vol. 123, Issue 2, pp. 419-427, 2001.

114. Naber, J. and Reitz, R., “Modeling Engine Spray/Wall Impingement”, SAE Technical Paper 880107, 1988.

115. Dukowicz, J.K. “Quasi-steady droplet change in the presence of convection, informal report Los Alamos Scientific Laboratory”, LA7997-MS, 1979.

116. Hélie, J. &Trouvé, A., “A modified coherent flame model to describe turbulent flame propagation in mixtures with variable composition”, Proc. Combust. Inst. 28: 193-201, 2000.

117. Colin, O., Benkenida, A., “The 3-Zones Extended Coherent Flame Model (ECFM3Z) for Computing Premixed / Diffusion Combustion”, Oil & Gas Science and Technology – Rev. IFP, Vol. 59, No. 6, pp. 593-609, 2004.

118. Subramanian, G., Vervisch, L., and Ravet, F., “New Developments in Turbulent Combustion Modeling for Engine Design: ECFM-CLEH Combustion Submodel”, SAE Technical Paper 2007-01-0154, 2007.

119. Shi, X., Li, G., and Zhou, L., “DI Diesel Engine Combustion Modeling Based on ECFM-3Z Model”, SAE Technical Paper 2007-01-4138, 2007.

120. Colin, O., Pires da Cruz, A., Jay, S., “Detailed chemistry-based auto-ignition model including low temperature phenomena applied to 3D engine calculations”, Proceedings of Combustion Institute 30, pp 2649–2656, 2005.

121. Hanson, R.U. and Salimian, S., “Survey of Rate Constants in the N/H/O-System”, Combustion Chemistry, William C., Gardiner Jr., Springer Verlag, 361-421, 1984.

122. Bowman, C. T. “Chemistry of Gaseous Pollutant Formation and Destruction, in Fossil Fuel Combustion.” A Source Book. 215-260, 1991.

123. Fenimore, C.P. 13th Symposium (International) on Combustion, The Combustion Institute, Pittsburgh, pg. 373, 1971.

124. Zeldovich, Y. B., Sadovnikov, P. Y. and Frank-Kamenetskii, D. A., Oxidation of Nitrogen in Combustion., Translation by M. Shelef, Academy of Sciences of USSR, Institute of Chemical Physics, Moscow-Leningrad, 1947.

125. Bogensperger, M., “A Comparative Study of Different Calculation Approaches for the Numerical Simulation of Thermal NO Formation”, Diss. U. Graz, 1996.

126. Lam, S. H., “Reduced Chemistry Modeling and Sensitivity Analysis”, Lecture Notes for Aerothermochemistry for Hypersonic Technology, Lecture Series Program, at the Von Karman Institute For Fluid Dynamics, April 24-28, Brussels, Belgium, 1995.

127. Maas, U. and Pope, S. B., “Simplifying Chemical Kinetics; Intrinsic low dimensional Manifolds in Composition Space”, Combustion and Flame 88: 239-264, 1992.

128. De Soete, G.G., “Overall reaction rates of NO and N2 formation from fuel nitrogen”, 15th Symposium (International) on Combustion”, The Combustion Institute, Pittsburgh, pg. 1093, 1975.

129. Bockhorn, H., Fetting, F., Heddrich, A. and Wannemacher, G. “Investigation of the Surface Growth of Soot in Flat Low Pressure Hydrocarbon Oxygen Flames”, Twentieth International Symposium on Combustion. Pittsburgh: The Combustion Institute, 1985: 879, 1985.

130. Magnussen, B.F. and Hjertager, B.H. “On mathematical modeling of turbulent combustion with special emphasis on soot formation and combustion”, Sixteenth International Symposium on Combustion. Pittsburgh: The Combustion Institute, 1977.

131. Tatschl, R., Riediger, H., Bogensperger, M., “Multidimensional Simulation of Spray Combustion and Pollutant Formation in a Medium Speed Marine Diesel Engine“, Proc. FISITA World Automotive Congress, Paris, 1998.

132. Kent, J.H. and Honnery, D.R., “Soot Mass Growth in Laminar Diffusion Flames - Parametric Modeling”, Soot Formation in Combustion. Henning Bockhorn (Ed.), Springer, 1994.

133. Gülder, Ö.L., “Soot Formation in Laminar Diffusion Flames at Elevated Temperatures”, The Combustion Institute Publishing Co. Inc., 1992.

134. Böhm, H., Bönig, M., Feldermann, Ch., Jander, H., Rudolph, G. and Wagner, H. Gg., “Pressure Dependence of Formation of Soot and PAH in Premixed Flames”, Soot Formation in Combustion, Springer, 1994.

135. Mobasheri, R., Peng, Z., and Mirsalim, S., “CFD Evaluation of Effects of Split Injection on Combustion and Emissions in a DI Diesel Engine”, SAE Technical Paper 2011-01-0822, 2011.

136. Mobasheri, R. and Peng, Z., “Investigation of Pilot and Multiple Injection Parameters on Mixture Formation and Combustion Characteristics in a Heavy Duty DI-Diesel Engine”, SAE Technical Paper 2012-01-0142, 2012.

137. Mobasheri, R., Peng, Z., and Mirsalim, S., “Analysis the Effect of Advanced Injection Strategies on Engine Performance and Pollutant Emissions in a Heavy Duty DI-Diesel Engine by CFD Modeling”, International Journal of Heat and Fluid Flow 33: 59-69, 2012.

138. Wiedenhoefer, J.F. and Reitz, R.D., “Modelling the Effect of EGR and Multiple Injection Schemes on I.C. Engine Component Temperatures”, Numerical Heat Transfer, Part A: Applications, 37: 7, 673-694, 2000.

139. Mobasheri, R., Peng, Z., “A Computational Investigation into the Effects of Included Spray Angle on Heavy-Duty Diesel Engine Operating Parameters”, SAE Paper 2012-01-1714, 2012.

140. Mobasheri, R., Peng, Z., “Using Large Eddy Simulation for Studying Mixture Formation and Combustion Process in a DI Diesel Engine”, SAE Technical Paper 2012-01-1716, 2012.

141. Mobasheri, R., Peng, Z., “Analysis of the Effect of Re-Entrant Combustion Chamber Geometry on Combustion Process and Emission Formation in a HSDI Diesel Engine”, SAE Technical Paper 2012-01-0144, 2012.

142. Mobasheri, R., Peng, Z., “3D-CFD Modelling of the Effects of Injection Timing on the Combustion Process and Emissions in a High Speed Direct Injection (HSDI) Diesel Engine”, Proceedings of the ASME 2012 Internal Combustion Engine Division Spring Technical Conference ICES2012, Paper number ICES2012-81137, 2012.

143. Zhu, Y., Zhao, H., and Ladommatos, N., “Computational Study of the Effects of Injection Timing, EGR and Swirl Ratio on a HSDI Multi-Injection

Diesel Engine Emission and Performance", SAE Technical Paper 2003-01-0346, 2003.

144. Zhu, Y., Zhao, H., Melas, D. A., and Ladommatos, N., "Computational study of the effects of the geometry of piston bowl pip for a high-speed direct-injection diesel engine", Proc. IMechE, Part D: J. Automobile Engineering, 218, 875-890, 2004.